



저작자표시-비영리-변경금지 2.0 대한민국

이용자는 아래의 조건을 따르는 경우에 한하여 자유롭게

- 이 저작물을 복제, 배포, 전송, 전시, 공연 및 방송할 수 있습니다.

다음과 같은 조건을 따라야 합니다:



저작자표시. 귀하는 원저작자를 표시하여야 합니다.



비영리. 귀하는 이 저작물을 영리 목적으로 이용할 수 없습니다.



변경금지. 귀하는 이 저작물을 개작, 변형 또는 가공할 수 없습니다.

- 귀하는, 이 저작물의 재이용이나 배포의 경우, 이 저작물에 적용된 이용허락조건을 명확하게 나타내어야 합니다.
- 저작권자로부터 별도의 허가를 받으면 이러한 조건들은 적용되지 않습니다.

저작권법에 따른 이용자의 권리는 위의 내용에 의하여 영향을 받지 않습니다.

이것은 [이용허락규약\(Legal Code\)](#)을 이해하기 쉽게 요약한 것입니다.

[Disclaimer](#)

August 2020

Ph.D. Dissertation

**Evaluation of reliability and monitoring capability
of multipurpose CNT-CF cement composite sensor
for concrete structures**

Graduate school of Chosun University

Department of Architectural Engineering

Major: Construction and Building Material

Million Tafesse Bedso

Evaluation of reliability and monitoring capability of
multipurpose CNT-CF cement composite sensor for
concrete structures

콘크리트 구조용 다목적 CNT-CF 시멘트 복합재료
센서의 신뢰성 및 모니터링 성능 평가

August 28, 2020

Graduate School of Chosun University

Department of Architectural Engineering

Major: Construction and Building Material

Million Tafesse Bedso

Evaluation of reliability and monitoring capability of multipurpose CNT-CF cement composite sensor for concrete structures

Advisor: Professor Hyeong-Ki Kim

This dissertation is submitted to graduate school of Chosun
University in partial fulfillment of the requirements for the degree of
Doctor of Philosophy in Architectural Engineering

May, 2020

Graduate School of Chosun University

Department of Architectural Engineering

Major: Construction and Building Material

Million Tafesse Bedso

The doctoral dissertation committee for
Million Tafesse Bedso certifies that this is the
approved version.

Committee:

Professor Chang-Geun Cho, Chosun University (Chair Member)	(sign)
Professor Hee Young Lee, Chosun University (Committee Member)	(sign)
Professor Beomjoo Yang, Chungbuk National University (Committee Member)	(sign)
Professor Bang Yeon Lee, Chonnam National University (Committee Member)	(sign)
Professor Chosun University (Committee Member)	(sign)

July, 2020

Graduate School of Chosun University

Table of Contents

Table of Contents	i
Abstract....	x
Abstract in Korean (초록).....	xii
Chapter 1. Introduction	1
1.1 Introduction	1
1.2 Objective and scope of the dissertation	5
1.3 Outline of the dissertation	5
Chapter 2. An introduction to structural health monitoring: Literature review	7
2.1 Introduction	7
2.2 Structural health monitoring.....	7
2.2.1 Concrete and SHM	7
2.2.2 Types of sensors	11
2.2.3 Functional filler sensors	17
2.4 Previous works on crack, chloride and carbonation-literature review	21
2.4.1 Crack sensing	21
2.4.2 Chloride and carbonation Sensing.....	25
Chapter 3. Unwanted electrical fluctuation of CNT/cement composite using CNT as a sole agent: Pilot experiment	29
3.1 Introduction	29
3.2 Materials and methods.....	29
3.2.1 Materials and mix proportion (orange).....	29
3.2.2 Experimental methodology	32
3.3 Results and discussion.....	39
3.3.1 CNT/cement mortar composite mixed with NaCl.....	39
3.3.2 CNT/cement composite immersed in chloride solution	44
3.3.3 Accelerated carbonation of CNT/cement composites	46

3.3.4 CNT/cement composites embedded in reinforced mortar	47
3.6 Discussion: On electrical properties fluctuation causes	49
3.7 Conclusions	60
Chapter 4. Reliability of CNT-CFs hybrid cement composite on dimensional stability and electrical stress-strain sensing capability	62
4.1 Introduction	62
4.2 Materials and methods.....	62
4.2.1 Materials and mix proportions.....	62
4.2.2 Experimental Methodology	67
4.2.3 Working principle of the hybrid cement composite sensor	71
4.3 Results and discussion.....	73
4.3.1 Preliminary study	73
4.3.2 Dimensional stability.....	77
4.4 Discussion	93
4.5 Conclusion.....	97
Chapter 5. Chloride profiling and conductivity relation of CNT-CFs hybrid cement composite following the rapid chloride penetration test and monitoring evaluation	99
5.1 Introduction	99
5.2 Materials and method	99
5.2.1 Materials and mix proportions.....	99
5.2.2 Experimental methodology	100
5.3 Result and discussion	103
5.3.1 Chloride profiling of hybrid cement composite	103
5.3.2 Mortar embedded hybrid cement composite sensors	113
5.3.3 BSE-SEM, EDX, and EPMA analysis	117
5.4 Discussion	120
5.5 Conclusion.....	124
Chapter 6. Multiple CNT-CFs hybrid cement composite sensors embedded in reinforced mortar for crack and moisture monitoring.....	126
6.1 Introduction	126

6.2 Materials and method	126
6.2.1 Materials and mix proportions.....	126
6.2.2 Experimental methodology	126
6.3 Result and discussion	129
6.3.1 Moisture monitoring.....	129
6.3.2 Crack monitoring.....	131
6.4 Discussion	142
6.4 Conclusion.....	146
Chapter 7. Conclusions	149
7.1 Summary	149
7.2 Recommendations	154
7.3 Future studies	155
References..	157
Appendix...	168
Appendix A. Glossary of electrical terms and definitions.....	168
Appendix B. Supplementary data of chapter 4.....	173
Appendix C. Supplementary data of chapter 5.....	179
Appendix D. Supplementary data of chapter 6	180
Acknowledgment	185
Curriculum Vitae	187

List of Tables

Table 2-1 Summary of characteristics and cost of cement composites incorporated with carbon materials	20
Table 2-2 Literature review on self-sensing properties of cement composite sensors based on functional fillers	28
Table 3-1 Summary of mix proportion and experimental procedure	31
Table 4-1 Physical properties of the functional fillers (CNT and Carbon fiber).....	64
Table 4-2 Chemical composition of Portland cement and silica fume	65
Table 4-3 Mix proportion of mortar samples	66
Table 4-4 Resistivity of hybrid cement composite samples before and after boiling based on their resonant frequency (Dry and SSD)	75
Table 4-5 The total intruded volume of hybrid cement composites	89
Table 4-6 Comparison of the hybrid cement composite sensing capability results with previous literature reviews	97
Table 5-1 Mix proportion of chloride profiling samples and embedding mortars	100
Table 5-2 Chloride concentration of the hardened hybrid cement composite based on ion-chromatography	106
Table 5-3 Total intruded volume of the hybrid cement composite samples with chloride ingress.....	108
Table D-1 Flexural crack widths measured by portable microscope	181
Table D-2 Resistivity measurement before, during and after cracking of the sensors ..	182
Table D-3 Resistivity measurement before and after cracking of the surrounding reinforced mortar sample.....	183
Table D-4 Resistivity measurement before and after crack healing.....	184

List of Graphs

Figure 2-1 A typical algorithm for structural health monitoring.....	10
Figure 3-1 Schematic illustration of reinforced mortar embedded with the CNT/cement composite	39
Figure 3-2 Resistance of CNT/cement mortar composites mixed with various chloride contents: before drying.....	40
Figure 3-3 Change of resistance of CNT/cement mortar composites mixed with different chloride contents by drying cycles (1 cycle: 1 day of air-drying and 2 days of sealing) 42	
Figure 3-4 Saturation degree of CNT/cement mortar composites mixed with different chloride contents by drying cycles	43
Figure 3-5 Resistances of CNT/cement mortar composites mixed with various chloride contents after completely dried (measured with different electrode types).....	44
Figure 3-6 Changes of resistance of paste composites with CNT 0.6 % immersed in chloride solution (measured with different electrode types)	45
Figure 3-7 Changes of resistance of mortar composites with different CNT contents immersed in chloride solution	46
Figure 3-8 Changes of resistance of CNT 0.6 % paste composites by carbonation (measured with different electrode types)	47
Figure 3-9 Resistance of CNT/cement composites (CNT 0.6%) embedded in a mortar beam: before and after embedding.	49
Figure 3-10 A schematic illustration of generation mechanism of macrocrack in cement composite sensor embedded in concrete or mortar.	52
Figure 3-11 A schematic illustration of blocking of tunneling region by hydration products	54
Figure 4-1 Raman spectroscopy analysis of Pure CNT and NaOH treated CNT	64
Figure 4-2 FT-IR spectra of CNT and superplasticizer	65

Figure 4-3 Flow chart showing the shrinkage cycle of Phase one (left), Phase two (mid), and Phase 3 (right).....	70
Figure 4-4 Shrinkage measuring demec gauge with embedded pin setup.....	71
Figure 4-5 Schematic illustration of the hybrid cement composite and BSE-SEM image of CCF2.....	73
Figure 4-6 Change in resistivity by percentage of samples based on their resonant frequency (SSD condition and 7 day air dried)	76
Figure 4-7 Phase angle Vs. frequency value of preliminary samples	76
Figure 4-8 Shrinkage cycle of the hybrid cement composite for phase one.....	79
Figure 4-9 Mass loss result of the hybrid cement composite for phase one.....	79
Figure 4-10 Scattered graph of the hybrid cement composite resistivity (a) stainless steel electrode (b) silver paste electrode	81
Figure 4-11 Shrinkage cycle of the hybrid cement composite for phase two	82
Figure 4-12 Mass loss result of the hybrid cement composite for phase two.....	83
Figure 4-13 FCR Vs shrinkage cycle of the hybrid cement composite for phase one	85
Figure 4-14 FCR Vs shrinkage cycle of the hybrid cement composite for phase two	86
Figure 4-15 Relationship graph of FCR and strain for Phase one and phase two	88
Figure 4-16 MIP result of the hybrid cement composites for shrinkage samples (a) incremental pore volume (b) cumulative pore volume in percentage by pore size	90
Figure 4-17 Total deformations of phase one and two.....	91
Figure 4-18 Pictures of microcrack (a) cracks during phase two cycle (b) After healing on phase 3.....	92
Figure 4-19 Deformation after end of phase two of the hybrid cement composite in phase three (dormant period) during air curing for 6 months.....	92
Figure 5-1 Custom made rapid chloride penetration testing instrument setup.....	102

Figure 5-2 Schematic diagram showing the embedded sensors inside a reinforced mortar for chloride monitoring	103
Figure 5-3 Hybrid cement composite samples sprayed by AgNO_3 based on the profiling depth after the rapid chloride penetration test (a) C3CF2 (b) CCF2	105
Figure 5-4 Pore size distribution of chloride ingress samples following the profiling depth for (a) C3CF2 samples and (b) CCF2 samples	110
Figure 5-5 Relationship of the total intruded volume and chloride concentration in the hybrid cement composite.....	110
Figure 5-6 Non-evaporated water-to-cement ratio (W_{ne}/C) of the hybrid cement composite based on the profiling depth of the chloride ingress samples	111
Figure 5-7 Chloride concentration and resistivity result of the hybrid cement composite by the profiling depth	112
Figure 5-8 Chloride concentration and resistivity relationship of the hybrid cement composite sensing capability	113
Figure 5-9 Chloride concentration of each profiling depth of the hybrid cement composites based on ion-chromatography test result.....	114
Figure 5-10 Embedded sensors change of resistivity for chloride monitoring (a) individual sensors result (b) seriously connected sensors result	116
Figure 5-11 Embedded sensors change of capacitance for chloride monitoring (a) individual sensors result (b) seriously connected sensors result	116
Figure 5-12 BSE-SEM, EDX mapping and element composition of CCF2 hybrid cement composite immersed in chloride for 90 days.....	118
Figure 5-13 BSE-SEM and EPMA image mapping of CCF2 hybrid cement composite immersed in chloride for 90 days	119
Figure 5-14 Chloride depth mapping in different levels using EMPA image of CCF2 hybrid cement composite immersed in chloride for 90 days.....	120

Figure 6-1 Schematic diagram of moisture samples showing the embedded sensors inside a mortar	128
Figure 6-2 Schematic diagram of crack samples showing the embedded sensors inside a reinforced mortar	129
Figure 6-3 Relative humidity and resistance relationship of the hybrid cement composite embedded in reinforced mortar for moisture monitoring	131
Figure 6-4 Measurement directions of the hybrid cement composite and the mortar between the hybrid cement composites	132
Figure 6-5 Initial resistivity relationship measurement of crack specimens due to change in moisture	133
Figure 6-6 Three-point bending test setup and crack propagation directions	134
Figure 6-7 Real time monitoring of the resistivity change of sensors during a three-point bending test for crack monitoring	136
Figure 6-8 Crack width Vs change of resistivity relationship of the hybrid cement composite during cracking	137
Figure 6-9 Relationship graph of the change on resistivity and crack width based on the effect of moisture	139
Figure 6-10 Resistivity measurement of the surrounding mortar using the hybrid cement composite as an electrode: (a) Sample 1 (b) Sample 2.....	140
Figure 6-11 Relationship of the change in resistivity after crack and after healing (a) specimen placed underwater (SSD) (b) specimen placed in the air (Dry)	142
Figure 6-12 Flow chart showing the multi-functionality of the hybrid cement composite to detect crack, chloride, and moisture.....	146
Figure B-1 Phase angle Vs frequency value for new samples at dry state	173
Figure B-2 Phase angle Vs frequency value for new samples at SSD state	174
Figure B-3 Impedance Vs frequency value for new samples at dry state	175

Figure B-4 Real Vs imaginary Impedance measurement values for new samples at dry state.....	176
Figure B-5 Images taken after phase 2 and phase 3 during cracking and healing.....	177
Figure B-6 SEM images for the hybrid cement composite (CCF2).....	178
Figure C-1 Backscattering images for the hybrid cement composite (CCF2).....	179
Figure D-1 Crack patterns of specimens cracked under three-point bending test.....	180

Abstract

Evaluation of reliability and monitoring capability of multipurpose CNT-CF cement composite sensor for concrete structures

Million Tafesse, Bedso, M.Sc

Advisor: Prof. Hyeong-Ki Kim, Ph.D.

Department of Architectural Engineering

Graduate school of Chosun University

The long-established way of examining the concrete structure requires a professional inspection to analyze the damage through visual inspection. In most cases, when further investigations are necessary, a small part of the structure will be raked and tested. However, in the past few decades, the construction industry used structural health monitoring (SHM) to achieve a higher degree of serviceability and to cut the cost of maintenance through signals from the sensors for early maintenance.

In this study, a cement composite based on carbon nanotube (CNT) and carbon fiber (CFs) were examined for its capability to act like a sensor by the change of electrical resistivity. This paper follows a sequential pattern to explore and advance the potential of CNT/cement composite sensors. To make a baseline, different case studies were undertaken as a pilot study to widen the understanding of the problems. Following the result of the pilot study, which is related to the unnecessary fluctuations, a reliability study was carried out to improve the properties of the CNT/cement composite using mortar-

based CNT and CFs hybrid cement composite. In this part, a new approach was used to evaluate the self-sensing capabilities of different hybrid composites using the stress-strain cycle by drying and wetting the shrinkage samples. Afterward, the specimens set to dry for an additional six months exposing them to the outside environment to investigate the healing capability. Furthermore, for detailed analyses, the mechanical properties, porosity, total deformation, and microcrack images were taken. From the result, most of the hybrid composite showed a substantial sensing capability with significant reliability.

Once the reliability study was done, the hybrid cement composite, which showed the steadiest result was selected for further investigation. Of this investigation, chloride profiling was examined using a rapid chloride migration test to understand chloride concentration and conductivity relations. Moreover, the sensors were also embedded inside mortar specimens. Furthermore, cracking and relative humidity were also examined by embedding different types of hybrid cement composite sensors inside a mortar sample to show the multifunctionality. Cracking was done under a three-point bending test embedding several sensors in one reinforced mortar specimen while investigating the relationship between the crack width and location with the conductivity, including the healing capability of the cracks. In addition, for the first time the hybrid cement composite was used as an electrode to investigate the surrounding mortar resistivity. This will add a new approach to the research area. In general, the result of the hybrid cement composite to sense chloride and crack was good. However, even though the relationship between the moisture and resistivity was good, the sensing capability was very low.

Abstract in Korean (초록)

벡소 밀리언 타페세

지도교수: 김형기

조선대학교 대학원 건축공학과

콘크리트 구조물을 진단하는 가장 일반적인 방법은 전문적인 인력이 직접 방문해 구조물의 상태를 육안 혹은 장비를 이용해 파악하는 것이다. 대부분의 경우, 장기적인 조사가 필요할 뿐 아니라 경우에 따라 구조물이 일부 손상되는 경우도 있다. 그러나 최근 몇 십년 간 건설분야에서는 구조물 안전성 모니터링 (Structural health monitoring, SHM) 기술이 개발되어 왔으며, 이를 통해 높은 정밀도의 결과를 얻을 수 있을 뿐 아니라 진단과 관련된 사회비용을 줄이는 것이 가능해졌다.

본 연구에서는 탄소나노튜브(Carbon nanotube, CNT) 및 탄소섬유(Carbon fiber, CF)를 혼입한 시멘트 복합재료의 전기저항 변화를 활용해 센서로서 사용이 가능한지에 대해 확인 하였다. 이 논문에서는 CNT 시멘트 복합재료 센서의 활용 가능성을 높이기 위해 다음의 순서에 따라 진행된 연구 결과를 정리하였다. 먼저 기초적인 성능수준을 확인 하기 위해 다양한 변수의 파일럿 실험이 진행되었다. 그리고 기초결과에서의 결과값의 편차를 고려해, 이 편차를 줄이기 위한 한 방법으로 CNT 시멘트 복합재료 자체에 CF 를 같이 혼입하였으며 이에 대한 신뢰성을 확인 하였다. 이 때, 시편을 반복하여 건조 및 포화 시켜 응력-변형률 변화를 확인하였다. 이후 시편의 자기치유에 의한 전기전도도 변화를 검토하기 위해 6 개월간 추가로 외부에 폭로되었다. 그리고 물리적인 특성 및 공극, 최종변형률, 미세균열 발생여부들을 확인 하였다. 실험결과 대부분의 CNT-CF 하이브리드 복합재료가 만족할만한 신뢰성, 즉 안정적인 전기전도도 특성을 갖는 것으로 확인 되었다.

신뢰성 결과를 기반으로 가장 안정적인 하이브리드 복합재료를 이용해 추가 연구를 진행하였다. 먼저 급속 침투시험을 이용해 염소 프로파일링을 수행하였으며, 염소농도와 전기전도도 간의 관계에 대해 검토 하였다. 또한 복합재료 센서를 콘크리트 구조를 모방한 일반 모르타르에 매립해 실험 하였다. 매립된 복합재료 센서가 모르타르 구조의 균열 및 상대습도 변화에 따라 전기전도도가 변화하는 정도에 대해 검토하였으며 이를 통해 센서의 다목적성이 확인 되었다. 3점 재하를 통한 힘에 의해 균열이 발생한 모르타르 내에, 매립된 복수의 복합재료 센서가 그 자체 및 서로간의 전기전도도가 변화하는 형태를 확인 하였다. 이 때 균열 폭과 균열 발생 후 자기치유에 의해 전기전도도가 변화하는 정도 역시 확인 하였다. 실험결과, 염소침투 및 균열에 의해 복합재료의 전기전도도가 변화하는 정도가 큼을 확인하였으며, 동시에 상대습도에 의한 변화는 없는 것을 알 수 있었다.

Chapter 1. Introduction

1.1 Introduction

Reinforced concrete is still the major construction material and widely known way of building infrastructures in almost all over the world, despite their very nature of permeability and deterioration over time. To develop sensors that could monitor these heterogeneous structures is a wise move and necessity, rather than to stick to the age-old methods of inspection using damages that are exposed to the outside surface (Clemente, 2017). In overall, the porous nature of concrete allows different substances to enter into the concrete, such as water, chloride, sulfate, and carbon dioxide (Lin, 1990; He and Shi, 2008; Miloud, 2005, de Mederios, et al., 2014).

For instance, water and chloride use the permeability of concrete to get inside the pore structures to form ice during freezing temperatures and salt crystals to be build up over time inside the concrete to corrode the bars inside the concrete, respectively (Roberts, 1962; Cai and Liu, 1998). Eventually, the ice and corroded reinforcement initiate an outward force from the inside of the concrete, putting the concrete to a susceptible position of strain (Marchand, 1996; Bamforth, 1997; Angst et al., 2009). Carbonation and sulfate attack also create the same expansive forces. In the case of carbonation, the reduction in passivation of the surrounding concrete leads to steel corrosion (Chang, 2006). During the sulfate attack, the intruded sulfate reacts with calcium aluminate hydrate or calcium hydroxide to form ettringite (Mindess, 2019; Delatte, 2009). Both the steel corrosion and ettringite formation, lead the concrete to be under a tensile force. It is a well-known fact that concrete is not good on strain forces. Therefore, for this and many other reasons monitoring concrete structures is essential to ensure early maintenance.

Early maintenance is one of the crucial things for concrete structural sustainability. Some of the benefits are safety, extend service lifetime, and also could save a large amount of money and resource (Ko, 2005). However, indifferent is not the problem for early maintenance; instead, it lays on the complexity and difficulty to detect the damages sooner. An expert personal investigation is required on the site based on a frequently timed mode, and in some cases, it could demand a downtime on the building or road. Overall, this is a time taking process, which involves a considerable amount of resources, workforce, and expertise on the area beside the extra outflow of cash just for the sake of investigation prior to the major cost of maintenance. With the advancements of technology Structural Health Monitoring (SHM) has evolved to detect degradation and damages due to internal and external factors (Song, 2017).

In earlier times, SHM has been performed traditionally on a global scale, having a larger area to monitor with a limited number of sensors, which could pick only on severe damages (Rainieri, 2011). Most of the SHM sensors provide the necessary information for the intended area since they are being done on a global scale using a limited number of sensors on fewer locations. However, for large-area data collection, they fall short because most sensors are not compatible with the surrounding concrete. To overcome the limitation, either a network of sensors should be embedded inside the structure, or the structure itself should be smart enough for self-sensing. The latter being uneconomical for its high volume of functional filler requirements. This dissertation will focus on fostering the development of embedded type functional fillers based on cement composite sensors.

Currently, the development of the SHM is going towards a more sophisticated sensor system demanding, large sensor grid networks, minute size sensors, and a way to monitor the overall system wirelessly. Therefore, researchers are working on the development of sensors that can be distributed in a large area and can be inspected remotely on a wireless network by mimicking the human nerve system (Lynch, 2006). These will help to detect any small defects as early as possible in real-time, which apparently will benefit from wasting too much time, money, and service that come from late inspection and maintenance. However, one of the major challenges in developing SHM systems for any structure is the quality of sensors and their versatility.

In the construction industry, there are different types of sensors, such as piezoelectric ceramic, shape memory alloys, strain gauges, fiber optic sensors, half-cell electrolyte sensors, and many others. Most being embedded inside the concrete and some attached to the surface and few being destructive tests, which requires raking to examine the surrounding environment. Most of the sensors that are available in the current market are based on temperature and humidity measurement to assist on-site construction, mainly focusing on the early age of concrete during placing and curing. Besides, predicting the strength of the concrete using the mix proportion, temperature, and humidity of the concrete following the maturity concept. However, the sensors have their drawbacks on long term monitoring of major durability problems of reinforced concrete. In general, the majority of the sensors detect one or two specifically targeted problems. This helps the sensors to predict the damage accurately; however, due to the heterogeneous nature of concrete, the problem is complex, diverse, and interconnected to evaluate the durability through time, which requires the same solution as the problem, a multipurpose sensor.

In addition, most of the sensors are not easily compatible with their surroundings caused by the weak bond between the constituent material of the sensor and the concrete interfacial character (Lee et al., 2017). Furthermore, the cost of most sensors is expensive to use in a large area, and the metallic sensors capability to corrode and lose their sensitivity as a sensor is another problem that cannot be ignored since most of them are metal-based sensors (Han and Ou, 2007). To solve those major problems of sensors (Multipurpose, Compatibility, Cost, and Corrosion) for the construction industry, this dissertation paper recommends sensors, which are manufactured from cement by adding functional fillers.

The trend of looking for cement composite sensors is growing due to the ease of integrating the sensors with the surrounding concrete without any significant defects [Compatibility]. The research community is now trying to advance the cement-based composite sensors, thanks to nanomaterials and their property, with an overall low cost of production [Cost]. These functional fillers could change the property of the bulk cement composite, which is originally a non-conductive material into a conductive and strain sensitive material giving the cement composite the ability to picking changes without the need for metallic elements [Corrosion] (Kim, 2014; Han and Ou, 2007). Carbon-based functional fillers inside cement composite sensors have great potentials for the future SHM system. Furthermore, unlike most sensors, rather than having a single or fewer goal to achieve, the carbon-based functional fillers could be able to monitor different conditions like carbonation, crack, chloride penetration, and moisture condition of their surrounding concrete [multipurpose].

1.2 Objective and scope of the dissertation

The main objective of this dissertation is to develop a CNT/cement composite sensor with exceptional reliability and the ability to monitor different defects of concrete with multipurpose capability. The scope of this research includes: 1) a pilot study to pinpoint the major shortcomings of a CNT/cement composite sensors were carried out to lay the foundations of the research focus points, 2) the limitations discussed in the pilot study, especially in terms of the dimensional stability was studied by merging CNT and CFs using both functional fillers as a hybrid cement composite sensor by following a relatively new way of methodologies, 3) detailed investigations on the capability of the sensors to pick changes by using chloride profiling and cracking samples, additionally the ability of carbonation and moisture detection were also studied.

1.3 Outline of the dissertation

This dissertation is composed of 7 chapters, each of which are interconnected and follow a progression pattern until the end.

Chapter 1 briefly describes the limitations of the traditional and current SHM systems and an overview of the benefits of cement composite sensors based on functional fillers. The objective, scope, and outline of the research are presented in this section.

Chapter 2 A brief introduction on structural health monitoring is done, followed by a discussion on the pros and cons of the different types of sensors that are common on structural concrete monitoring. In addition, a short synopsis was written about functional fillers and also gives an idea about what has been done in previous literature reviews in detail, focusing on CNT and CFs based cement composite application for the SHM system.

Chapter 3 deals with the characteristics of CNT/cement composite by investigating the limitations they have based on various case studies using a diverse methodological approach for each study. This section will be treated as a pilot study, which will be counted as foundation work for the other chapters to come.

Chapter 4 investigates the reliability of the CNT-CFs hybrid cement composite sensor using a unique approach from previous works. In this chapter, the dimensional stability and microcracking of hybrid cement composite sensors were studied using slender shrinkage samples through different phases of a stress-strain cycle in-depth.

Chapter 5 presents the studies made on hybrid cement composites using a rapid chloride penetration test to evaluate the relationships between the conductivity of the matrix and its chloride concentration on the cement matrix following a novel approach. In addition, the hybrid cement composite sensors embedded inside mortar to detect chloride also included inside this chapter.

Chapter 6 tries to show the multifunctional capability of the hybrid cement composite sensors by embedded inside reinforced concrete to monitor cracks, moisture, and carbonation besides the chloride penetration, which is discussed earlier in chapter 5. Crack detection and location, including the healing properties in time, will be the focus area of this chapter while introducing only the potentials on monitoring carbonation and moisture.

Chapter 7 summarizes the findings and core points of the dissertation with concluding remarks, including recommendations for future studies.

Chapter 2. An introduction to structural health monitoring: Literature review

2.1 Introduction

In this chapter, the main technical terms used in the paper will be discussed briefly, focusing on electrical terminologies and theory, which are outside of our field of study in order to highlight the main words in the dissertation.

This study tries to overview different literature works based on what the sensors can actually detect. Some of the nanomaterials composites can help in picking problems such as chloride penetration, crack propagation, carbonation depth, moisture detection, traffic management and can be used for non-distractive testing as well on objects made of concrete. This paper also tries to evaluate each problem based on the literature available on the area and tries to see their limitations.

2.2 Structural health monitoring

2.2.1 Concrete and SHM

The world has come far from the ancient Egyptian, and Roman Cement to the closest discovery of modern-day cement patented and named by Joseph Aspdin in 1824 as Portland cement, after a place in the United Kingdom where strong stones were found. Later in 1845, Isaac Johnson calcinated the Portland cement at a high temperature of 1400-1500 °C to improve and create the Portland cement we know today. The Portland cement is a strong binder and can be mixed with sand, aggregate, and water to produce concrete. All the materials used to create concrete are readily available in almost every part of the world, making concrete the most consumed material next to water in the world. However, concrete is weak when it comes to a tensile force to avoid

that in 1984 Ernest L. Ransome introduced the Reinforced concrete. His innovation leads to the world's first reinforced concrete skyscraper in Ohio, the USA showing an alternative material to mostly steel dominated construction at the time. Since then, the world is using concrete as a primary building material and has made many signs of progress through research and study by improving the strength and durability of concrete. Currently, preserving the concrete structures for a long time is a challenge.

To curb the durability issues of concrete early maintenance is the key. It is almost not practical to avoid all kinds of defects in the concrete due to the heterogeneous and porous nature of concrete. All that can be done is to address the defects as soon as possible before severe damage has occurred. Since most concrete structures resist isolated damages, until these separate damages started to gather and bring colossal and sudden damage to the structure due to natural disaster or fatigue. To control that monitoring structural parts of the infrastructure is required, which also increases the serviceability and safety of the structures. To control or monitor the structure means to maintain the damage at an early age with minimum cost and possibly a short term or no interruption at all in the operation of the infrastructure. Currently, the world is looking for much longer service life in concrete structures in terms of natural resource management, carbon footprint reduction, and cost-effectiveness.

To control or monitor a concrete structure requires sensors to collect data and analyze it for decision making in real-time; this is called structural health monitoring (SHM). ASTM – E2983 defines SHM as a field of engineering that deals with the diagnosis and monitoring of structures during their operation. Affirming the primary goal of SHM is to detect, identify, assess, and monitor the flaws that may occur and affect the structure. Figure 2.1 shows a typical flow chart

or algorithm that shows the SHM flow of a concrete structure should look like when it is under monitoring. Whenever a change in the surrounding environment is detected, the information will be stored as a benchmark, and the severity will be analyzed. If the damage is vast, it will be addressed automatically by identifying the kind of damage, and a response should be given for the maintenance call to solve the damage detected early.

On the other hand, if the damage is minor, an assessment study will be done with additional already stored trivial damage information, based on the assessment the future impact in the structure will be categorized as likely and unlikely to have an impact on the structure. If it is “likely” the maintenance should be started soon. However, if the inspection personnel ignore the maintenance call or if the future impact is considered “unlikely,” the data will be stored in the “store information” section. When further new changes are detected, either minor or major, an assessment will run again, this time will run considering the new cases as well with the old stored information to make it more precise and to solve at the right time.

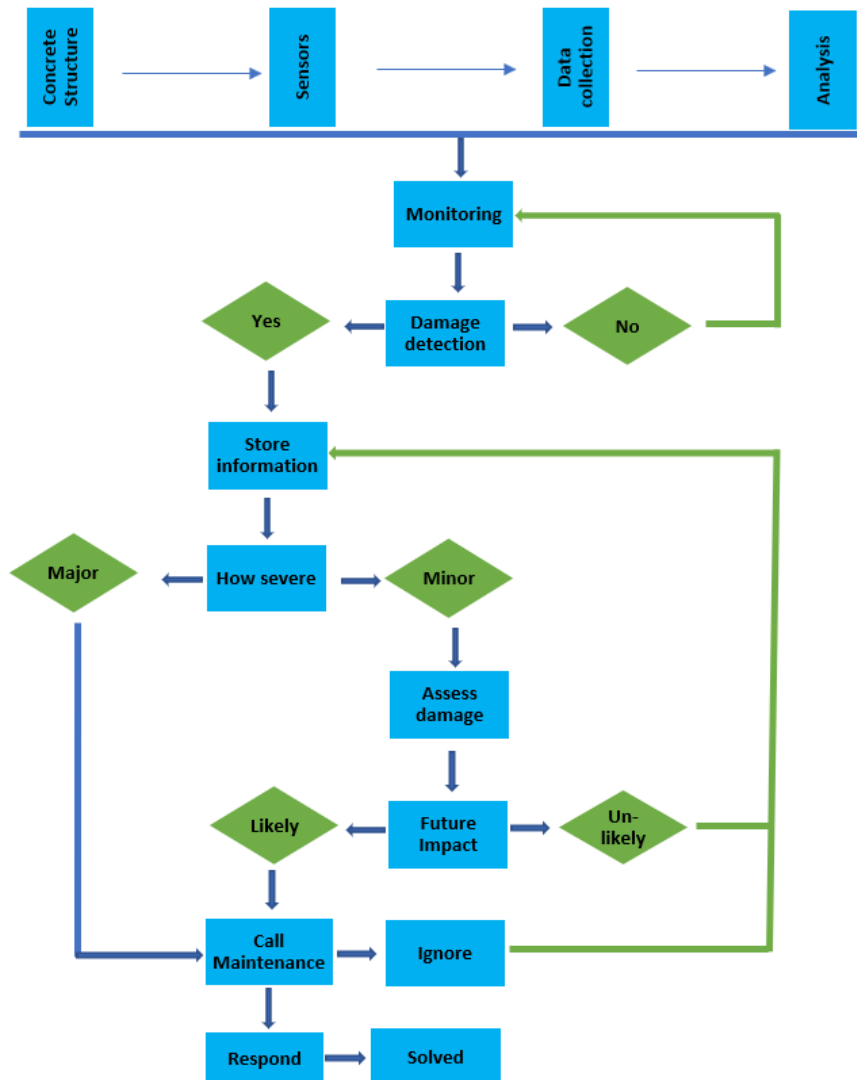


Figure 2-1 A typical algorithm for structural health monitoring

SHM monitoring is not only bounded in civil engineering; instead, it is much advanced in the aerospace and mechanical engineering departments as well (Yuan, 2016). As a new and multidisciplinary field, SHM is a relatively new skill that started to grow, starting from the '90s, gets its foundation from non-destructive testing (NDT). However, NDT and SHM have a distinct approach to the way the test is performed, in case of NDT, to examine a structure external

equipment will be used on a periodical base to assess the structure by an expert or skilled worker. In SHM, sensors will be embedded permanently to collect data on real-time bases, and analysis will be done based on an algorithm feed to a central brain-like system. The information will be used to assess the structures continuously without any human intervention, which makes SHM the best alternative over NDT. However, there are many difficulties in order to implement SHM, of this, the complexity to install the system in a structure, the kinds of sensors to use for data accusation, analyzing the data for damage detection, and to get a precise prediction in the future of the structure condition are some of the few obstacles to be addressed.

2.2.2 Types of sensors

There are different kinds of sensors each having their own pros and cons based on their way of response to a change in the surrounding they can be categorized in to: Piezoresistive, Piezoelectric, fiber optic Bragg gratings (FBG), accelerometer, micro-electromechanical system (MEMS), magnetostrictive and shape memory alloys (SMA) are the few from the different kinds of sensors.

2.2.2.1 Shape Memory Alloys (SMA)

SMA are sensors with a unique capability of reminding their previous shape after a change in shape while being heated or cooled. This can be done due to an inside molecular rearrangement of the SMA metals back and forth by either temperature or external forces having a higher and lower phase called austenite and martensite, respectively. They can be used as an actuator, energy dissipater, and microstrain for different applications. The sensors are made by an amalgamation of metals, for this reason it is also called smart metals.

The cost of the SMA sensor is relatively high, and most sensors have difficulty in retaining post-tensioning force shapes. Besides, most of the applications of these sensors are suitable for steel structures. The Low ductility properties of cement-based materials make the application of SMA sensors to fail shortly for many applications on concrete based infrastructures. However, they are also highly corrosion resistance, and in some cases, they can be replaced in place of tendons and can be used as one, in addition to their primary work of strain sensing.

A study made by Lee and Park showed that embedded SMA wires could be used to increase the ductility and recovery rate of reinforced concrete specimens in addition to deformation detection and monitoring of concrete structures (Lee and Park, 2017). A relatively modern and novel way of using magnetic sensing capabilities with SMA in order to monitor cracks that are internal or external on a local and global based magnetic field created using a permanent magnet was done by Davis et al. 2019. The results of the experiment showed great potential for detecting internal cracks and damages on the concrete structure, yet the study requires more detailed studies in the future (Davis et al., 2019).

2.2.2.2 Magnetostrictive

The same is true for magnetostrictive sensors made of ferromagnetic materials like nickel, cobalt, iron, and their alloys. The difference in magnetostrictive is that they change their shape mechanically when a magnetic field is exerted to the sensors, and the revers will occur whenever the magnetic induction of the material changed; this will help to monitor the material through the deformation. Furthermore, an alteration on the coil or magnet geometry will also affect the waves or signals that will be used for the damage analysis. These waves have an excellent potential for long-distance monitoring but, since they are applicable to the ferromagnetic

materials, only their wave is short-range and have low ultrasonic energy due to this measurement should be taken in a near distance to the specimens or infrastructures.

The sensors can be used for detecting corrosion, debonding of steel interface from the surrounding concrete, curing of concrete, and strain measurement on cables were reviewed by Bartels et al., 1999. The study showed promising capabilities of magnetostrictive sensors in all the listed aspects. However, it also indicates that the performance of the sensors in reinforced concrete was low compared to other materials like suspension ropes (Bartels et al., 2019). Different studies have been made to monitor wire strands, especially for a suspension bridge. Khazem et al., 2001 made practical field evaluation studies on a sidewalk suspension bridge wire strands in New York. The result showed that defects could be monitored from a single location in the wire as far as a distance of 100 meters without using multiple sensors. Furthermore, the results indicated that magnetostrictive sensors could be cost-effective with a good performance to monitor strand wires (Khazem et al., 2001).

2.2.2.3 Micro-Electromechanical System (MEMS)

MEMS are miniature sensors with exceptional sizes ranging from millimeters to micrometers having components of an electrical and mechanical system. These can be used where many sensors cannot reach due to limitations of size or accessibility. The basic principle of MEMS lies in a tiny chip, which uses the standard integrated circuits technologies. MEMS have been used for decades in diverse sectors such as Automotive, military, electronics, communication, medical, aerospace, and many other industries for a different purpose. They have revolutionized most of the sectors by increasing data sensitivity and accuracy with minimum power

consumption and cost of production, including its operation. However, they have an intricate design and need different expertise to collaborate to make MEMS sensors.

Saafi and Romine.,2001 studied the feasibility of embedding MEMS sensors in terms of durability and sensitivity inside concrete structures for a SHM purpose. The studies showed that the sensors have capabilities to changes of moisture, temperature, shrinkage, stresses, or any damages inside the concrete structure with high sensitivity. However, the sensors were affected by the moist and alkaline environment from the surrounding concrete, and furthermore, the stress-bearing capacity of the sensors should be improved more in order to integrate with structural concretes, which requires high strength (Saafi and Romine, 2001). The same studies have been done by many researchers in order to evaluate the capability of MEMS as a valuable sensor, and most studies should that this technology has the potential to be the cheapest way of monitoring in the future (Ribeiro and Lameiras, 2019). However, currently, the durability, frequency variation, water resistance, alkali resistance, and external power supply sources and the wireless monitoring range should be addressed (Lynch et al., 2003; Kavitha et al., 2012; Ham et al., 2015). In addition, even if the MEMS has already revolutionized many industries, it is still at the early stage for the construction sector (Oppenheim., et al 2000). Since MEMS have the potential to SHM, further studies should be done in detail.

2.2.2.4 Fiber optics

From fiber optics, the most used are the fiber optics sensors (FOS) and fiber Bragg grating (FBG). These kinds of sensors are relatively well known compared to the others and already have applications in many areas, including the construction sector. The sensors work based on a stranded metal wire in a tube to detect any change in strain or deformation on the surrounding

area. The principle is based on incident light interference, which detects the shift of the light spectrum from the source while going across a couple of intrinsic sensors deployed throughout the length of the optical fiber due to a shift in a specific wavelength (Mahdikhani and Bayati, 2008). Fiber optic sensors are not affected by water and temperature so that they have good stability. They can be used as a temperature, crack, and corrosion indicator inside a concrete structure. In addition, the size of a typical sensor is very small, mostly in millimeters (2 to 10 mm) and also lightweight. This gives plenty of advantages to distribute it in mass and assesses the concrete structure in-depth (Uva et al., 2014; Rajabzadeh et al., 2019; Fedorov et al., 2015).

Furthermore, since they require no electric energy source for operation, this makes them very suitable for remote SHM system sensing. However, the cost of fiber optic sensors is comparatively high, and the understanding or knowledge about the sensors between experts in the construction sector is low. Leng and Asundi, 2003 used two kinds of fiber optic sensors, Fabry-Perot interferometer, and FBG, and measured real-time response of curing composite materials. From the result, both fiber optic sensors can be used to monitor the progress of curing and any damage while casting the composite material (Leng and Asundi, 2003). Another study by Lau et al., 2001 studied strain monitoring on composite-strengthened concrete structures embedded by FBG sensors, and real-time monitoring was done remotely. The results of the embedded FBG sensors in the experiment was compared to a conventional strain gauges, which were mounted on the surface. The comparison shows that the FBG sensors have a high accuracy in measuring strain and indicating any kind of microcrack or debonding (Lau et al., 2001).

2.2.2.5 Piezoelectric

Piezoelectric sensors are one of the major types of sensors that have been discovered before a century, and now it is one of the most well-known sensors for different applications such as temperature, strain, pressure, and acceleration. The measurement is taken by the change in electrical charge or voltage due to the application of mechanical force or vibration on the sensor. And the reverse is true, which is by applying a voltage to the piezoelectric sensor, the shape of the sensor will change or have a different physical form. A typical example for this kind of sensors is a silicon crystal, which can be found mostly by nature and an artificial man-made ceramic. Shen et al., 2006 used commercially available plate-like ceramic piezoelectric sensors and bonded the sensor in between two hardened cuboid-shaped cement paste in order to reduce the interface problem and give it aggregate-like shape and performance. The sensors were tested for basic performance and have shown good compatibility with the surrounding concrete and have also picked any vibrations on the concrete structure (Shen et al., 2006). Wu and chang., 2006 tried successfully to indicate a debond between the concrete and rebar. Also, the yielding of the rebar in a reinforced concrete structure was monitored using piezoelectric plate sensors and actuators together in a Pitch-catch mode (Wu and chang., 2006). A smart aggregate study for SHM using piezoelectric sensors was done by Hu et al., 2013. The study used embedded sensors to evaluate the effectiveness of crack detection in a concrete structure using a notch, hole, and three-point bending test. The result has shown the potential for piezoelectric sensors to detect cracks in a concrete structure as an SHM system (Hu et al., 2013).

2.2.2.6 Piezoresistivity

A change in resistivity of material by mechanical distress or a pure strain is called as Piezoresistivity. Currently, piezoresistive sensors are getting recognition from the research community in the construction industry because of the nano-materials capability to change the bulk cement composite properties, if nano-materials are added in a small amount during the mixing. This technique helped piezoresistive sensors to come in different materials like metal, ceramic, polymer, and composite. In this study, the composite type piezoelectric sensors are used as a piezoresistive sensor, which is a variation of electrical resistivity due to strain, by adding different types of functional fillers inside the cement composites a detailed approach will be made in the next section of this chapter.

2.2.3 Functional filler sensors

Functional fillers will change the way we understand, make, control, and design materials over the nanoscale level. Nanotechnology is one of the most advanced and contemporary time science fields with enormous potential for the construction field (Ielusz, 2014; Zhu et al, 2004). Some of the nanomaterials are graphene oxide (GO), carbon nanotube (CNT), carbon nanofiber (CNF), nano-silica (NS), iron oxide (FO), titanium oxide (TO), aluminum oxide (AO) and many others are used for different purposes to modify construction materials (Norhasri, 2017). However, the interest of the paper is on nanomaterials that can enhance or change the electrical properties of cement composites such as graphene oxide, carbon nanotube, iron oxide, and carbon nanofiber, which can act as a sensor. Of those, the study of this paper will focus on the carbon nanotube due to their superior conductivity and higher aspect ratio to act as filler inside the cement matrix and carbon fiber. These properties have been used to boost both the physical and electrical

stability of the cement composite sensors (Kim, 2014; Han, 2015; Reales et al, 2017; Azhari & Banthia, 2012).

To increase the life span of concrete SHM is getting acceptance in the research community as a way to indicate different types of defects in/on the concrete prior to colossal damage happened. There are different types of sensors develop to support the SHM in terms of how they work, some attached to the surface, embedded in the concrete, and some being self-sensing structural materials. The attached types of sensors are the usual type of non-destructive (NDE) techniques with some disadvantages like limited area coverage, complicated signal processing, and mechanical distortion due to the surrounding condition (Olivera, 2014). On the other hand, self-sensing concrete structural members are relatively a modern way of monitoring concrete, having a massive advantage to assess on a large area. However, doing so would require a large amount of functional fillers (Han, 2015). With the current technology, most of the functional fillers are expensive to use in large amounts, especially carbon-based fillers. To ease these, using embedded types of sensors can give a reduction in the cost without affecting the mix design of the original concrete, unlike the self-sensing concretes.

Table. 2.1 shows the economic perspective of different carbon-based functional fillers with the amount required to achieve a higher conductivity (Lee et al, 2019). To understand the full picture, it would be necessary to compare the total volume needed for functional fillers to achieve the specific level of conductivity regarding the cost. It is possible to achieve higher conductivity with a minimal amount of CNT compared to other types of carbon fillers because of their nanoparticle size effect, which can avoid the electrical conductivity blocking effect of cement particles by ultimately reducing the cost. Currently, the research community is trying to develop

different types of embedded sensors from various kinds of carbon functional fillers to make the sensors smaller enough to be distributed in large areas without any major defect.

Carbon-based functional fillers inside cement composite sensors have great potentials for the future SHM system. Since they are made from some of the basic ingredients of concrete itself with the addition of functional fillers this makes their production process extremely simple and reduces the cost the sensor in general compared to the sophisticated sensors that are currently available in the market. Moreover, due to their very nature, they are easily compatible with the surrounding concrete. Furthermore, unlike most sensors, rather than having a single or fewer goal to achieve, the carbon-based functional fillers could be able to monitor different conditions like carbonation, crack, chloride penetration, and moisture condition of their surrounding concrete, since the sensors are also cement-based materials.

Table 2-1 Summary of characteristics and cost of cement composites incorporated with carbon materials

Characteristics and cost	Conventional macro/micro materials	Nanomaterials (CNMs)
Required dosage (wt.% by cement) ^{a)}	<ul style="list-style-type: none"> - Graphite powder (10-100 μm): 30~50 % (Cao and Chung, 2003; Chung, 2004). - Graphite chip (100-2,000 μm): 40~100% (Cao and Chung, 2003; Chung, 2004) - Coke particle (1~3 mm): 70~120% (Son, 2010) - Carbon fibers: 1~10% (Wei et al., 2012; Laukaitis et al., 2012; Wei et al., 2018) 	<ul style="list-style-type: none"> - Multiwalled Carbon nanotube (MWNT): 0.6-1.2 % (Li et al., 2007; Han et al., 2012; Kim et al., 2014a) - Graphene: 0.5-1.5 % (Jin et al., 2017) - Graphite nanoplatelets: 2~5 % (Le et al., 2014)
Cost of carbon materials for required dosage ^{b)}	<ul style="list-style-type: none"> - graphite powder: 0.25-0.4 USD/kg of cement - Carbon fiber 0.4-4.0 USD/kg of cement 	<ul style="list-style-type: none"> - MWNT: 0.6-1.2 USD/kg of cement
Pressure sensing capacity (Piezoresistive sensitivity)	<ul style="list-style-type: none"> - Carbon fiber: Low (electrical resistance change range by external service load: less than 2 %) (Chung, 2002; Chung, 2012)). 	<ul style="list-style-type: none"> - CNT case: High (resistance change range by external service load: 5-20 %) (Jianlin et al., 2017; Han et al., 2012; Kim et al., 2014a)
Mechanical strength of composite with required dosage	<ul style="list-style-type: none"> - Powder type: decrease up to 40~60 % (Cao and Chung, 2003; Chung, 2004) - Fiber type: Less changed (Wei et al., 2012; Laukaitis et al., 2012; Azhari and Banthia, 2017; Wei et al., 2018) 	<ul style="list-style-type: none"> - (Less than 1 %) Less changed or increased some cases (Konsta-Gdoutos et al., 2010; Parveen et al., 2013; Pan et al., 2015; Kim et al., 2014b) - (Higher than 1%) Decreased (Pan et al., 2015; Kim et al., 2014b)

^{a)} Required dosages to achieve the electrical resistance of the composites lower than $10^3 \Omega \cdot \text{cm}$

^{b)} Approximate costs in the local market (South Korea) – graphite powder: 0.8 USD/kg; carbon fiber: 40 USD/kg; multiwalled CNT 100 USD/kg (<https://korean.alibaba.com>, referred at 2018.06.12)

2.4 Previous works on crack, chloride and carbonation-literature review

2.4.1 Crack sensing

Crack by itself is an indication of internal distress. Monitoring and detection of this internal distress in structural objects is crucial and also has multiple benefits beyond the reduction of maintenance cost and protecting the crack from widening. Sensors like strain gauges, Tiltmeter, Fiber Bragg grating (FBG), and LVDT can provide information about the crack only in a limited area and mostly surface conditions. A crack, especially on the surface of a structure, can introduce external hazardous substances such as chloride, carbonation, and moisture that can affect the concrete reinforcement in general and put the whole structure in danger. For many reasons current SHM system on cracking is getting lots of attention for sensors based on cement composite.

To detect the damage of a civil structure, Mohammed saffi, 2009 developed an in situ wireless and embedded CNT/cement composite sensor. By measuring the change in the electrical resistance of the composite sensor by applying a monotonic and cyclic tensile loading, while monitoring the initiation and progress of the crack in the study. The electrical resistance response of the embedded CNT/cement composite sensor for the deflection created by the tensile cyclic load showed good sensitivity, excellent repeatability, and low hysteresis (Saffi, 2009). A similar experiment using cyclic loading was done by Azhari and Banthia., 2012 while in this case, the loading being axial compression and the materials used as a sensor being hybrid CNT and CFs cement composite. Sensor response for both the cyclic and monotonic strain due to the compressive stress was good enough to identify the microcracks by the steady rise in resistivity

and the failure was identified by the unexpected and steep rise in resistivity (Azhari and Banthia., 2012).

Furthermore, the above studies were confirmed by Konsta-Gdoutos and Aza., 2014. The study showed the capability of nanocomposites reinforced by CNT and CNF to be piezoresistive using strain sensing under compressive cyclic loading (Konsta-Gdoutos and Aza., 2014). Mosavinejad et al., 2018 conducted a study on high-performance carbon fiber reinforced cement composite (HPCFRCC). The study on the piezoresistivity properties indicates that a higher percentage of CFs needs, which is about 0.6% by weight of cement. In addition, using the four-point bending technique a thin HPCFRCC specimen plate containing 0.8% CFs was cracked while measuring the resistivity simultaneously. Based on the study finding, it was possible to detect and monitor the cracks. However, for specimens containing a low amount of CFs the electrical resistance change was insignificant and highly variable (Mosavinejad et al., 2018).

Lim et al., 2015, conducted a relatively direct study on crack sensing, and the research has systematically studied the feasibility of CNT/cement composite as a crack sensor. The study was mainly based on the electrical conductivity of the CNT/cement composite in relation to the crack width and moisture content. The experimental study was done after cracking the specimens and compressing them in a perpendicular direction to that of the crack path. The specimens, CNT/cement composite, and mortar embedded CNT/cement composite were compressed in stages while the crack gap was measured along with the conductivity and profiling were done. From the result, it was concluded that the composite sensor could detect the crack closure even though it cannot fully recover the initial conductivity. The Authors suggested that by increasing

the conductivity, dimensional stability, and by monitoring in real-time, the feasibility of the sensor can even get better (Lim et al., 2015).

Naeem et al., 2017 studied experimentally the flexural stress sensing capability of CNT/cement composite embedded in a reinforced mortar beam and the effect of its location inside the mortar beam. The study has confirmed that the stress and crack sensing under a flexural load is possible, and with the increase in CNT content, the sensing capability was enhanced up to 0.6% by weight of cement. The collapse of the reinforced mortar was identified by the sudden change in the resistance value, and the study also pointed out that the location of the sensor has no effect on identifying the specimen failure (Naeem et al., 2017).

In recent years, advanced and more in-depth researches are being done towards the self-sensing ability of cementitious composites. Al-Mufadi and Sherif., 2018, tried to investigate the crack initiation and a way to identify the cracks. In the study, they tried to use the temporal slope of the normalized electrical resistance derivative with respect to time. By doing so, the effect of polarization can be minimized since the slope of the polarization is much smaller than the cement composite electrical resistance change. This can easily help to identify and monitor the crack (Al-Mufadi and Sherif, 2018).

Siad et al., 2018 have studied enhancing the self-sensing capability of engineered cementitious composites (ECC) not only for the crack sensing ability but also on precracked specimens healing properties on different moisture condition and curing time making it a pioneer study. The study used different amounts of CNT and CFs to investigate each material individually. The result showed that the CFs have a lowering effect on the deflection and an increase in stiffness,

on the other hand, the CNT has no or negligible impact on the deflection and stiffness of ECC. After the initial crack of ECC specimens with CNT, an increase in the number of cracks and a decrease in the width of crack were seen, and the opposite was true, for ECC specimens with CFs. In general, it was possible to improve the sensitivity of ECC by increasing the conductivity and recovering of the specimens through self-healing. However, after healing the ECC specimens with CFs could not recover their sensing ability, unlike the specimens with CNT (Siad et al., 2018).

CNT and CFs sensors or hybrid sensors of both materials have been shown in the above literature. Even though the research is growing, but it is far from being accurate to detect, locate, and tell the depth or width of the crack in both micro and macro level cracks. Some of the difficulties that should be addressed are the mechanical strength of the sensors itself, the effect of the electrodes, the effect of polarization during measurement, the self-healing capability study of the sensors and the high cost for the production is becoming an obstacle for the sensors to be real and commercialized. However, the progress in overcoming these problems is ongoing. For example, some researchers are focusing on changing the structural material itself to a conductive and self-sensing material without the need for an additional embedded sensor. This is referred to as Intrinsic self-sensing concrete (ISSC). However, this requires large amounts of functional fillers to be dispersed in the concrete, in this case, CNT and CFs, which would make it expensive. Furthermore, the addition of aggregate in the concrete has a blocking effect on the conductivity (Han, 2015).

The other drawback of developing a sensor is the polarization effect. The simplest way to avoid this effect is to use AC rather than a DC resistance measurement (McCarter, 1995; Konsa-

gdoutos., 2014; Cho 2004). However, this is not economical, accessible, and portable for easy use. On the other hand, almufadi and sherif, 2018 had used a mathematical way to eliminate the polarization before crack and used the increase of the polarization effect after once the crack occurred due to the capacitance properties developed by the micro cracks insulated by water or air in between. This will give a chance to systematically monitor the cracks inside the composite using the polarization effect as a parameter (almufadi and sherif, 2018). Chacko., 2007 study suggests a high volume of conductive fibers with low water to cement ratio can bypass the capacitance and induction effects by acting as a pure resistor (Chacko., 2007).

Another major drawback of developing sensors is that there is little research on the self-healing properties of the sensors. As of known concrete cannot be hydrated fully even after many years, and the hydration products of the cement will change their form in time. This quality of concrete will sometimes help the concrete to heal after a crack. However, the properties of most sensors after a crack heals are not fully understood (Siad et al., 2018). Table. 2.2 shows the major review points in the literature review described in a convenient way for comparison and a better understanding.

2.4.2 Chloride and carbonation Sensing

Chloride and carbonation have their effect on corroding the reinforcement bars of concrete, and both prefer higher moisture conditions for in-depth penetration. However, carbonation needs carbon dioxide for its reaction to being initiated, and chloride penetration requires oxygen for the oxidation reaction to take place in the reinforcement. Both have a devastating effect on today's structural objects, where construction in the coastal area has increased, and the carbon emission of cities is getting worse every year.

If care were given to protect the concrete structures, the durability and service life of the structures would be longer. For that, the available sensors currently are not good enough in predicting and monitoring on a real-time base. Most of the sensors require a timely fashioned inspection, a professional to investigate. Furthermore, the test is mostly a destructive type of testing, especially to know the depth of the penetration, which makes this area still challenging for the research community until today to get a sensor that can pick the defects at an early age (Taheri, 2019). Some of the sensors types used are fiber optic, FBG, half-cell, rebar probes, acoustic emission, embedded electrodes, and may others (Taheri, 2019).

A study made by Chacko, et al., 2007 using CFs as functional filler studied the effect of chloride content on the resistivity of carbon fiber reinforced cement paste (CFRC) as ISSC material. Water with and without chloride was used to prepare two different samples. From the result, the specimens without chloride showed an increase in resistivity in 28 days both for longer and shorter specimens, each by 52% and 26%, respectively. However, samples with chloride have shown a slight or negligible change in resistivity compared to the other specimens, which can be used as an indication for chloride ingress.

Azhari and banthia., 2010 used different proportions of CFs to assess chloride ingress. Specimens fabricated with and without CFs were immersed in chloride solution for one month. The resistivity value before and after one month showed a reduction in resistivity, including a slight change in the control samples. Besides, to avoid the effect of the moisture, another resistivity measurement was done. The specimens were fully desiccated and dried to get a precise result on the chloride ingress (Azhari and banthia., 2010). Hoheneder et al., 2014 also faced the same challenge to separate the effect of moisture from chloride ingress while comparing

reference FRC and FRC mixed with 0.2% CNF by volume. For that, the identical specimens prepared and immersed in a water and chloride solution for 24 hours before measuring the conductivity response for each while applying four-point bending. Both samples subject to water and chloride showed almost the same electro-mechanical response. However, a change was observed between the water and chloride exposed specimens on their slope after differential conductivity was done, showing the capability to identify chlorides. Furthermore, the authors have suggested further studies to develop the method fully (Hoheneder et al., 2014).

Kim et al., 2015 have made a detailed feasibility study on real-time chloride ingress monitoring in reinforced concrete structures using embedded CNT cement composite. In addition, the amount of chloride ingress inside the composite was estimated through regression analysis based on the electrical characteristics. In the study, different amount of NaCl solution and CNT was used to run experimental investigations. Based on the results, the conductivity of CNT has increased as the chloride content increased, indicating chloride ingress, especially in the case of moist specimens since it increases chloride ion movement through the pores. By drying, the specimen loses some amount of their conductivity due to less ion movement while being capable of monitoring. However, as the CNT amount increases in the composite, the effect of chloride will be low due to the CNT cement composite higher conductivity over the chloride ions. Note that despite the monitoring capability, there was a higher fluctuation of data even between the identical specimen types. Some of the chloride content estimation formulas derived based on regression showed the corresponding R^2 values to be lower than 0.6 due to the conductivity fluctuations. However, by combining different amounts of CNT composites together, the accuracy of the estimation improved profoundly (Kim et al., 2015).

Table 2-2 Literature review on self-sensing properties of cement composite sensors based on functional fillers

Citation	Functional fillers	Cement Composite type and resistivity	Research target	Methodology	Result	Detection mechanism
Mohammed saffi, 2009	CNT (1%)	Paste 150-200 Ω -cm	Crack monitoring	monotonic and cyclic tensile loading	0.5% swnt content failed to pick crack propagation whereas 1% shows good sensitivity until failure.	Change in resistivity
Azhari and Banthia., 2012	CFs alone and Hybrid CNT and CFs	Paste 371 Ω -cm	Piezoresistive sensing	Cyclic loading with axial compression	Hybrid sensors Provide quality signal, improved reliability and increased sensitivity than CFs sensors.	Change in resistivity
Mosavinejad et al., 2018	CFs (0.2% to 0.8%)	High performance cement composite 62 - 5 K Ω -cm	Crack monitoring	four-point bending technique	Meaningful variations where observed for higher CFs content in the matrix. low CFs content show higher fluctuation	Change in resistivity and current
Lim et al., 2015	CNT (0.3% & 0.6%)	Paste 1.8-250 k Ω -cm	feasibility study as a crack sensor	Crack closing using compression force while measuring crack width and resistivity	Higher Recovery rate was obtained for higher initial conductivity composite (0.6% CNT). Moisture effect was high due to low conductivity.	Change in resistivity
Naeem et al., 2017	CNT (0.6%)	Paste 650 Ω -cm	Effect of sensors geometry (relative position) inside RC mortar beam	Crack sensing under a flexural load	Dramatic and steep changes in resistivity was shown regardless of the sensor location in the mortar	Change in resistivity
Siad et al., 2018	CNT (0.5% & 1%) & CFs (0.25% & 0.5%) (tested individually)	Engineered cementitious composites (ECC) 0.560 to 36 K Ω -cm	Pre-cracked specimens healing properties	Curing cracked samples under different moisture condition	Both ECC specimens (CNT and CFs) showed crack recovery by self-healing but CFs specimens showed low self-sensing after healing unlike CNT specimens.	Change in resistivity
Chacko, et al., 2007	CFs (5%)	Carbon-fiber reinforced cement paste 33 to 69 Ω -cm	Study the influence of chloride infiltration	Two samples were mixed with and without NaCl and resistivity taken for 28 days	Samples with NaCl showed lower resistivity compared to the equivalent samples without NaCl.	Change in resistivity
Azhari and banthia., 2010	CFs (0%, 3.5%, 7% & 15%)	Paste (1,400 to 10000 Ω -cm)	Chloride monitoring	Samples were immersed in 10% NaCl solution for 1 month	Monitoring was possible to due to the decrease in the resistivity but requires further study	Change in resistivity
Kim et al., 2015	CNT (0%, 0.3% & 0.6%)	Paste (1.5 to 250 k Ω -cm)	feasibility study as a chloride sensor	Mixing samples with different NaCl concentrations and estimating Chloride content were based on resistivity	NaCl content not only shown by the decrease in resistivity but also the amount of chloride was estimated, even though, there is a fluctuation.	Change in resistivity

Chapter 3. Unwanted electrical fluctuation of CNT/cement composite using CNT as a sole agent: Pilot experiment[†]

3.1 Introduction

This chapter is a preliminary study to investigate and shed light on the limitations of the CNT/cement composite for further studies. To do that, four different scenarios were considered: case 1) were conducted by direct mixing of sodium chloride together with the CNT/cement composite, case 2) is immersing the CNT/cement composites inside sodium chloride solution rather than mix together like case one, which is because of the different effects occurred by following both approaches, case 3) use the accelerated carbonation effect to study on the CNT/cement composites, and case 4) was conducted by embedding the CNT/cement composite inside reinforced concrete.

3.2 Materials and methods

3.2.1 Materials and mix proportion (orange)

Type I Portland cement satisfying the specifications of ASTM C 150 and natural sand with specific gravity, water absorption, and fineness modulus of 2.64, 3.2 %, and 2.83, respectively, were used. Multi-walled CNTs were purchased from a South Korean firm Hanwha Nanotech with a product name HANOS MWCNT CM-130 having a diameter and length ranges of 12-18nm and 15-25 μm , respectively. The CNT has a purity of around 90 %, and its production was done by an improved virtue method in the synthetic process following a catalytic CVD process.

[†] This chapter has been published "Lee, H. K., Nam, I. W., Tafesse, M., & Kim, H. K. (2019). Fluctuation of electrical properties of carbon-based nanomaterials/cement composites: Case studies and parametric modeling. *Cement and Concrete Composites*, 102, 55-70."

Silica fume a byproduct in the production of silicon metal and ferrosilicon alloys were applied in the mix for mechanical dispersion of CNT by using it as a mineral admixture due to their small size range (13,000-30000 m²/kg), which is 1/ 100th of an average single cement grain. Silica fume (EMS-970D, Elkem Inc.) satisfying ASTM C 1240 was utilized in the cement matrix. In addition, a high range water reducer, polycarboxylic acid-based, superplasticizer was used to help the dispersion of cement, silica fume, and CNTs in the mix.

A case by case study is done for the pilot experiment the water to cement ratio (w/c) and the CNT ratio for each condition is shown in table 3.1 including mixture type, curing condition, type of electrode, and measurement condition. Silica fume was used in all the mixtures, 10% by weight of cement was added. In addition, the weight ratio of sand and cement was 1:1 for mortar mixtures. Furthermore, the dosage of superplasticizer was 1% by the weight of cement. The NaCl content and carbonation ratios used in each case is described for each case in table 3.1. Note that the mix proportions used in this study are almost similar to the previous studies made by Kim., 2015 except that the natural sand is added in mortar samples. In addition, further information on the mix design, mix procedure, and desperation techniques of CNT can be found in previous studies (Kim, 2015; Kim et al., 2016b; Lim et al., 2017). In addition, some CNT cement composite specimens were embedded inside a reinforced mortar, which has a weight proportion of water, cement, and sand ratio of 0.5: 1: 2.5, respectively.

Table 3-1 Summary of mix proportion and experimental procedure

Study	Mixture level	Mix-ratio subject to change			Curing condition	Electrode used	Measurement of resistance
Case 1	Paste (Kim, 2015)	W/C 0.3	CNT	NaCl (%)	Sealed curing for 5 days from mixing, and water curing after then	-stainless steel platelets	- At 28 days from mixing (saturated) - After 7 days of air-drying from then (partially dried)
			0	0, 0.5, 1, 1.5, 2 & 2.5			
			0.3				
	Mortar	0.3	0	0, 0.5, 1, 1.5, 2 & 2.5	Sealed curing for 3 days from mixing, and water curing after then	-stainless steel -silver paste	- At 28 days from mixing (saturated) - At each air-drying cycles (×5 cycles) - After oven-drying (110°C for 1 day)
			0.3				
			0.6				
Case 2	Paste	W/C		CNT (%)	Sealed curing for 28 days. After that immersed in a 10% NaCl solution for two years	-stainless steel -polymer	-At 28 days from mixing (saturated) -once every month (SSD)
		0.3		0.6			
		0.5					
	Mortar	0.35	0, 0.3 & 0.6		Sealed curing for 28 days. After that immersed in a 5% NaCl solution for 1 year	-stainless steel	-At 28 days from mixing (SSD) -every month once (SSD) -After vacuum drying (50°C for 1 day)
Case 3	Paste	W/C		CNT (%)	Water curing for 28 days. After were placed in a carbonation chamber with 10% CO2, 50% humidity, and 20°C temperature for 120 days	-stainless steel -polymer	-At 28 days from mixing (SSD) - Measurement was taken at 1, 2, 28, 56, 84 and 120 days
		0.3		0.6			
		0.5					
Case 4	Mortar (embedde d in a reinforced mortar)	W/C		CNT (%)	Water curing for 28 days. The specimens were placed in 3 d/f types of locations from the bar.	-stainless steel	-before pouring -after pouring -after oven-drying and cooling for a day inside the reinforced mortar.
		0.3		0.6			

3.2.2 Experimental methodology

3.2.2.1 CNT/cement mortar composite mixed with NaCl (Case 1)

A 10-litter capacity Hobert type automatic mixer was used for mixing. After beaching all the solid ingredients, including the CNT and NaCl powder, dry mixing was conducted for 5 minutes, and then by adding the liquid ingredients, water, and superplasticizers, respectively additional 10 more minutes were mixed. Note that the mixing procedure and time is typical for all cases in this section. The specimens were casted using a $2 \times 2 \times 8$ cm mold and $1.5 \times 1.5 \times 0.1$ cm stainless steel platelets were used as an electrode. The electrodes were embedded sidewise along the edges using a two-point method (Kim, 2015). After casting, the samples were kept at a temperature of 20 °C and relative humidity of 50% chamber. Both times, during the first 3 days where the specimens are sealed by cellophane and after the removal of the plastic wrap and immersion of the specimens inside the water until 28 days.

After 28 days of curing, the samples resistances were measured using a simple digital multimeter (SK-104, Samkwang Inc., South Korea) designated to measure the direct current (DC) of the samples. Measurement was first taken immediately after taking out the samples from the water after 28 days of curing in order to evaluate the moisture condition at a saturated condition. To understand the relation between the resistivity and moisture condition the samples were subjected to a step by step drying cycle for five times. A cycle contains a one-day air drying of the samples inside the curing chamber followed by two-day sealing of the specimen using cellophane inside the chamber. Two-day sealing is adopted in order to avoid resistivity fluctuation due to a moisture difference inside the specimen by depth. This will help to unify the moisture distribution of the samples after each air-drying cycle. After five cycles of drying, the

samples were vacuum-dried under the condition of a temperature of 50 °C and a pressure of 6×10^{-5} atm.

In addition, to evaluate the stainless-steel electrodes reliability after drying the specimens in vacuum chamber, the electrodes were removed from the edges of the specimens by cutting with a high-tech diamond saw having less disturbance less than 2 mm of both edges were removed. The Cutted-surface of the specimens were painted by a highly conductive silver paste having a resistivity lower than $10^{-2} \Omega \cdot m$ was brushed on both sides, and resistance measurement was taken. The reason is that by drying the specimen, dry shrinkage might occur, and this can have an effect on the interface of the electrode and the CNT/cement composite leading to debonding and leads to a fluctuated result of the measured data.

Case 1 was conducted as one part for applying the CNT/cement composite as a chloride sensor in reinforced concrete structures, where the chloride penetration may yield corrosion of reinforcement steel bars. The electrical resistance of chloride solution, i.e., seawater, generally has a range of electrical resistivity of 10^{-2} - $10^2 \Omega \cdot m$ depending on the concentration of ions, which is lower comparing that the resistivity of the CNT/cement composite is 10^3 - $10^6 \Omega \cdot m$ (Rhoades, 1996; Kim, 2015). Since the resistivity of ordinary water is 10^3 - $10^8 \Omega \cdot m$, the resistivity of the composite seldom influenced by moisture contents in the matrix but was likely to be changed by chloride concentration (Rhoades, 1996). In our previous research results (Kim, 2015), NaCl powder was mixed with the fresh CNT/cement paste mixture. By increasing NaCl contents up to 5 wt.%/cement, i.e., 3.034 wt.%/cement of chloride ion, the resistivity of CNT/cement paste composites at 28 days was drop down up to $1/10^3$ - $1/10^2$ of control mixture without NaCl. This result was consistent with the study of Jin et al. (2017) that resistivity decreases of

graphene/cement paste composite by chloride contents. It was confirmed that the resistivity was decreased up to about 1/6 times when the chloride ion increased to 3 wt.%/cement in the cement paste containing 2 wt.%/cement of graphene (Jin et al., 2017).

Lim et al., 2017 studied the effects of embedding CNT/cement composite inside a reinforced mortar lead to a high resistivity and loss of conductivity due to the cracks that occurred by dry shrinkage (Lim et al., 2017). In order to improve the dimensional stability in this study, the use of fine aggregate is evaluated. In general, the goal of this study is to assess the reliability of using a mortar type CNT/cement composite to improve the dimensional stability and overall sensing ability of the composite.

3.2.2.2 CNT/cement composite immersed in chloride solution (Case 2)

The mixing procedure used in the above section is typical, which is similar to all the sections in this chapter. After mixing the paste type mixtures, the specimens were casted using a $2 \times 2 \times 8$ cm prism mold, and electrodes were embedded, this time 50 mm apart from each other while keeping the center of the specimens. Two types of electrodes were used in this study a thin copper plate coated with a silver paste of 1.5×3 cm dimension and a conductive epoxy, which is a non-corrosable electrode. The conductive epoxy having a resistivity of about 8 Ohm·m was made by mixing the conductive epoxy with 5% CNT to the total weight and to make sure the blending was uniform a two steps ultra-sonication processes was used: bath-type sonicator for 30 min followed by tip-type sonication for an hour. For the mortar mixtures, a stainless-steel electrode was embedded at the edges of the specimens having the same dimension with the paste mixtures.

After mixing, the specimens were kept in the mold for three days until all the specimens were hardened. After hardening, all the samples were kept inside a distilled water for 28 days. Completing the 28 days curing the paste composite samples were immersed in chloride solution with NaCl 10 wt.%, and the weight ratio of the specimen to chloride solution was fixed at 1.65. Measurements of resistance were done once every month for two years. For measuring the direct current, the same test equipment was used as of case 1. Note that the NaCl solutions were the specimens were immersed is not changed throughout the two years. However, for the mortar type specimen, the measurement was taken for a year while changing the 5% NaCl solution once a month while taking the measurement as well. The measurement was done twice: immediately after taking out of the NaCl solution and after drying the samples in a vacuum chamber at 50 °C for one day. This is done in order to evaluate the effect of moisture contents inside chloride-penetrated CNT/ cement specimens. In addition, to avoid chloride binding in the cement matrix, vacuum-drying was adopted to minimize the effect of hydration acceleration by oven-drying, unlike the vacuum.

The difference between case 1 and case 2 is that the NaCl was directly mixed inside the mix for case 1 and in this case (case 2) the specimens were immersed in a chloride solution. This is done to simulate the chloride diffuses into the cement matrix in actual environments, unlike direct mixing. The direct mixing introduces the sodium chloride into the cement mix, which is different from the situation of chloride attack on concrete structures in real conditions. And in order to apply electrical charges through specimens to drive the chloride ions in the concrete have their limitations for CNT/cement composite specimens. Methods like NT BUILD 492, or ASTM C1202 use electric charge; however, specimens having functional fillers could generate high

heat (Kim et al., 2016a). The heat could have a binding effect chloride ion on the chloride ion to the cement by increasing the degree of hydration during the test time. For this reason, the application of electrical charges through the specimens is complicated. In the next chapter of this dissertation, a detailed study will be made by a custom-made rapid chloride migration test.

3.2.2.3 Accelerated carbonation of CNT/cement composites (Case 3)

The paste-type mixtures were prepared for this experiment having $2 \times 2 \times 8$ cm prism with a silver paste coated copper, and conductive CNT/epoxy plates were used as electrodes. After casting, the specimens were immersed inside water for 28 days for curing than to carbonate the samples 200 litter-capacity carbonation chamber was used. The accelerated carbonation is done in a controlled environment where all the 6-faces of the specimens are exposed inside the chamber for 4 months at 10 % of CO_2 , 50 % of relative humidity (RH), and 20 °C of temperature. Since this study is a primary work to evaluate the effect of carbonation of the CNT/cement composite, the carbonation profile, pH, or ion concentration of pore solution of the samples is not evaluated in depth. The carbonation depth of cement composites with water to cement ratio of 0.5 and 10 % of silica fume, exposed in 3-10 % of CO_2 for 100 days, was about 3-10 mm, which measured by 1 % of phenolphthalein solution, and the composite with w/c of 0.3 and same silica fume content was almost zero (Papadakis, 2000; Sulapha et al., 2003). Note that, to measure the resistance of the samples the same instrument was used as the above sections.

It is a common problem for a reinforced concrete structure to be susceptible to corrosion by the carbonation effect. This is due to the carbon dioxide from the air penetrate the concrete surface by decreasing the pH of the surrounding alkali environment surrounding the rebars or in short by lowering the passivation properties of the concrete the rebars will be subjected to corrosion. The main goal of this section is to understand the effect of accelerated carbonation on the electrical properties of a CNT/cement composite. It is expected that the calcium hydroxide, which is electrolyte dissolved in the pore solution of the cement, reacts with the carbon dioxide and precipitates in the form of calcium carbonate. This leads to a decrease in electrolytes concentration in the pore solutions, which decreases the conductivity.

Furthermore, the formation of a crystal calcium carbonate might block the CNT network connectivity as well having the same decreasing effect. Based on this principle, the CNT/cement can be used as a sensor for carbonation following the change in the resistivity of the CNT/cement composite. To avoid any experimental error due to parallel results from a different problem, such as crack, moisture, or chloride, is necessary by quantitatively analyzing the results. However, for this study, accelerated carbonation is used in a controlled environment to avoid any kind of meddling.

3.2.2.4 CNT/cement composites embedded in a reinforced mortar (Case 4)

The same type of specimens, $1.5 \times 1.5 \times 8$ cm prism CNT/ cement composite samples was used after curing for 28 days for this section. Measurement was done with the same instruments described in case 1. Stainless steel plates were used as electrodes, and an electric wire was welded on the surface of each electrode. Note that the initial resistivity measurement of all the CNT/cement composites was taken. After curing, the CNT/cement specimens were placed in 3

different places inside a 15 cm cubic mold, as shown in Figure 3.1, including D10 rebar satisfying the ASTM A615 standard. The bar and the CNT/cement specimens were separated by a plastic-thin plate spacer to keep it in place while pouring the mortar. A conventional mortar, 0.5: 1: 2.5 ratio, was used to mix the water, cement, and sand, respectively, by weight ratio. Three types of geometries were prepared: Type 1 was the case where the CNT sensor was exposed only on one side of the mortar surface; Type 2 was the case where all sides of the composite are faced to the mortar, and Type 3 was the case where the composite is placed on the corner of the mortar. As shown in figure 3.1, rebar and composite were located with 1, 2, 3, and 4 cm of distances. After casting, all the specimens were cured by immersing inside water for 28 days for the mortar to get full strength. Then the second resistivity measurement was taken after 28 days of curing the mortars using the embedded wire, and the final measurement was taken after drying the samples inside an oven chamber at 100 ° C and cooling it in the air for one day.

The experiment in the present section was carried out to evaluate the effect of rebars on the electrical resistance of the CNM/cement composite when both the rebars and the composite were embedded in the concrete. Similar studies have been done in the Kim (2015) and Lim et al. (2017) that the paste-type CNT/cement composites were embedded in the mortar with rebar having fixed distance, and their resistances were not affected by the existence of rebars. In the present section, the rebars and the mortar-type CNT/cement composites were embedded parallelly in the mortars having various positions with different distances, and the resistance of the composites was measured.

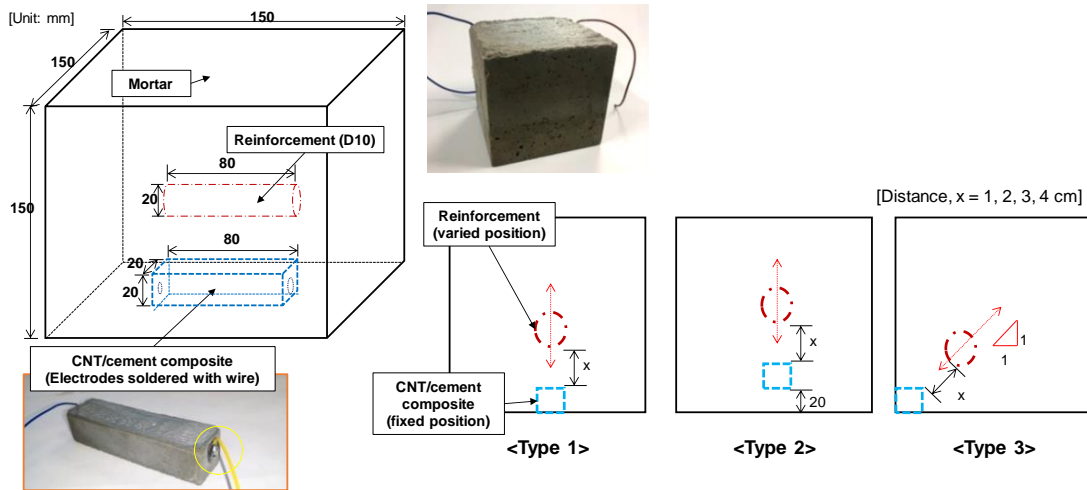


Figure 3-1 Schematic illustration of reinforced mortar embedded with the CNT/cement composite

3.3 Results and discussion

3.3.1 CNT/cement mortar composite mixed with NaCl

Figure 3.2 shows the resistance of the prism samples after 28 days curing, which was saturated, surface dried condition. It should be mentioned that, since this study dealt with some cases of the fluctuation of electrical properties and was not for establishing accurate guidelines of their properties, the results of resistance of bulk samples were not converted to the specific conductivity or resistivity. As mentioned above, in relevant previous studies (Kim, 2015; Jin et al. 2017), the resistivity of the paste composites with CNTs or graphene showed a very clear decrease with an increase in chloride content. However, in the case of mortar composite in the present section, such changes could not be found. The coefficients of determination, R^2 results, for CNT 0.6% and 0.3% mixtures obtained from regression analysis were very low about 0.4 and 0.01, respectively, which indicated that the influence of chloride contents on the resistance of composites was negligible.

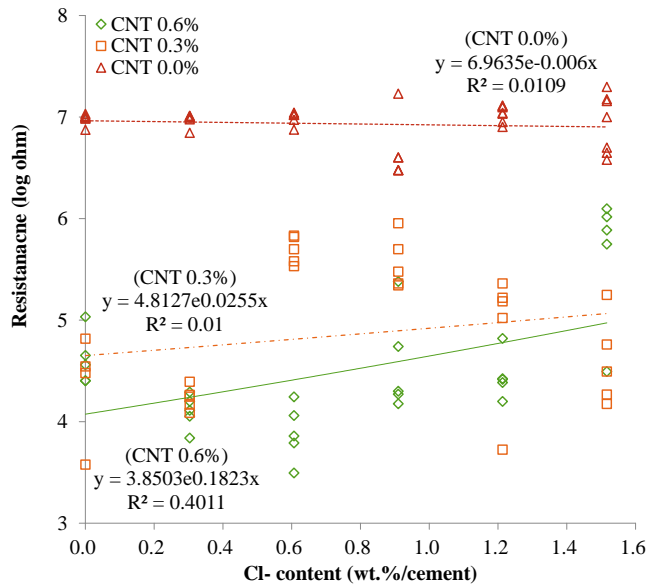


Figure 3-2 Resistance of CNT/cement mortar composites mixed with various chloride contents: before drying

Figure 3.3 is a series of graphs showing changes in electrical resistance of the cement composites by drying cycles. Figure 3.4 represents the degree of saturation, i.e., the ratio of remained water weight of dried samples at each step to the initial water weight of saturated samples. Although the moisture in the samples was dried step by step, as shown in Figure 3.4, the overall changes of resistance of the samples were insignificant, within the range of less than 50%, for all types of mixtures. It should be mentioned that, except for the case of the samples having very low resistivity, such as 0.6% of CNT, the previous studies reported that the resistance of the paste composites with low resistivity, i.e., 0% and 0.3% of CNT, was increased within ranges of 10^1 - 10^2 times by drying (Kim et al., 2014a; Wei et al., 2017). Due to the introduction of fine aggregates, which act as nonconductive macro-fillers, the volumes of capillary pores formed in cement paste matrix were water may be retained was reduced and thus the effect of moisture

contents on the resistance of mortar composite was considered to be decreased compared with the case of the paste composites.

However, the result which should be focused in this study was that some irregular fluctuations of resistances in Figure 3.3. Although the minimum values of resistances of the CNT 0.6% samples with NaCl 0% was quite constant, about $10^{3.5} \Omega \cdot \text{cm}$, regardless of drying states, some of the fluctuations for this mixture was found in the resistance range of 10^4 - $10^6 \Omega \cdot \text{cm}$ depending on the drying step. A similar phenomenon occurred even in the cases of other CNT and NaCl contents. It is worth mentioning that the samples for each mixture were fabricated with the identical procedure, including mixing time, compacting method, and curing process. These fluctuations will decrease the reliability of this cement composite sensor with CNMs.

Moreover, measured values of resistances of the cement composites were also strongly influenced by electrode types. Figure 3.5 presents resistances of the composite after vacuum-drying measured with embedded metal electrodes and those with silver paste after removing the metal electrodes. Note that both the metal plate and silver paste used as electrodes had much lower conductivity than the CNT/cement mortar composite, i.e., about $1/10^6$ times so that the measured values of resistance of the composite should seldom be affected by the type of electrode. However, as shown in Figure 3.5, the resistances measured with a metal electrode was, in actual, higher about 10^1 - 10^2 times compared with those measured with brushed silver paste. This gap was relatively large range compared to the resistance change by NaCl contents (Figure 3.4).

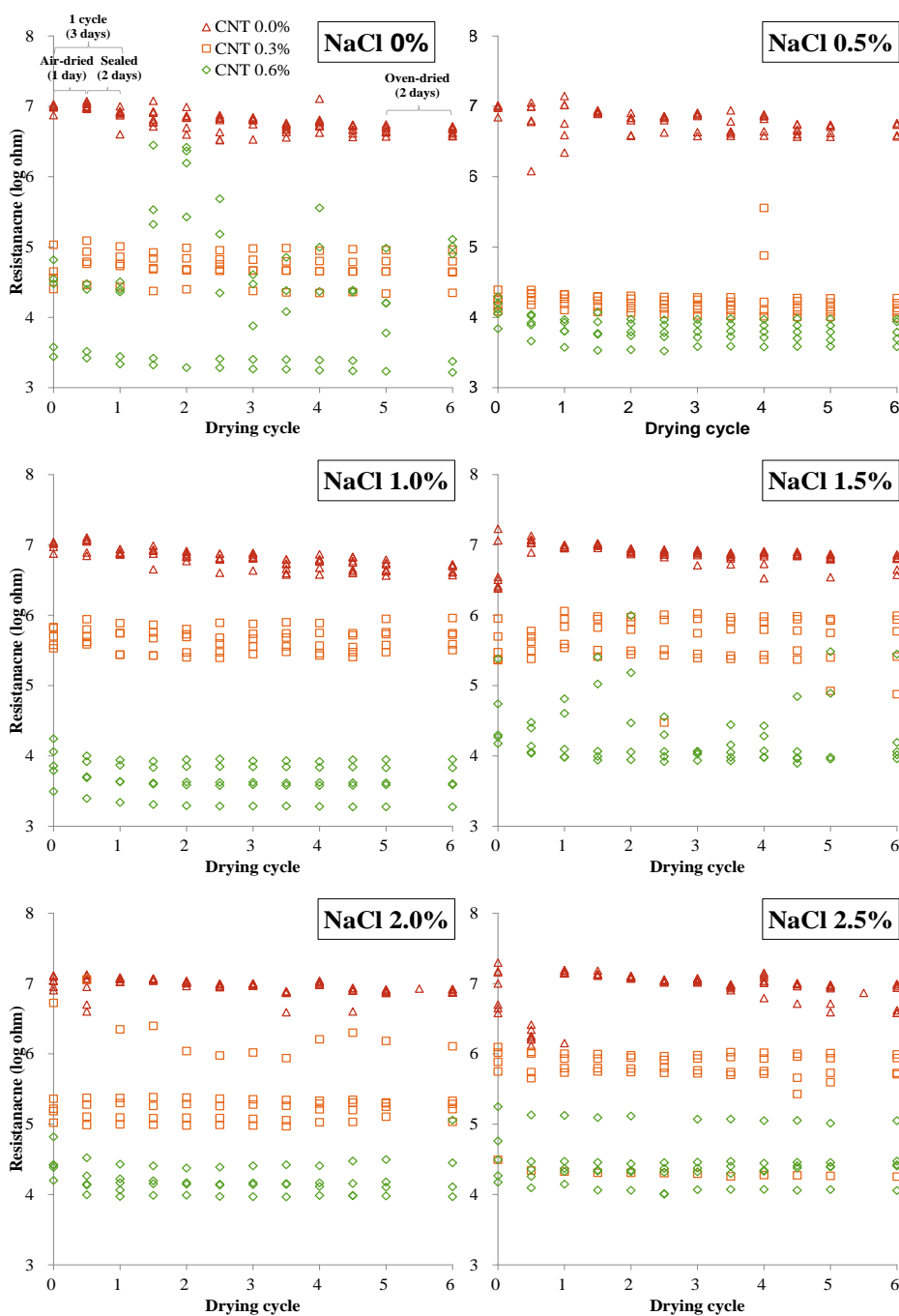


Figure 3-3 Change of resistance of CNT/cement mortar composites mixed with different chloride contents by drying cycles (1 cycle: 1 day of air-drying and 2 days of sealing)

In summary, the results of the experiments performed in this section indicate that the addition of chloride ions to the CNT/cement composite was expected to decrease in electrical resistance, but it was not clearly shown in mortar type samples. Moreover, although the drying of the composite samples without any restrained physical condition seldom influenced the resistance, the effect of electrode types on the resistance of the composites was significant compared to the effect of chloride contents.

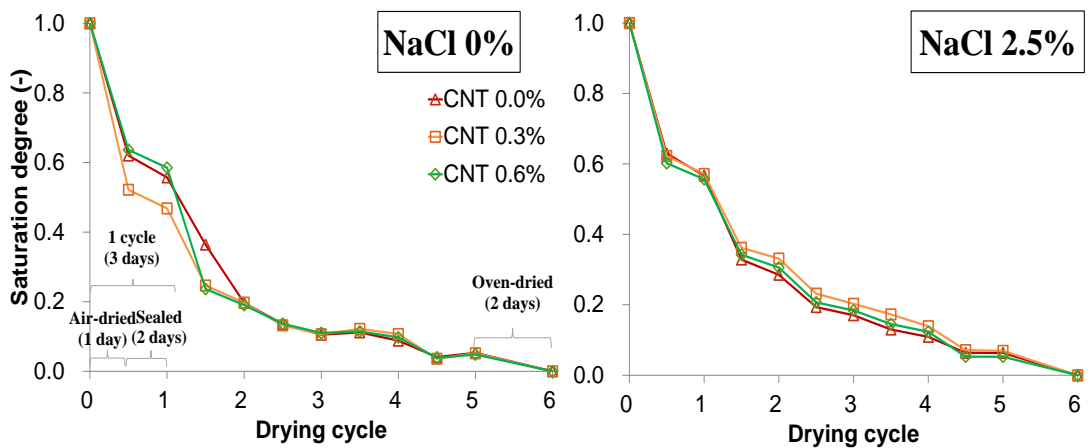


Figure 3-4 Saturation degree of CNT/cement mortar composites mixed with different chloride contents by drying cycles

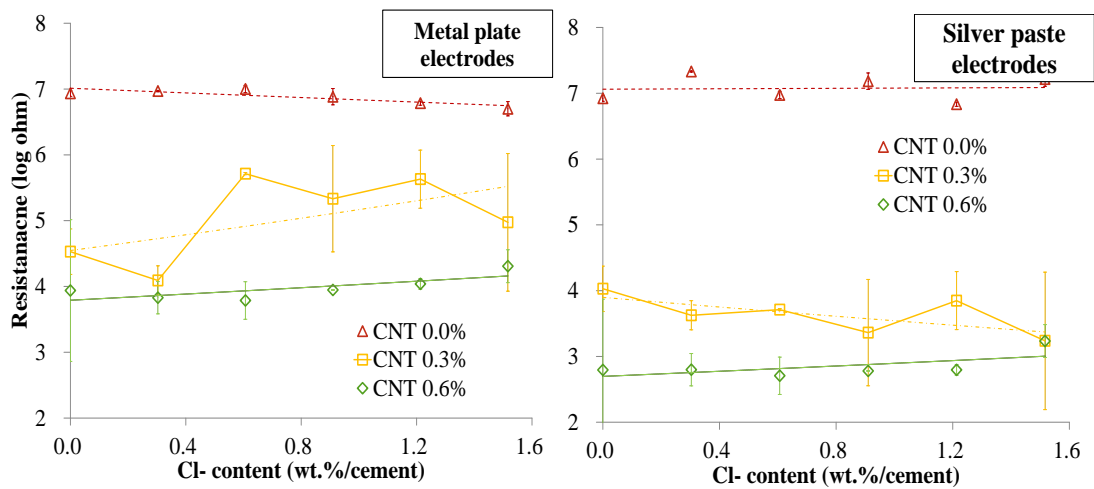


Figure 3-5 Resistances of CNT/cement mortar composites mixed with various chloride contents after completely dried (measured with different electrode types)

3.3.2 CNT/cement composite immersed in chloride solution

Figure 3.6 shows the resistance change of the CNT/cement paste specimens immersed in NaCl 10 wt.% solution for two years, while Figure 3.7 presents the resistance of mortar specimens stored under 5 wt.% NaCl and seawater for one year. The error bars in figures 3.6 and 3.7 represent the standard deviations of the 6-8 numbers of samples, and the trend lines drawn here are based on the exponential function calculated by nonlinear regression.

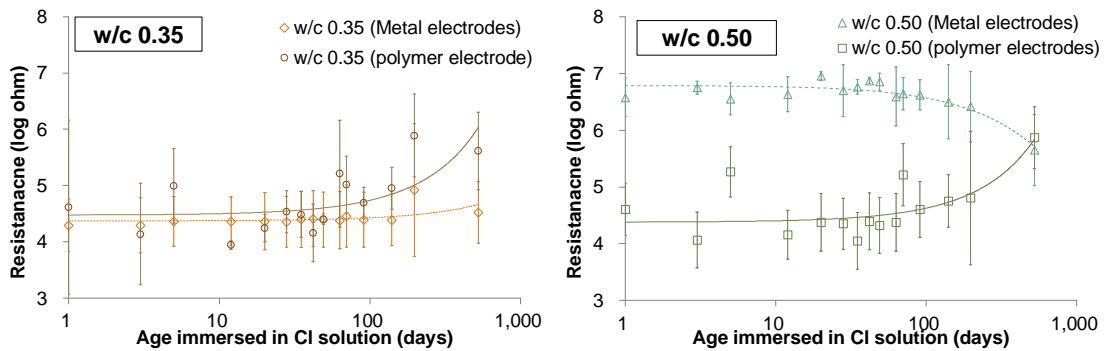


Figure 3-6 Changes of resistance of paste composites with CNT 0.6 % immersed in chloride solution (measured with different electrode types)

In general, measured values of the resistances of the composites were increased by immersing time except for the case of the paste samples of w/c 0.50 with metal electrodes. The range of increase in resistance was about 10^1 times in the case of paste composites for two years, while for mortar composites, the range was $10^{1.5}$ - $10^{2.5}$ times for one year. It also can be seen that there were always fluctuations in the range of $\pm 10^1 \Omega$. Only for the case of paste samples with w/c 0.50, the electric resistance value measured by metal electrodes was exceptionally decreased from $10^{6.5} \Omega$ to $10^{6.0} \Omega$ for two years of immersion in chloride solution. However, in the case of the resistance of the paste samples measured with non-corrosable conductive polymer electrode (Figure 3.6), it was confirmed that the increase ranges in resistance with time was identical regardless of w/c, i.e., from $10^{4.3} \Omega$ to $10^{5.6} \Omega$. In addition, as shown in Figure 3.7, the resistance changes with moisture contents were negligible in the mortar composites, as that resistance gap between saturated and dried samples were within the range of $\pm 10^{0.5} \Omega$. In summary, the electrical resistance of CNT/cement composites immersed in chloride solution in actual

increased, unlike the expectation that the resistance would decrease due to the increase in chloride contents in the pore solution of the cement matrix.

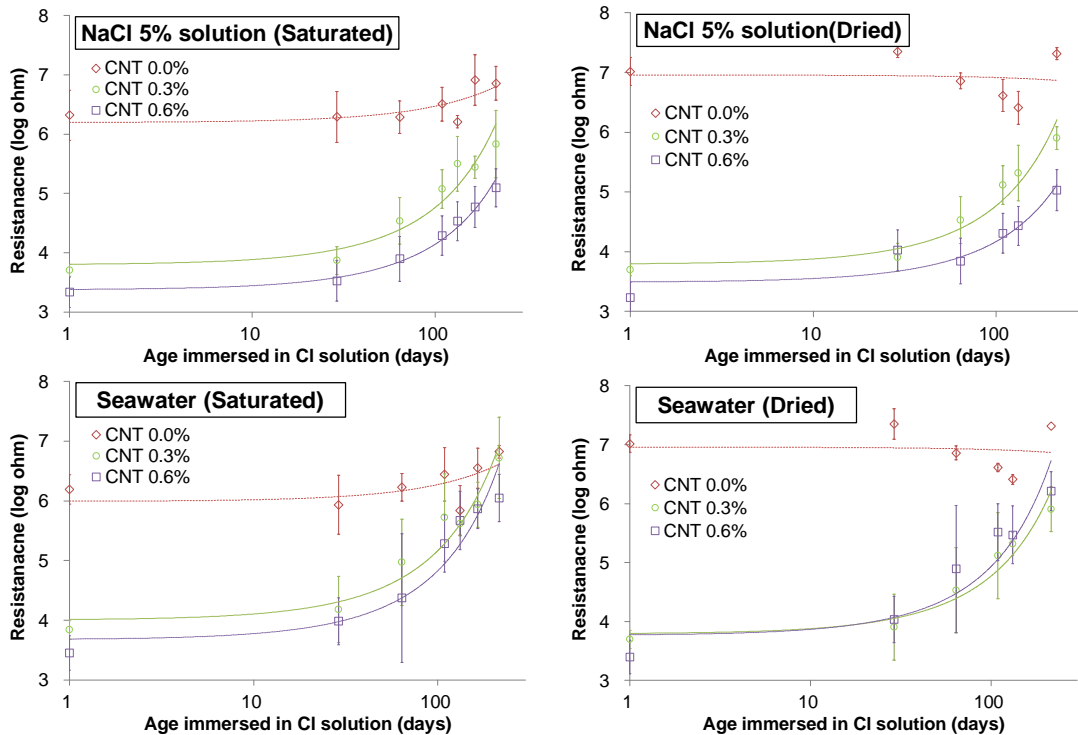


Figure 3-7 Changes of resistance of mortar composites with different CNT contents immersed in chloride solution

3.3.3 Accelerated carbonation of CNT/cement composites

Figure 3.8 shows the change in resistance of CNT/cement paste composites during carbonation over 120 days. The electrical resistance by the carbonation was increased as expected, but the variation range was significant. It should be mentioned that this experiment was conducted twice for the same experiment to confirm the results. Although the same mix proportion was used, the resistances of samples for the first and second tests were varied about 10^1 times. Even that, the resistances of the samples were found to be increased with the range of 10^2 - 10^3 times, regardless of w/c and type of electrode.

If the electrical flow in the samples was just through the physical connection of CNT networks, this large increase in resistance would not have occurred. Moreover, considering general results of carbonation depths of cement composites with silica fume in previous studies having similar mix proportion with this study (Papadakis, 2000; Sulapha et al., 2003), the carbonated area might be concentrated on the surface in the case of w/c of 0.3, while, the carbonation was progressed throughout the cross-section of the samples in the case of w/c 0.5. Nevertheless, as shown in Figure 3.8, the fact that the range of increase in resistance did not depend on w/c.

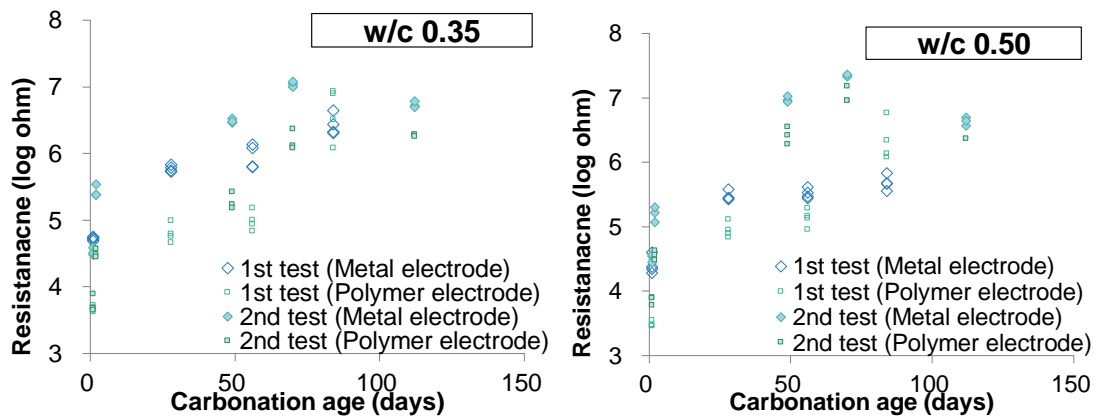


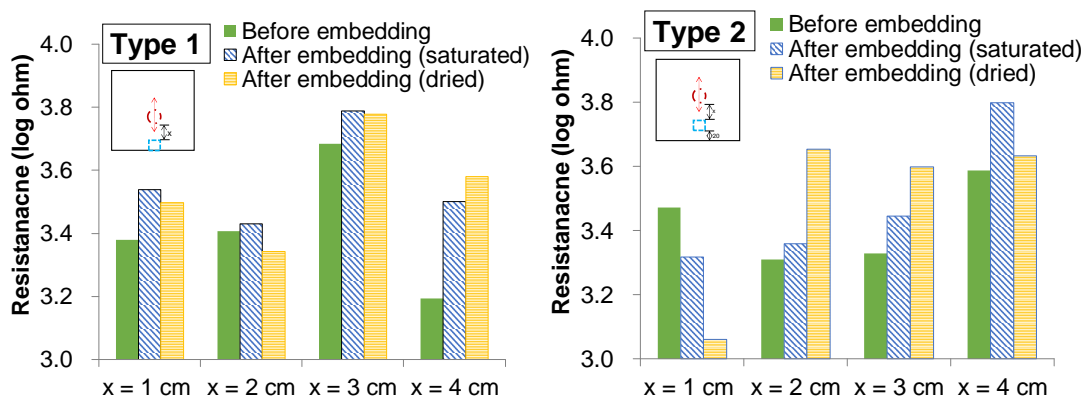
Figure 3-8 Changes of resistance of CNT 0.6 % paste composites by carbonation (measured with different electrode types)

3.3.4 CNT/cement composites embedded in reinforced mortar

Figure 3.9 presents the resistances of the CNT/cement composite measured before and after embedding in the reinforced mortar. As can be seen from the range of the y-axis, most measurement results of resistances were within a range of $10^{3.0}$ - $10^{4.0} \Omega$, and this deviation was considered as very narrow compared with the changes in resistance in other experimental series in above sections. This indicated that the mortar type CNT/cement composites used in the present section have higher dimensional stability so that, even after oven-drying, the composites

did not lose their conductivity. It is worth mentioning that in the previous study (Lim et al., 2017), the CNT/cement paste composite embedded in the reinforced mortar loosen their conductivity after air-drying.

The difference of initial electrical conductivity of each composite before embedding (green bars in Figure 3.9) could be negligible because it can be considered as the deviation of the composites themselves. An interesting finding from the figure was that the gradual change in the resistance by steps of before and after embedding, and after drying was also very small. Comparing with those before embedding, the resistances of the composites for most cases increased by slightly, about $10^{0.1}$ - $10^{0.2} \Omega$ after embedding, and this difference can be negligible, regardless of the distance between rebar and the composite. These results indicate that the surrounding mortar between rebars and the composite sensors, which has a much higher resistance than the composite about 10^4 - 10^6 times, was insulated the composite so that the electrical resistance of the composite was seldom fluctuated by the presence of the rebars. On the other hand, in the cases of $x=1$ cm in Type 2 and $x=4$ cm in Type 3 specimens, an exceptional slight decrease in the resistances after embedding was found.



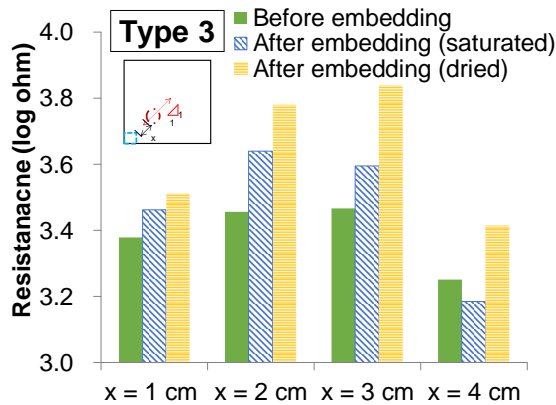


Figure 3-9 Resistance of CNT/cement composites (CNT 0.6%) embedded in a mortar beam: before and after embedding.

3.6 Discussion: On electrical properties fluctuation causes

Dispersion of CNMs in cement matrix

A phenomenon of non-uniform dispersion of CNMs has been observed in the present study as well as in other scientific reports, and especially the CNTs among various CNMs were reported to be hard to disperse uniformly in cement matrix due to their high aspect ratio and strong van der Waals force (Han et al., 2011; Kim et al, 2016; Jang et al., 2017; García-Macías et al., 2017). In an ideal case, the composite with an identical mix proportion and mixing procedure should have an identical range of resistance. However, as shown in the results of Figure. 3.3, 3.4, and 3.8, it was not for some cases which already mentioned above. Moreover, the resistance of the composite should decrease steadily as the concentration of chloride ions increases. However, in the results of experimental series 1, it was confirmed that the resistance of CNT/cement mortar composite were fluctuated even when mixed dosage of NaCl was increased. This means that there is a possibility that the electrical properties of the cement composites were strongly influenced by the CNT dispersion itself rather than the concentration of chloride ions.

In our previous paper (Kim et al., 2014d), it was reported that, even when the same amount of CNT was added, the electrical conductivity of cement composite can be increased from 10^1 to 10^2 times by incorporation of the silica fume, which helped mechanical dispersion of CNTs. Note that the improved dispersion of CNTs by silica fume in the study was evaluated via SEM images. In Kim (2015), CNT/cement paste composite incorporating the silica fume for mechanical dispersion was prepared, and in some cases, it was found that the conductivity does not increase or even decrease accordance with some ranges of increase in the CNT content. A similar phenomenon was also shown in Figure 10 of D'Alessandro et al. (2016) that considerable decreases in the conductivity of the CNT/cement mortar (about 10 times Level) were found for some ranges of increase in the CNT content. Note that, in the study, the CNT was dispersed using the sonication process.

If the dispersion is good, the probability of physical/electrical connection of the CNM network is greatly increased, and the conductivity of the composite with them thus should be increased (Jang et al., 2017). However, even if CNM/cement composites are fabricated under the same condition and process, it is still hard to control their electric properties as identical in actual.

In addition, limited numbers of studies on the difference in dispersion according to the type of CNM in cement composites have been reported, and conclusions on this cannot be reached yet.

Cracking of hardened cement matrix

One of the factors affecting the electrical properties of CNM/cement composites is the cracking of cement matrix. Microcracking developed by various causes, such as drying, fatigue, and creep, leads to a partial disconnection of the conductive CNM network. This microcracking have a seldom influence on the bulk resistance of the composites when these cracks were dried.

However, when the microcracks were saturated with pore solution having high conductivity, the bulk resistance became decreased.

Moreover, some case of increases in resistance under the conditions of drying was found in Experimental series 1 and 3, and this is considered to be due to that the microcracks were propagated by drying so grew to ‘macrocraks’. A clear example of resistance increase by the ‘macrocracking’ was shown in the study of Lim et al. (2016). The CNT/cement paste composite was embedded in the reinforced mortar and then dried. After the oven-drying, the conductivity of the embedded composites was completely lost. Although macrocracks were not directly found visually in the study, the possibility of macrocracks can be fully estimated by considering the general knowledge of the cement technology, including shrinkage.

Paste-type cement composite had relatively larger drying shrinkage compared with surrounding mortar due to lack of sand, which is a dimension-stable material. As the paste composites were embedded in the mortar, the surrounding mortar or concrete were physically acting as a fixed boundary condition for the composite, and thus microcracking in the paste composites became propagate and grow by the restrained stress, as described in figure 3.10. On the other hand, the mortar-type CNT/cement composite in Experimental series 4 in this study has lower shrinkage about 1/6-1/2 compared with paste composite, which was measured in the previous study (Tafesse and Kim 2016), and thus it has a low potential of microcracking (Hawreen et al., 2018). As shown in figure 3.9, the CNT/cement mortar composites embedded in reinforced mortar did not lose their conductivity even after drying.

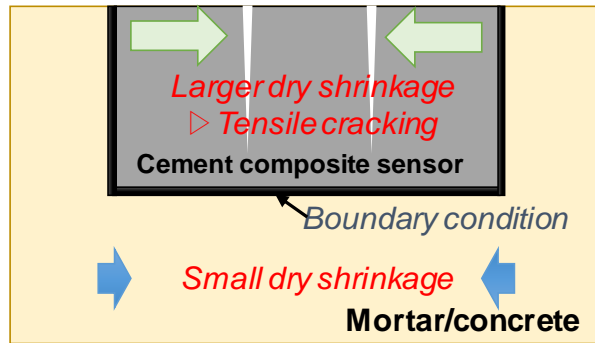


Figure 3-10 A schematic illustration of generation mechanism of macrocrack in cement composite sensor embedded in concrete or mortar.

Growth of hydration products between CNMs: tunnel blockage

The network of CNM dispersed in the cement matrix has three types of mechanisms of electrical flow. First is direct conduction due to physical contact between the CNMs, and this is not disturbed by other external factors, except lose of conductivity of CNMs themselves. The second is electron flow through ions in the pore solution of the cement matrix. This is influenced by the internal moisture content and will be explained in the following sections. The third is caused by the tunneling effect (Li et al., 2006).

As well known, the governing equation for the tunneling effect between two conductive particles, such as CNMs under the ideal condition, is as follows (Simmons, 1963).

$$R_T = \frac{h^2 d_{eff}}{A_{eff} e^2 \sqrt{2m\lambda}} \exp\left(-\frac{4\pi d_{eff} \sqrt{2m\lambda}}{h}\right)$$

(11)

where e the quantum of electricity, m the mass of electron, h the Planck's constant, d_{eff} the effective distance between conductive particles, λ the electrical height of the barrier, and A_{eff} the effective cross-sectional area of tunnel (Simmons, 1963)

Since most of the geometrical parameters in the equation have stochastic values in the cement matrix, numerical modeling considering the tunneling effect have been adopted fitting parameters obtained by try-and-error process (García-Macías et al., 2017a; García-Macías et al., 2017b). Even that, this equation represent the tendency that the resistance of CNT networks increases by an increase in distance between CNMs and decrease in values of tunneling area. When the hydration of cement and other hydraulic powders are progressed, the hydration products including calcium silicate hydrates having nano-sized particles became filled between CNMs (Kim et al., 2014b) and these may block the tunneling pathway (see Figure 3.11). This can be called the 'tunnel blockage effect'.

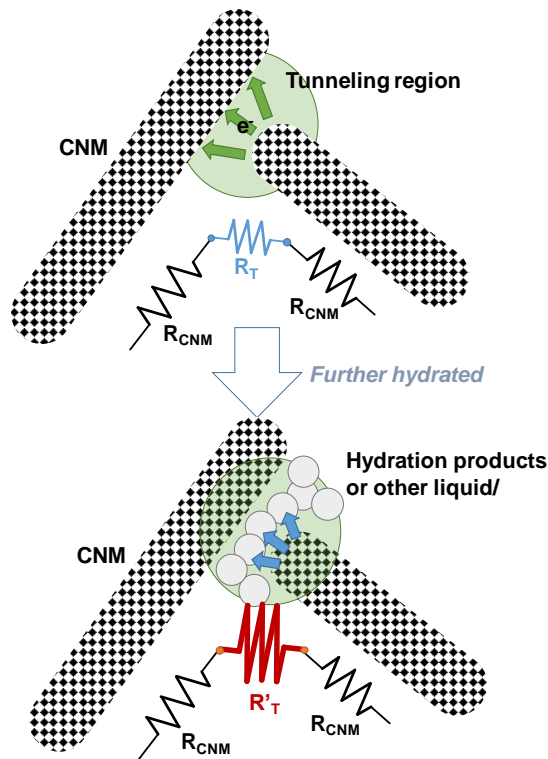


Figure 3-11 A schematic illustration of blocking of tunneling region by hydration products

The results of the Experimental series 2 and 3 in above are considered as evidence of this phenomenon. As shown in figure 3.6 and 3.7, the resistances of the CNT/cement composites were increased by increases in immersing period in the chloride solution. It is common knowledge in cement chemistry that the degree of hydration is increased by water curing periods, resulting the denser microstructure of cement matrix. Moreover, the friedel's salt $[3\text{CaO} \cdot \text{Al}_2\text{O}_3 \cdot \text{CaCl}_2 \cdot 10 \text{H}_2\text{O}]$, which is a crystalline phase of cement binding chloride ion, was nucleated in cement matrix due to chloride penetration, which may help denser microstructure (Yuan et al., 2009).

In the present study, CNTs are physically intermixed with the silica fume particles having similar size with the CNTs. In figure 4 in Kim et al. (2014), it was presented that silica fume particles were distributed between the CNTs in cement matrix. Thus, the silica fume between CNTs reacts with cement over time and it interferes with the electron tunneling between the CNTs. When carbonation proceeded as in the Experimental series 3, calcium carbonate crystals became filled in the existing pores of cement matrix, which can also prevent tunneling. From this reason, it was shown in figure 3.8 that the increase in resistance was up to 10^3 - 10^4 times as the carbonation and drying proceeded simultaneously.

In addition, there is a potential that that results of the experiment series 2 and 3, i.e., resistance increase of CNM/cement composite by immersing period, was induced from change of electrical properties of the CNMs themselves. It was hard to find on date the effect of strong basic condition in cement matrix, i.e., pH range of 13-14, on the carbon-to-carbon bonds of CNMs, which may influence their conductivity. This should be studied in future study.

Debonding of electrodes

Type and shape electrodes for the conductive cement composites has already been discussed in Han et al., (2007), and it was confirmed that when the mesh-type electrodes were used, the measured resistance was reduced by about 10 %, and the deviation of the results was reduced to about one third compared with plate-type electrodes. It was supposed to be due to the larger contact area of mesh than plates. Similarly, in the Experimental series 1-3 in this study, it was able to confirm the effect of the electrodes on the measured resistances. In the figure 3.5, the resistances measured via metal plate electrode embedded in the samples was higher approximately 10 times than those with perfectly attached silver paste. In figure 3.6, for the case

of samples with w/c 0.5 embedding metal plate electrodes, much higher resistances was considered to be due to debonding of electrodes from the beginning of the test. The initial resistance measured in this case was higher about 10^2 times than that with polymer electrodes and also time-dependent change in resistance showed different tendency.

In addition, mesh-type metal electrodes was not used in this study. Mesh-shaped electrodes having larger contact area than the plate possesses lower potential of debonding with cement matrix. In the case of plate, the debonding can easily grow because of its propagation direction is along with interface, while in the case of the mesh, the geometry of interface is more complicated. Even that, the metal mesh may also be corroded with time. Therefore, it was recommended to use carbon fiber mesh or conductive polymer mesh for cement composites considering long-term reliability of measurement results.

Interfacial void around composite sensors embedded in concrete/mortar

Although the CNM/cement composites themselves has no problem, but there is a possibility that the resistance of the composite may reduced owing to the surrounding voids in the composite-concrete interface. The resistances of the composites embedded in concrete structures can be significantly affected even when the area of the void is only 2 % of the cross section of the composite. In actual construction field, these types of voids can be frequently generated between rebars by imperfect compaction and this was more easily developed when the distance of between the rebars was narrower. Therefore, if the CNM/cement composite sensors are first installed with rebars and the concrete is then poured over them, the interface voids may developed. Moreover, if the fresh CNM/cement composites were installed to existence concrete

structures in any methods and forms, it is also hard to completely avoid these interfacial voids or gap.

It was difficult to find other papers reported on this phenomenon. Most of the test with conductive cement composites has been carried out in lab scale or test bed (Han et al., 2011; Naeem et al., 2017), and the fabrication of samples or specimens were carefully conducted to eliminate this void. However, as mentioned in the Experimental series 4 above, the case of resistance reduction with insignificant range was detected and the interfacial void was found. Although it cannot not be make the conclusion that the resistance reduction of the case of Figure 3.9 (samples of Type 2 and $x = 1\text{cm}$) was definitely induced by the interfacial void because of those the reduction range was within the acceptable deviation and the length of the void could not be measured, this supposition can be one possibility.

Moisture content, polarization and ion flow in the cement composites

Basically, hardened cement matrix contains connective pore networks between hydration products, which called as capillary pores. As mentioned above, even though the cracks induced by drying shrinkage do not occur, the volume of solid and liquid portions in cement matrix became reduced due to the phase transformation during hydration (Jennings et al., 2008). By the hydration, the water is changed to solid hydrates with cement, resulting the decrease in absolute volume of solid and liquid, while the volume of bulk hardened matrix was seldom changed (Powers, 1968). Thus, pore was generated by this and the water can be transfer through this. The electric properties of cement composites is strongly influenced by moisture content in the pore networks, as the pore solution contains high concentration of ions (Polder et al., 2000; Wei et al., 2017).

The CNT/cement composites used in this study showed insignificant changes in resistance by the moisture contents due to their low resistivity. For example, in the Experimental series 1, the resistance of the mortar composites under saturated condition was only 20-30 % smaller than that of the dried samples (Figure 3.3). Note that the resistances of samples exposed to accelerated carbonation and dry condition (the Experimental series 3) were increased about 10^3 for 120 days and this is more likely to be due to the tunnel blockage by carbonation, not by drying, considering the results of Experimental series 1. However, previous studies have shown that the electrical properties, including resistance and piezoresistivity (pressure sensitivity), of CNM/cement composites with high resistivity can be greatly influenced by amount of pore solution, i.e., moisture contents. For example, in Song and Choi (2017), it was found that the resistivity of CNT/cement composite was vary from $5 \times 10^3 \Omega \cdot m$ to $80 \times 10^3 \text{ ohm m}$ depending on the moisture contents. It was due to that the composites in the study have much higher resistivity compared with that in the present work ($1\text{-}3 \times 10 \Omega \cdot m$ for CNT 0.6 % mortar composite in Experimental series 1, 2, and 4). In the numerical approach of Jang et al. (2017), the effect of the moisture contents on the resistance of CNT/cement composites was evaluated, and the computational results on this effect was agreed with the experimental results.

The internal moisture affects not only to the change of resistance of the composite, but also to the polarization and ion flow. In Li et al., 2008, a conductive cement composite containing 120 nm carbon black was prepared for deformation sensing. The measured values of resistance of the composite were not only influenced by water content, but also changed by the measurement time. The increases in resistance and reduced piezoresistive sensitivity according to the curing time shown in the study are thought to be caused by tunnel blockage. However, it was stated

that, when the composites was under electrical charging by DC for a period, the resistance measured was fluctuated due to dielectric polarization. It was considered that ion flow by DC charging occurred through the pore solution networks at the same time, even though this was not mentioned in the manuscript. Note that the polarization is a phenomenon in which dipole moments are generated in molecules and atoms without ions diffusion, while the ion flow differs slightly from the polarization that the cation and anions in the pore solution are diffused. Even that, both phenomena are correlated with the fluctuation of electrical properties by the DC charging.

In Kim et al. (2014) and Kim (2015), it was found that the effects of moisture contents, polarization, and ion flow can be negligibly reduced when maximizing conductivity, i.e., minimizing resistivity, of the cement composite. The conductivity of the CNT/cement composites was maximized to the range of 10^1 - 10^2 mS/m (resistivity of 10^1 - 10^2 $\Omega \cdot m$), which brought the change of electric conductivity and piezoresistive sensitivity by DC charging less than 10 %. This range was negligible considering that the resistances of the composites with same mix proportion was varied about 10 times or more for each sample.

The effects on polarization and ion flow can be ignored when using alternating current (AC) rather than DC. In Jin et al. (2017), the graphene/cement composite was attempted to be used as a chloride sensor, and the conductivities of the composites mixed with various chloride contents was measured using the AC. Although the measurement equipments for AC resistance are generally much more expensive than the equipments for DC resistance, it is necessary to use AC in order to increase the reliability of sensor for the practical application.

3.7 Conclusions

A detailed investigation has been done on previous works and in the present study. In this study, different experiments have been conducted to assess the possible causes of CNT/cement composite sensors to fluctuate. The series of experiments carried out are mixing and immersing of CNT/cement composites with NaCl particles and chloride solution, respectively, to evaluate the chloride sensors. Accelerated carbonation tests for CNT/cement composites were designed to assess the carbonation effects. In addition, the effect of the rebar on the electrical behavior of the CNT/cement composite embedded in a mortar specimen was also investigated. Considering the experiments carried out including previous studies the causes for the fluctuation of electrical properties of CNM/cement composite sensor for the concrete structures can be summarized as follows:

- Dispersion of CNMs: ununiformed dispersion of CNM in a cement matrix could influence the electrical properties of the composite.
- Cracking: microcracking might lead to a partial disconnection CNM network affecting the electrical properties of CNM/cement composites and this will be worsen on paste composite.
- Growth of hydration products: By the increase of cement hydration in time the hydration products could be filled between CNMs (tunnel blockage effect) creating fluctuations.
- Debonding of electrodes: based on the electrode type debonding can grow between the interface of the composite and electrode affecting measurement results.

- Interfacial void around composite sensor embedded in concrete or mortar specimens can induce the possibility for resistance fluctuation.
- Moisture contents in cement composite (also correlated with polarization and ion flow) have a strong influence on the electrical properties of CNMs composites.

The fluctuation by these causes should be controlled in order to increase the reliability of the sensor, and thus future studies will be conducted to consider this.

In addition, the electrical properties of CNM/cement composite sensors may be changed by the damage of the sensor itself, which induced by freezing and thawing, acid, and other chemical attacks from outside or ASR. However, when the cement composite sensors are damaged, the same problem also should occur in the surrounding concrete. By measuring the change of the electrical properties of the composites in this case, the damage of the surrounding concrete can be monitored, which means that the composites work as the sensors.

Chapter 4. Reliability of CNT-CFs hybrid cement composite on dimensional stability and electrical stress-strain sensing capability

4.1 Introduction

In light of the literature review, this study follows a different approach to investigate the reliability of the CNT-CFs hybrid cement composite sensor. Unlike most researches, to improve the dimensional stability, mortar specimens are used in this study, as indicated in chapter 3. Furthermore, to enhance the steadiness of the conductivity in terms of response time and dimensional stability, CFs were introduced in this study.

To prove the reliability of the sensors slender shrinkage samples were prepared and put through a stress-strain cycle using drying and wetting. This done at 50°C in a vacuum chamber to desiccate any moisture for drying and wetting was done by immersing the samples in water at room temperature.

4.2 Materials and methods

4.2.1 Materials and mix proportions

In this study, two types of functional fillers were used for the experiment. Multiwalled carbon nanotube and pitch-based carbon fiber manufactured by Hyosung Inc and GS Caltex Co, respectively, were used in the experiment. Detail properties of the functional fillers are shown in table 4.1. Further information on the CNT and carbon fiber can be found in Tafesse et al., 2019, and Park et al., 2018, respectively (Tafesse et al., 2019; Park et al., 2018).

Raman spectroscopy was taken to evaluate the presence and purity of the CNT and the effect of alkalinity on the CNT, as shown in figure 4.1. A JASCO NRS-5100 Micro-Raman spectrometer

with 532 nm laser (JASCO, Tokyo, Japan) ($\lambda_{exc} = 532 \text{ nm}$) was used to conduct the experiment. The CNTs showed peaks at the D, G, and 2D bands around 1347, 1575, and 2922, respectively, including the derivative G' band (Boncel and Koziol, 2014). While comparing the ID/IG ratio, which indicates the purity as the D band decreases. The D band indicates the presence of defects in the CNT (Kim et al., 2018). From the result, both CNT samples, pure one, and NaOH treated, showed a higher degree of crystallinity having lower defects with a ratio of 0.85 for both cases. This also indicates the higher conductivity capability of the CNT and also has no effect on the NaOH treated CNT as well (Skakalova et al., 2005). Note that the CNT was treated by NaOH in order to simulate the high alkaline nature of the surrounding composite and to understand its effect on the purity and conductivity.

In addition, to check if there are no functional groups attached to the CNT, an FT-IR were taken using FT-IR/NIR spectrometer (Frontier™, PerkinElmer Inc.). Based on the analysis shown in figure 4.2 there was no functional groups attached to the CNT, except for the weak bonds around 2000 cm^{-1} (Nguyen, 2015). Besides, the superplasticizer used in this experiment was also were analyzed. However, the SP itself contained polycarboxylate ethers, which exhibit multiple peaks at 2920, 1460, 1340, 1240, 1080, and 940 cm^{-1} . The first three peaks correspond to C-H stretching in SP, and the peak at 940 cm^{-1} corresponds to C-H stretching in an alkene base; the remaining peaks indicate C-O stretching vibrations (Chen et al., 2018; Qian et al., 2017; Chen et al, 2018; Jun et al., 2015). Silica fume having a specific surface area of $19,620 \text{ m}^2/\text{kg}$ is used as a mechanical dispersal agent for the functional fillers with a specific gravity of 2.2, and type I Portland cement was used for the experiment with specific surface area and a specific gravity

of 3700 cm²/g and 3.17, respectively. The chemical compositions of both silica fume and cement, is demonstrated in table 4.2, which was originally from Kim et al., 2014 previous study.

Table 4-1 Physical properties of the functional fillers (CNT and Carbon fiber)

Functional fillers	Diameter (nm)	Length (mm)	purity (%)	Aspect ratio
CNT	5 - 10	0.01 - 0.05	95	1000 - 500
Carbon fiber	10000 - 20000	10	82.35	>500

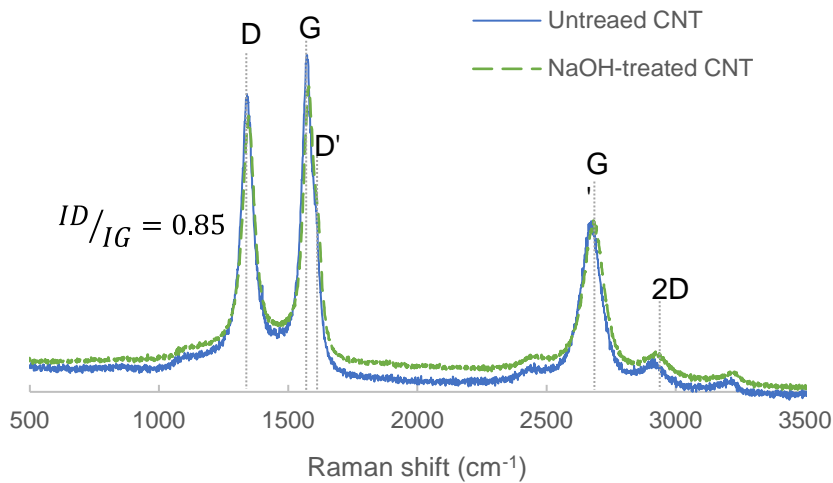


Figure 4-1 Raman spectroscopy analysis of Pure CNT and NaOH treated CNT

The mix proportion in this study can be categorized into three parts the first being the preliminary study to select the fitting mix ratio for further research and the second mix design part is designated for the study of the shrinkage properties by drying and wetting cycle the final, and the third is chloride penetration depth study. Table 4.3 shows all the mix designs, in addition to that mechanical strength and electrical resistivity values. Mortar type conductive cement composite is used in this study, having 1:1 cement to sand ratio. Most of all, the water-cement

ratio for all mix designs in this study was 0.4 and the amount of silica fume and SP being 10% and 0.9% by weight of cement, respectively for all mix designs in this study.

Table 4-2 Chemical composition of Portland cement and silica fume

Oxide (%)	OPC	Silica fume
SiO ₂	20.6	95.3
Al ₂ O ₃	5.0	0.1
Fe ₂ O ₃	3.4	0.4
CaO	60.7	0.2
MgO	2.6	0.8
SO ₃	2.4	0.6
K ₂ O	1.0	-
Na ₂ O	0.2	0.2
TiO ₂	0.3	-
P ₂ O ₅	0.1	-
Others	<0.3	-
LOI	0.8	2.5

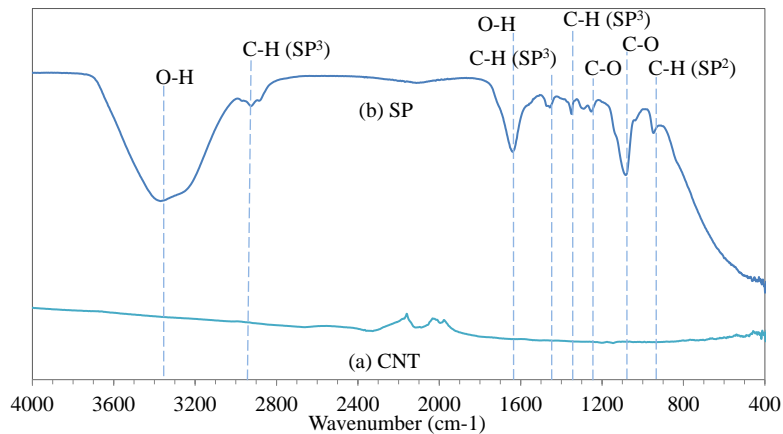


Figure 4-2 FT-IR spectra of CNT and superplasticizer

Furthermore, all of the mix designs that contain CNT were 0.6% by weight of cement. Note that the naming of the specimens was done in order to represent the experimental variables (CNT & CF) with the corresponding percentage amount in the mix. For example, CCF0.5 implies that the first “C” stands for CNT, and the “CF0.5” stands for a 0.5% Carbon fiber in the mixture. However, the control sample is indicated as “plain” and mix “C” indicates the there is only 6% CNT in the mixture with no CFs. Note that all the mixtures have a fair consistency for good workability.

Table 4-3 Mix proportion of mortar samples

Category		Mix-name	Cement	Water	Sand	Silica fume	Percentage (%)			Electrical Resistivity	Mechanical strength (181 days)		
							SP	CNT	CFs		Compressive strength	Flexural strength	Dynamic Young's modulus
										(Ω-cm) *			
Preliminary		Plain	1	0.4	1	0.1	0.9	-	-	10 ⁶ -10 ⁷	55	1.98	33.5
		C						0.6	-	80-90	37	1.8	32.6
		CF2						-	2	10 ⁵ -10 ⁶	60	2.02	32.8
	Shrinkage	CCF0.5						0.6	0.5	90-130	45	1.68	35.5
		CCF1							1	50-60	39	2.13	36.3
		CCF1.5							1.5	40-50	55	1.8	34.2
		CCF2							2	60-70	64	2	35.6

* Note that the resistivity result only indicates samples having a dimension of 1.5cm × 1.5cm × 8cm (W × H × L).

4.2.2 Experimental Methodology

4.2.2.1 Preliminary study

The preliminary study is required to understand the general properties like mechanical strength and electrical properties between different mix designs of the cement composites, which are indicated in table 4.3. Moreover, in this section, the electrical properties were evaluated based on AC and DC data at initial stage. And their effect due to hydration reaction in time on the conductivity of the specimens were also evaluated by boiling the samples at a temperature of 70°C for 1 month inside water using 1.5cm × 1.5cm × 8cm (W × H × L) specimen dimension. Note that AC and DC data measurements were taken using Agilent instruments E4980AL precision LCR meter and 34972A LXI data acquisition, respectively.

The study has been performed mainly based on hybrid CNT-CFs cement composite sensors. For fabrication, dry materials mentioned above like sand, cement, silica fume, and CNT were placed in the exact order and mixed using a standard 6-liter Hobart mixer in accordance with ASTM C305 for 3 min. After a well dry mix, water was added slightly followed by superplasticizer within 4 min, and for mixtures containing the carbon fibers, once the water and SP were completely poured in the mix, the fiber was added to the mix bit by bit while mixing within a 3 min range. Before completing the mix, two more minutes were given to combining it thoroughly, and then casting was followed based on the specified purpose of the mix. Note that the mixing procedure is similar for all cases in this research.

4.2.2.2 Shrinkage

To evaluate the stress-strain cycle with the electrical properties of the conductive cement composite, most researchers used tensile, compressive, and flexural forces or, in general, load-

based measurements. On the other hand, there is a limited or no article that use shrinkage measurement to evaluate the stress-strain cycle in detail to compare with the electrical resistivity, to the best of the authors' knowledge. This article aims to fill the knowledge gap in the research community.

Most studies use paste type cement composite to avoid the conductivity blockage by sand and aggregates. However, the dimensional stability of paste-type composite is low compared to mortar and concrete, making the conductive cement composite vulnerable to microcrack and eventually lead to losing their conductivity. Furthermore, the authors' previous study by Tafesse et al., 2019 shows the effect of shrinkage on a paste type CNT/cement composite is significant, even though it has a trivial effect for high water-cement ratio (0.4). However, for low water to cement ratio (0.25) mixtures, a significant increase in shrinkage from 3800 $\mu\text{m/m}$ to 4500 $\mu\text{m/m}$ was seen as the amount of CNT increase from 0% to 0.6% in the mixture. On the other hand, to show how reliable the conductive cement is in time the shrinkage measurement is a more significant and realistic way than the load base tests, which is done in a short period and has a limitation on the dynamic properties of concrete through time. In addition, mortar type conductive cement composite with carbon fibers is adopted for this study to enhance the dimensional stability of specimens for the cyclic tests and to enhance the stability of the conductivity. To do that, different mix ratios were tested by adding carbon fibers (0.5%, 1%, 1.5% and 2%) with CNT (0.6%) using 0.4 water-cement ratio.

The test samples were prepared in accordance with ASTM C490 using 2.5 cm \times 2.5 cm \times 30 cm (W \times H \times L) rectangular specimens for each mixture; three samples were prepared. Immediately after casting, the specimens were covered using cellophane for one day to avoid unnecessary

evaporation before demolding. After one day, all the samples were cured inside the water at 20 ± 1 °C and 60 ± 4 relative humidity for 28 days. The cycle of drying and wetting also started after 28 days of casting, having three different phases over time.

The first phase was measured every week/cycle. Measurement of one-cycle looks like this, the samples were vacuum saturated for 24 hours at 20 °C then shrinkage, mass, and resistivity data of specimens were taken starting from the SSD condition on the first day to air-dried 2nd-day and 3rd-day measurement. After the 3rd-day measurement, the specimens will be vacuumed again, this time at 50 °C for 3 days to desiccate water from the specimens. To avoid any errors from thermal expansion of specimens after vacuum drying due to the rise in temperature the samples were kept at 20 °C for 1 day, then measurements were taken.

The first phase was measured for 10 consecutive cycles or 10 weeks and then the second phase continued without any alteration on the processes of the first cycle only by changing the measurement frequency from every week to once in a month or in every 4 cycles one-time measurement, which was done for 24 cycles or for 6 months long. After completing almost 34 cycles, first and second phase, the specimens were left to be exposed to the outside environment for 6 more months, experiencing a temperature as low as 10 °C and as high as 28 °C which is phase three. For this phase, the measurement was taken only at the end of the phase.

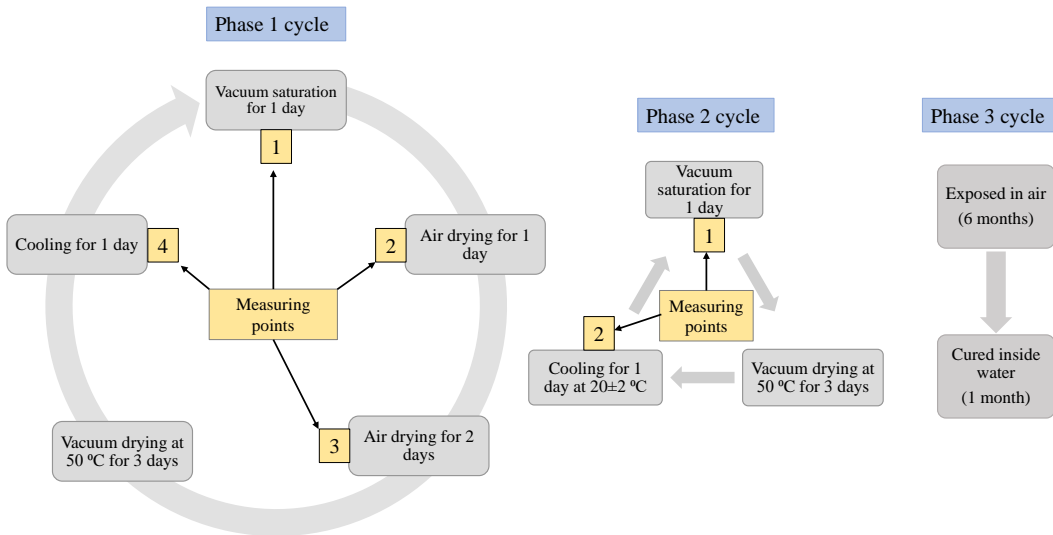


Figure 4-3 Flow chart showing the shrinkage cycle of Phase one (left), Phase two (mid), and Phase 3 (right)

The spotted microcracks on the surface of the hybrid cement composite throughout the phases were investigated by visual inspection. In addition, some pictures were taken using AM3111/3113 series Dino-lite digital microscope, and in order to explain the effect more clearly, the mercury intrusion porosimetry (MIP) was taken after phase 3 using an AutoPore IV 9500 series pore size analyzer. Note that shrinkage measurements were taken using a deformable mechanical gauge with a pin embedded inside the specimen, as shown in figure 4.4, and the electrical resistivity was taken using a simple digital multimeter (SK-104, Samkwang Inc., South Korea) for direct current measurement.

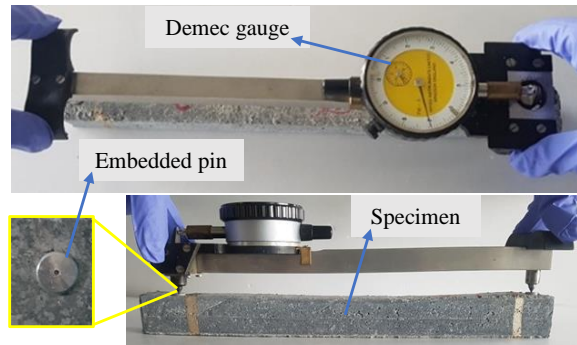


Figure 4-4 Shrinkage measuring demec gauge with embedded pin setup

4.2.3 Working principle of the hybrid cement composite sensor

The two sections discussed above are mainly concerned with the conductivity and stress-strain sensing ability of the cement composites listed in section 4.2.2.1 and 4.2.2.2, respectively. Integrating the CNT inside a cement composite mix using a mechanical dispersion method is a common way to disperse the CNT throughout the mix with the aid of mineral admixture, silica fume (Sanchez and Ince, 2009; Kim et al, 2014). The same is done in this study in order to disperse the CNT fairly with a slight agglomeration inside the cement matrix, as previous morphological studies indicated (Kim et al., 2014).

However, in this study pitch-based, carbon fiber was also included in some mixtures in order to reduce the resistance of the composite (Park et al., 2018). Furthermore, during DC measurement using a high-end multimeter, the mixture reinforced only with CNT has shown a significant fluctuation in reading for about 15 ± 5 seconds before the reading gets stable. On the other hand, for mixtures with both CNT and carbon fiber can be stable within 3 ± 2 seconds. This could be due to the voids inside the cement composite creating separate charges and helping the current to lead the voltage. However, note that the phase angle is much lower compared to the ideal capacitors, -90° (Cseresnyés et al., 2013).

The conductivity of the hybrid cement composite is a complex task, which requires multiple connections in order to pass a current from one end to the other. Some of the connections are, carbon fiber to carbon fiber, CNT to CNT, CNT to carbon fiber, pore to carbon fiber, pore to CNT and tunneling effects are the ways to pass current through. The carbon fiber and CNT connection to their correspondent materials is the common one, and much of the conductivity is done through this technique. In addition, the connection of the carbon fiber to the CNT and the vice versa will also enhance further the conductivity of the cement composite.

Furthermore, when CNTs are encountered with small electrolyte pores in the hydration products, the electrons could easily jump by the tunneling effect (Park et al., 2018). This is not only in the pore solution but also inside the hydration products also the electrolytes from the portlandite will further boost the conductivity of the cement composite, which is the basic principle to sense carbonation in the cement composite due to the loss of the electrolytes like CaOH to a crystalline phase CaCO_3 by carbon dioxide diffusion (Lee et al., 2019). However, when the CNTs encountered large size pores, the tunneling effect will be no use, this is where the importance of the carbon fiber comes in. The carbon fibers can easily intersect and pass this large size pore physically at the early stage during casting due to their length in millimeters. These carbon fibers can adhere to the CNTs on the surface throughout the length of the carbon fiber, which will have a major effect on the CNT dispersion and conductivity (Lee et al., 2017).

On the other hand, the unhydrated cement particles and the fine aggregates are fully insulating points, including the micro cracks in some cases. However, the microcracks might also be governed by the tunneling effects, if microcracks are not larger enough. In case these microcracks are larger, it would create a dielectric part (air) between the direction of the current

flow. This has its pros and cons, the advantages being the cement composite could have a capacitive sensing ability, which could help on monitoring the chloride ingress, in different circumstances these microcracks could increase the capacitance nature by simultaneously increasing the reactance of the impedance, which creates a fluctuation. And in case of direct current measurement, the steadiness of the resistance measurement will be lost and will take time. In order to show schematically, the above discussion is illustrated in figure 4.5.

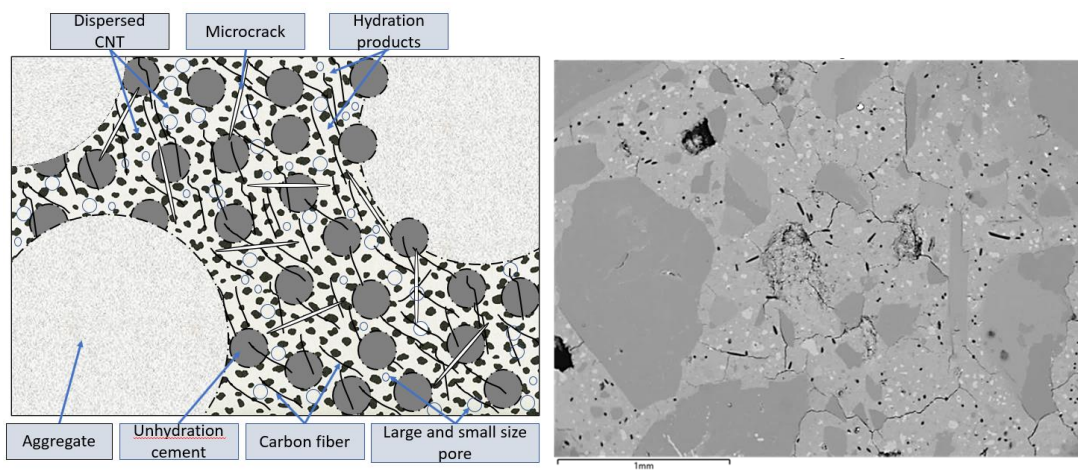


Figure 4-5 Schematic illustration of the hybrid cement composite and BSE-SEM image of CCF2

4.3 Results and discussion

4.3.1 Preliminary study

The preliminary study was conducted with the main aim of finding a mixture having all the qualities required to produce a good piezoresistive sensor for structural concrete monitoring. So, the first problem would be the mechanical properties of the samples to bear the applied force while they are embedded inside a concrete structure as a smart concrete aggregate. And the

second problem is to enhance the conductivity of the specimens with great stability. In order to achieve the above goals, the pitch-based CFs were selected and used.

All the samples have the same water to cement ratio of 0.4, and all are mortar samples with natural sand included in the mix to enhance the overall strength, as discussed in chapter 3 of this dissertation. Table 4.3 shows the mechanical and electrical properties for 181 days of specimens cured in water. The mechanical strength of the specimens was evaluated by using compressive, flexural, and dynamic Young's modulus. The compressive strength for the plain specimen being 55 MPa the strength mostly increases as the amount of CFs increase in the mixtures. The maximum strength was achieved by CCF2 specimens, 64 MPa. The same is true for the flexural result, as the amount of CFs in the mix increases the strength also increases. However, a maximum strength of 2.13 MPa is achieved by specimens with 1% of CFs in the mortar mix of CCF1. This mix, CCF1, also have attained the ultimate dynamic modulus of 36.3 GPa. From the result, it was clear that the C mixtures have shown almost the least performance in all the mechanical strength evaluation techniques. However, the electrical resistivity value of C specimens was as good as the specimens with both CNT and CFs combined. For the plain and CF2 samples, the resistivity was high, as expected. Even though the low resistivity was achieved by hybrid and C samples, the stability of the samples is one of the most important factors to manufacture a good sensor.

Table 4.4 indicates the impedance result of all the preliminary specimens based on their resonant frequency and figure 4.6 shows the change in resistivity of the samples at dry and SSD condition. Measurement was taken after curing samples for 91 days and then boiling it for additional 28 days, twice. This is done to investigate the late hydration reaction effect on the electrical

conductivity of the specimens. Furthermore, in both cases before and after boiling the samples, the dry and SSD conditions were measured to get a clue on the influence of moisture. From the results, the plain samples showed a very high resistivity, which can be categorized under an insulator.

The CF2 also showed a high resistivity in kilo-ohms, and both the plain and CF2 samples showed a high resistivity decreased by the influence of moisture. For CF2, since it has a conductive and the reduction of resistivity due to water was around 51% and 23% before and after boiling of the samples, respectively being highly influenced among the conductive samples. For samples, which contain both the CFs and CNT or the hybrid samples, the moisture has slightly influenced the samples from a minimum of 6% to 20%. On the other hand, C samples were influenced the least by the moisture and by the hydration product increase after boiling the samples.

Table 4-4 Resistivity of hybrid cement composite samples before and after boiling based on their resonant frequency (Dry and SSD)

Sample condition		Resistivity (Ω -cm)						
		Plain	C6	CF2	CCF0.5	CCF1	CCF1.5	CCF2
New Samples	Dry	67110.6	83.7	1327.8	97.7	48.9	31.4	49.2
	SSD	25312.9	81	641.7	103.6	39.6	36.9	55.3
Boiled Samples	Dry	24416.8	83.6	579.1	145.4	45.6	42.9	58.5
	SSD	17051.9	102.8	446.4	110.1	44.5	40.4	63

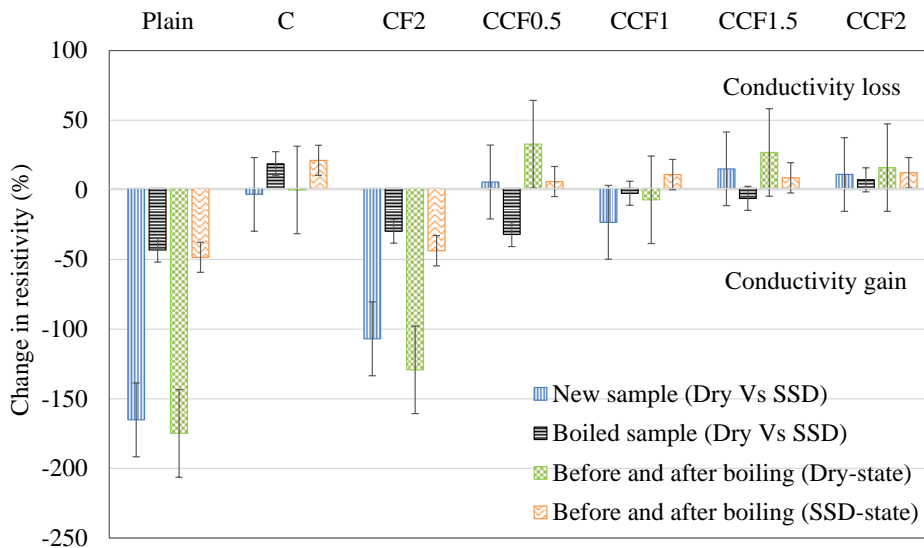


Figure 4-6 Change in resistivity by percentage of samples based on their resonant frequency (SSD condition and 7 day air dried)

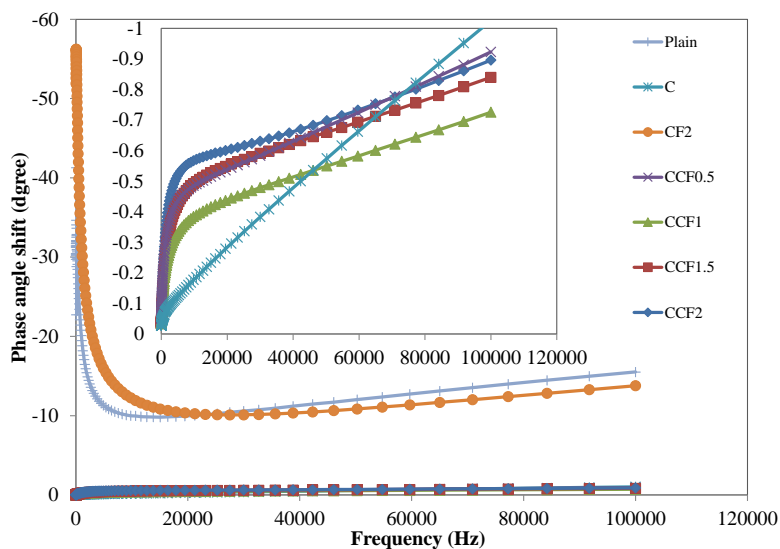


Figure 4-7 Phase angle Vs. frequency value of preliminary samples

The other critical study made in this preliminary section is to define the fundamental nature of the sensors, besides their piezoresistive capability. To analyze that, the phase angle was used based on a frequency range of 20Hz to 100 kHz. From the result in figure 4.7 all of the specimens

are in a negative value, which means the phase shift under impedance measurement indicates that the current is leading the voltage, which shows that the material being measured has a capacitive reactance (Azhari, 2012). The same is true, when voltage leads the current, the reactance will show a more inductive value, which is positive. However, in this study, only the capacitive nature of the specimens was seen. This could be attributed to the porous and heterogeneous nature of the composite samples. CF2 and the plain samples both showed a high capacitive nature at low-frequency ranges below the 20 kHz. On the other hand, the rest of the specimens showed the reverse, which is the capacitance of the specimens was high at higher frequencies even though, the total range was not high, $< -1^\circ$. However, the increase was constant, and no fluctuations have occurred while the frequency increased. Note that to avoid the geometrical effect of frequency on the phase angle, the shapes of all specimens were kept identical.

4.3.2 Dimensional stability

In this experiment, only the hybrid samples were used this is done by considering the above results in the preliminary results. From the results, the remaining samples that are not hybrid have shown different performance that was a top and bottom performance for different cases. However, the hybrid samples have shown a constant and good performance in all the scenarios made in the preliminary study, unlike the other types of specimens. To see one by one, plain and CF2 samples have a good mechanical strength performance and have a high capacitive response at a lower frequency like the hybrid samples but in a reverse mode. However, their electrical properties are not under the required range, while the plain samples have almost no conductivity. The CF2 samples have a conductivity in Kilo-ohms, which makes them easily suspectable to

moisture influence. For C samples, even though the electrical resistivity was good enough for the proposed study, the mechanical strength performance was inferior compared to the remaining specimens. This could harm the dimensional stability of the specimen in general and could lead to microcracks and harm the conductivity of the specimens. Due to the above reasons, the hybrid samples were chosen to be investigated on the long-range study, which lasts for a year studying the stress-strain properties of the hybrid cement composite based on slender shrinkage samples by wetting and drying. This research will have an impact on the future development of cement-based composite sensors.

4.3.2.1 Phase one (Initial Period)

Phase one is introductory part for the early age of the wetting and drying cycle of the slender samples. In this part, two things will be discussed: one is the early age shrinkage effect, and the second is the effect of stainless-steel electrode and silver paste on the resistivity result. The first ten cycles/weeks recorded by the wetting and drying cycle are considered as phase one. One cycle/week has four steps, which looks like this, In the 1st step, the specimens were vacuum saturated for 24 hours in room temperature, and measurements were taken in SSD condition. Then after the specimen was left to be dried in air for two consecutive days while taking measurement on both days, which is the 2nd and 3rd step and for the final and 4th step the samples were dried in a vacuum in 50 °C for three days, as shown in figure 4.3.

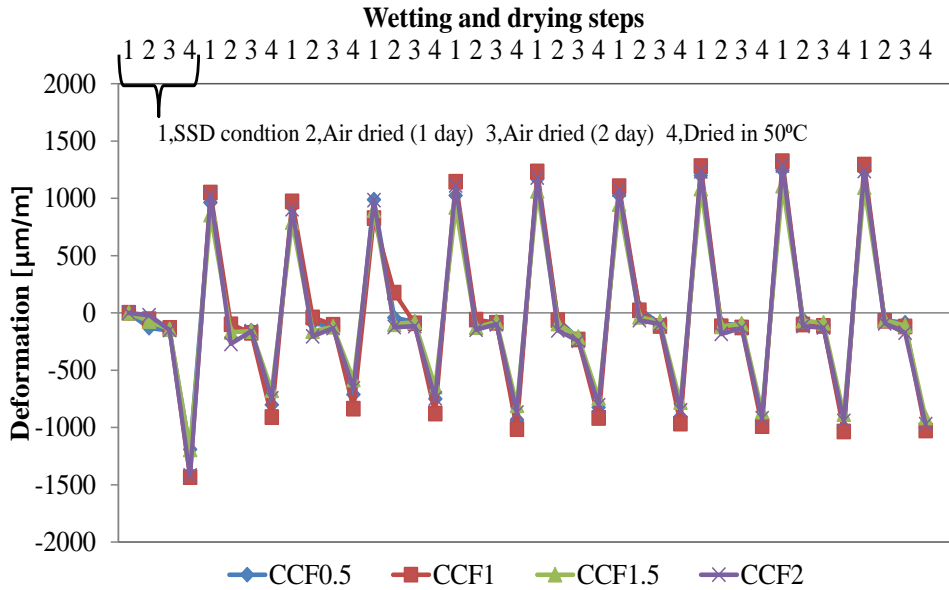


Figure 4-8 Shrinkage cycle of the hybrid cement composite for phase one

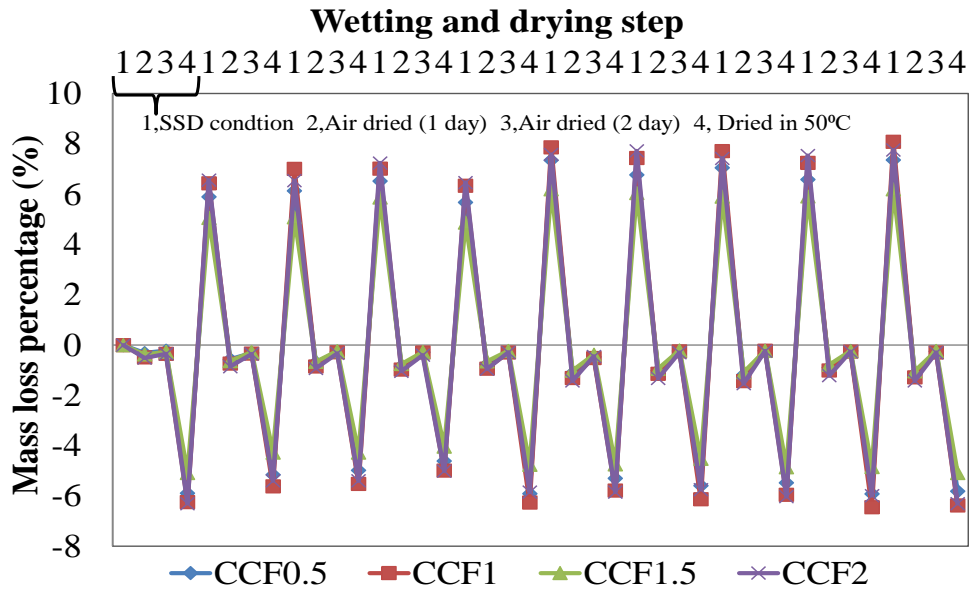
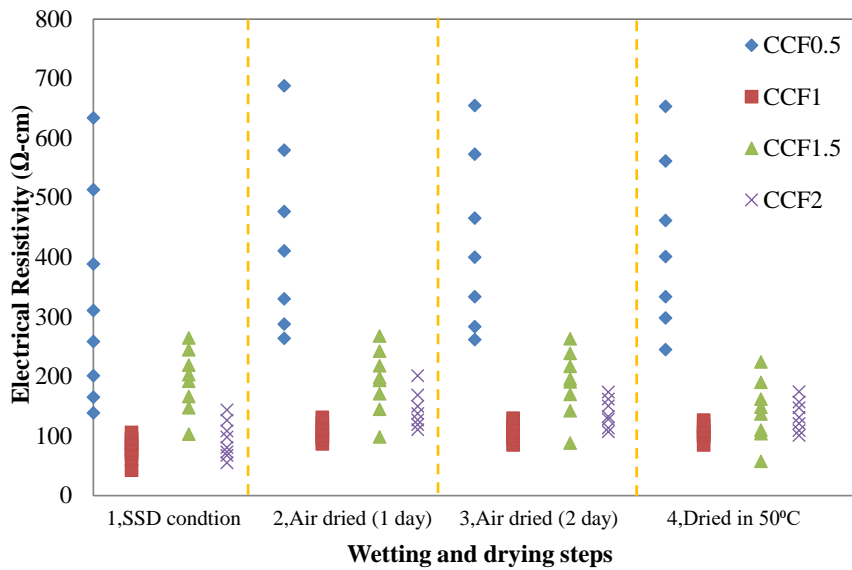


Figure 4-9 Mass loss result of the hybrid cement composite for phase one

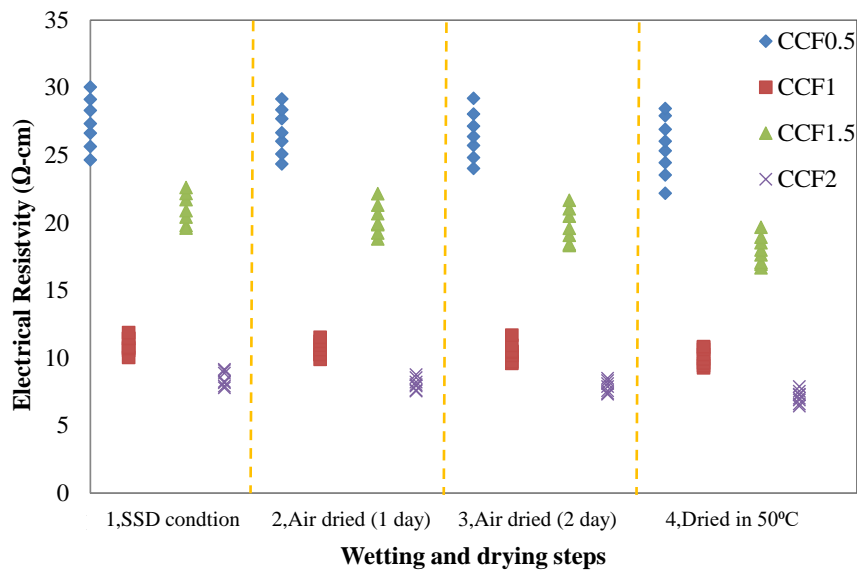
Figure 4.8 shows all the 4 steps with their respective deformation values. It is clear from the graph that all the specimens were in line with each other showing a great performance in all the steps. Approximately, a maximum of $-1400 \mu\text{m/m}$ and $1300 \mu\text{m/m}$ shrinkage and expansion were seen in phase one, respectively. The deformation is consistent with the mass loss result shown in figure 4.9. Having a -6% and 8% mass loss while the sample was in shrinkage and expansion, respectively. Both the maximum results seen in the deformation and mass loss as a positive and negative value are for the SSD and vacuum dry condition that is for steps 1 and 4. In the case of steps 2 and 3, even though the shrinkage effect was clear but it was a slight difference, mostly less than $75 \mu\text{m/m}$.

The second intention in this phase is to isolate the performance of the electrodes. Figure 4.10 shows a scattered graph of both electrode (stainless steel and silver paste) resistivity results on all the four steps. Even during the initial measurement, there was a slight difference in the initial resistivity values between identical specimens measured by the electrode and silver paste. However, the variation has increased during every cycle for the steel electrodes, especially for CCF0.5 specimens. The difference has reached around $600 \Omega\text{-cm}$ within the first ten cycles.

On the other hand, for CCF0.5 specimens measured using the silver paste, the variance was as little as $6 \Omega\text{-cm}$. These results were also implicated in other hybrid samples, even though the gap was not as high as CCF0.5 specimens. This shows the reliability of the steel electrode is not as good as the silver paste, for this reason, all the upcoming phases in this chapter and next chapters will be conducted based on the silver paste electrode.



(a)



(b)

Figure 4-10 Scattered graph of the hybrid cement composite resistivity (a) stainless steel electrode (b) silver paste electrode

4.3.2.2 Phase two (Evaluation period)

In this section, the shrinkage result that were taken for more than 6 months in two steps: 1st one is by wetting the specimens for 24 hours in a vacuum chamber and measuring the SSD condition and the 2nd step measurement were taken after vacuum drying the specimen in 50 °C for 3 days. This phase has two main goals: (1) is to analyze and discuss the shrinkage cycle and (2) to investigate the sensing capability of the hybrid composite samples in detail based on their resistivity and shrinkage cycle. This evaluation stage is very important due to the most cycles during the whole experiment were conducted at this stage.

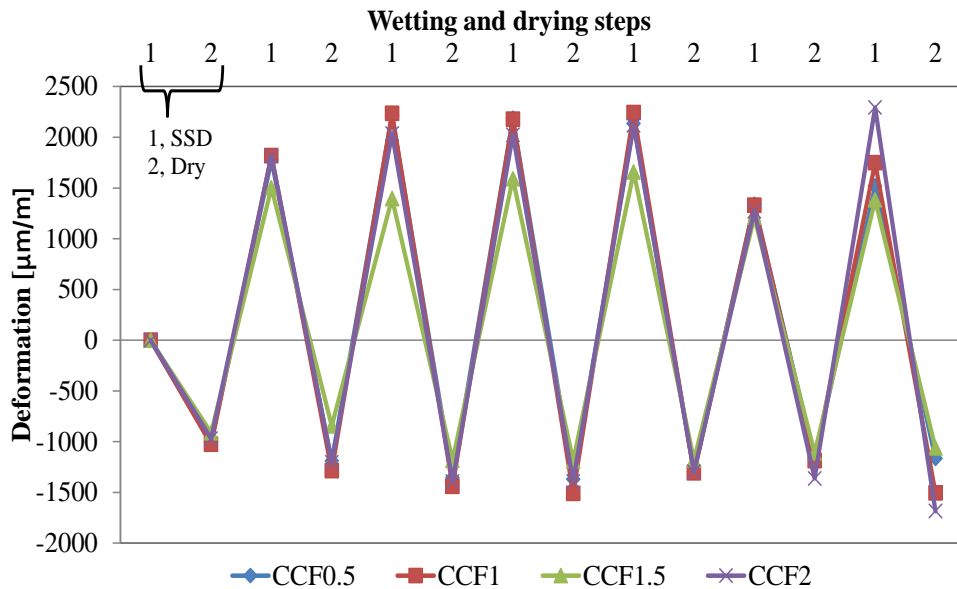


Figure 4-11 Shrinkage cycle of the hybrid cement composite for phase two

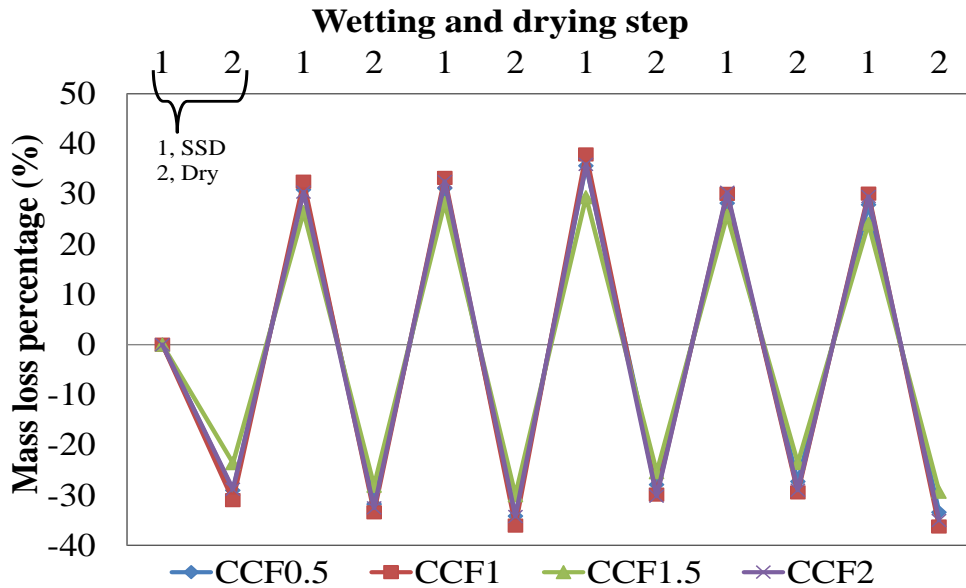


Figure 4-12 Mass loss result of the hybrid cement composite for phase two

The shrinkage cycle for phase 2 is shown in figure 4.11. From the result, it is clear that even though the cycles were too intense, the samples have shown an excellent resistance against the shrinkage and expansion having a deformation of top $-1700 \mu\text{m/m}$ and $2300 \mu\text{m/m}$, respectively. The mass loss measurements have been clearly supported these results in figure 4.12, which validates the shrinkage results, and the experiment was done with great care and excellence. The detailed analysis on the cumulative shrinkage result on phase one and two are done on phase 3, including the porosity results.

The second aim of this section, which is the relationship of the stress-strain cycle by the wetting and drying cycle of the slender samples, will have a great implication on the upcoming chapters of this dissertation. In short, the goal is to investigate the reliability of the hybrid cement composites self-sensing capability. To do that, the stress-strain values from the shrinkage samples measurement were compared with the fractional change of resistivity (FCR). FCR is a

ratio of change in resistivity or resistance by the original value of the specimen resistivity or resistance, as shown in equation 4.1. The formula below is true for specimens having a uniform contact area, the distance between two electrodes and temperature, which is all true in our case. Even though the distance between the two electrodes was changed during the shrinkage and expansion by -0.0017 m and 0.0023 m, respectively, the change is too small and negligible to have an effect on the result.

$$FCR = \frac{\Delta\rho}{\rho_0} = \frac{\Delta R}{R_0}.....4.1$$

Where FCR is the fractional change of resistivity, $\Delta\rho$ is the change in resistivity, ρ_0 is the initial resistivity of the specimen, ΔR is the change in resistance, and R_0 is the initial resistance of the specimen.

Both the initial and evaluation period self-sensing capability during the stress-strain cycle will be discussed on this section for convenience. During the initial period, the shrinkage cycle shown in figure 4.8 is discussed with respect to the FCR. The results demonstrated in figure 4.13 shows high resemblances for all the hybrid cement composite specimens between the stress-strain cycle and FCR. The maximum ratio of FCR was seen in CCF2 samples, and the minimum change were for CCF0.5. The change was incremental based on the carbon fiber amount in the mix. However, note that all the hybrid cement composite samples have a great self-sensing capability in spite of their change in FCR. By comparing the average strain of the samples with the FCR of the samples, as shown in figure 4.15 by comparing the relation using linear regression.

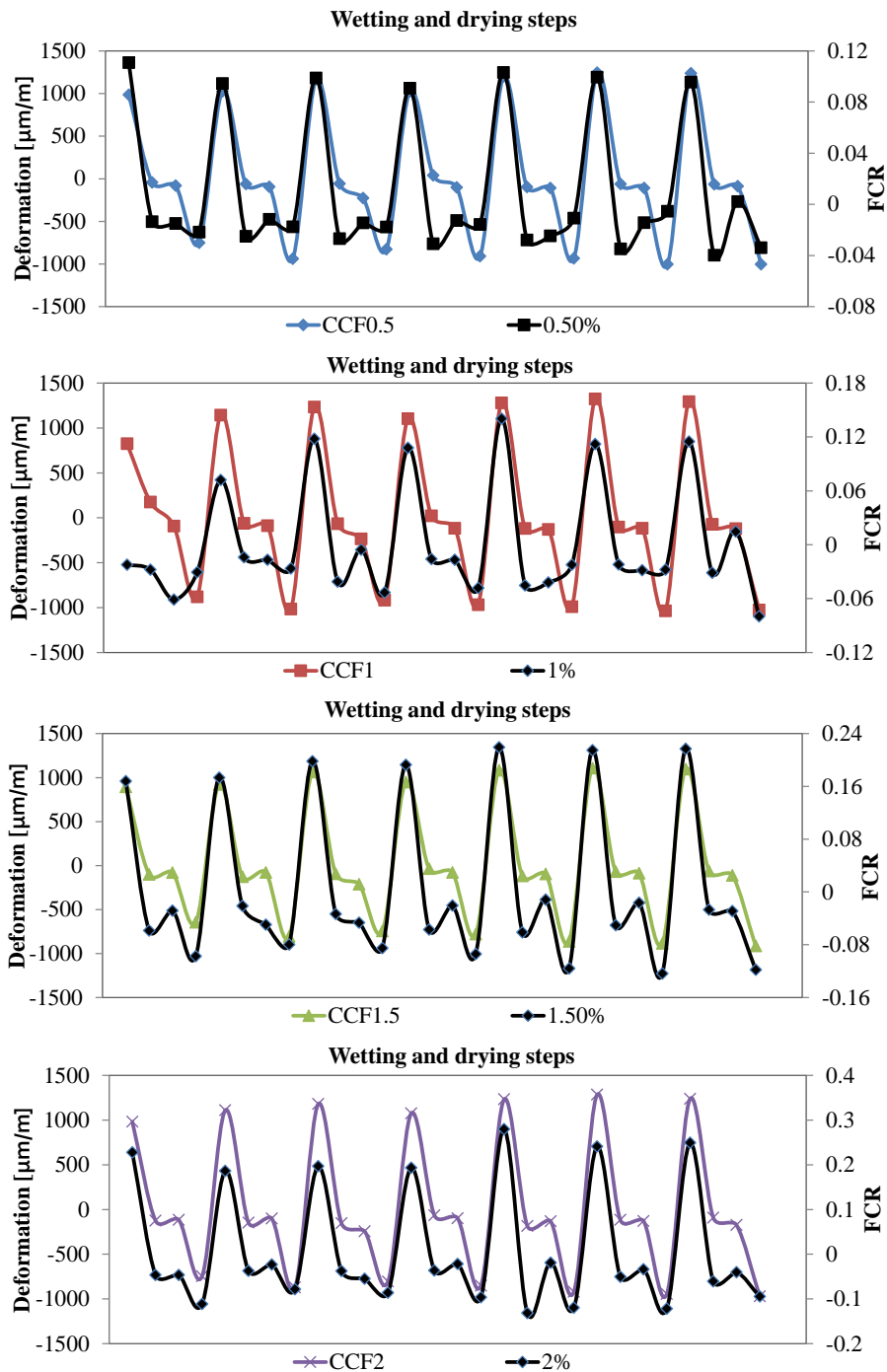


Figure 4-13 FCR Vs shrinkage cycle of the hybrid cement composite for phase one

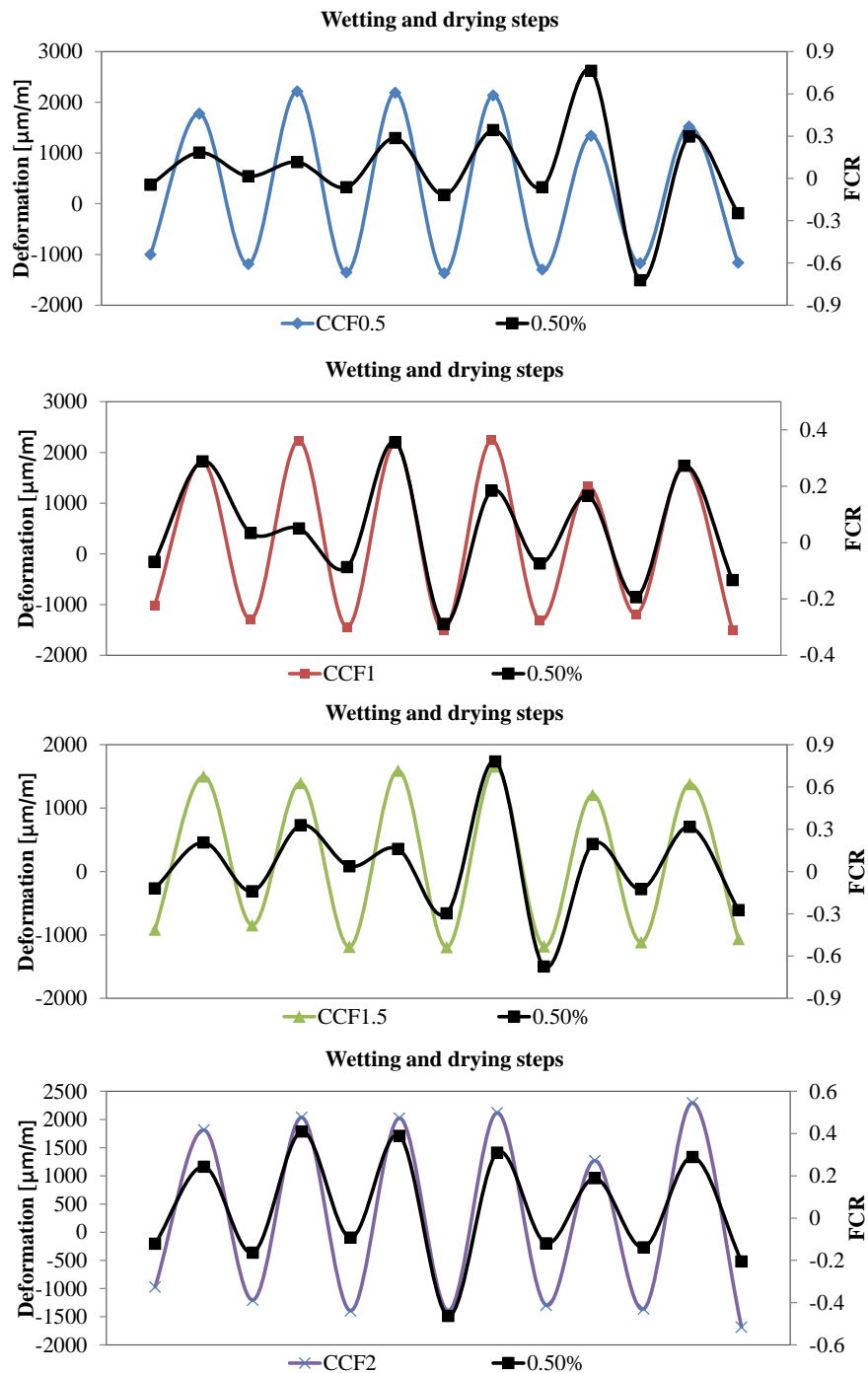


Figure 4-14 FCR Vs shrinkage cycle of the hybrid cement composite for phase two

The strain values have seen a negative value during their initial shrinkage stage, and a positive value is seen after microcracks were started, and the specimens were relaxed. In addition, the slope indicated in the equation of the regression results indicates the gauge factor of the hybrid cement composite samples. Gauge factor (GF) is a common evaluation unit for the sensitivity of any strain sensor. Sensors made of metal have around 2-5 GF, and single crystal silicon and polysilicon-based sensors have -125 to 200 and ± 30 GF, respectively. For this case, the GF sensitivity was high around 60 to 170, with an R^2 value of 0.7089 and 0.9366, respectively, which shows a linear relationship with the strain of the hybrid cement composites, as shown in equation 4.2 (Lee et al., 2017).

$$GF = \frac{\Delta\rho/\rho_0}{\varepsilon} = \frac{FCR}{\varepsilon} \dots\dots\dots 4.2$$

Where GF and FCR is the gauge factor and fractional change of resistivity, respectively, $\Delta\rho$ is the change in resistivity, ρ_0 is the initial resistivity of the specimen, and ε is the strain of the specimen.

In phase two, the relationship between the deformation of the samples and the respective FCR values was, to some extent, deflected, showing a less similarity between the cycles. This is because of the intense wetting and drying cycles (34-cycles) made in this phase. From figure 4.14, it is evident that the CCF0.5 and CCF1.5 samples were showing much lower similarities than in phase one. On the other hand, sample CCF1 and CCF2 have shown a fair and good cyclic trend, respectively. Both samples have shown a GF of 101 and 151 with an R^2 value of 0.7414 for CCF1 and 0.8786 for CCF2, consecutively. While CCF0.5 and CCF1.5 showed a less linear relation having an R^2 value of 0.4833 and 0.6738, respectively, as shown in figure 4.15. The

result discussed above were exceptional for the development of the self-sensing sensor in the future. Notably, the CCF2 specimens have shown a tremendous self-sensing capability even after all the 34 wetting and drying cycles.

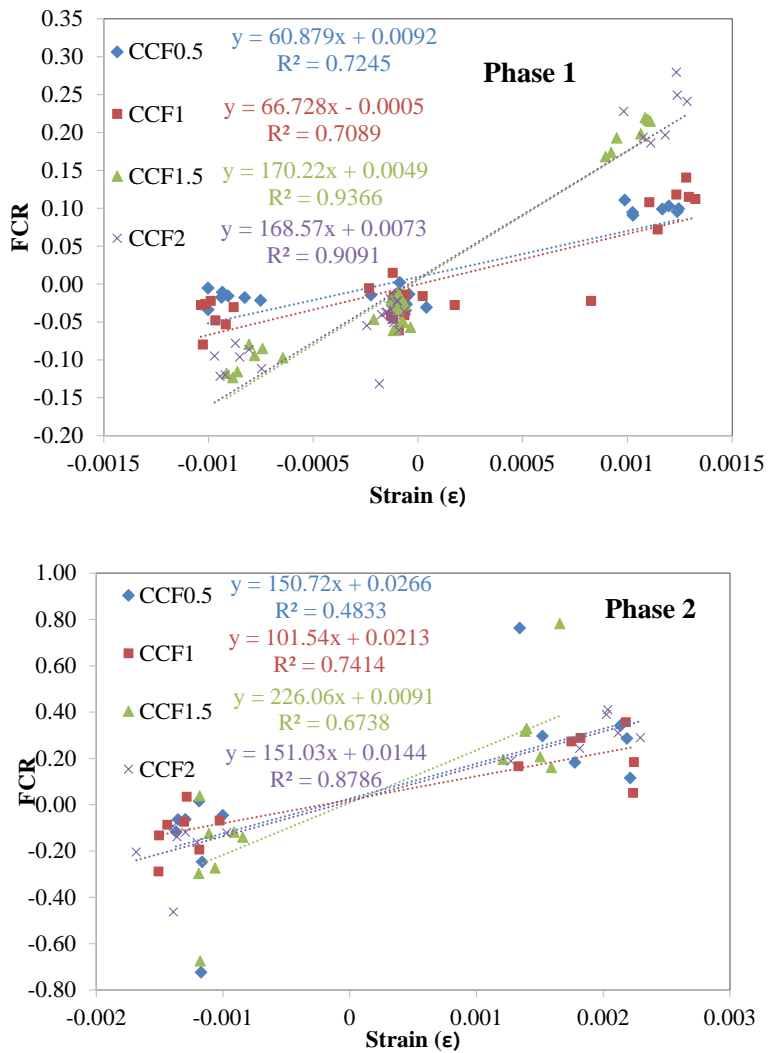


Figure 4-15 Relationship graph of FCR and strain for Phase one and phase two

4.3.2.3 Phase three (Dormant/ healing period)

Phase 3, the Dormant period, is where the specimens were left in the air to be subjected to the outside condition of temperature 10 °C minimum and 28 °C maximum during the 6-month period. The objective in this phase is to analyze the MIP result, inspect the microcracks of the specimens using a portable microscope, and to analyze the total deformation of the hybrid cement composite samples until this phase in the exact order. Figure 4.16 and Table 4.5 shows the MIP results of the hybrid cement composite incremental pore volume, and the total intruded volume, respectively. The total intruded volume is divided based on the three main pore sizes, mesopores [5 to 50 nm], capillary pores [50 to 100 nm], and the large capillary pores [> 100 nm]. The division was made in order to simplify and create a clear understanding.

Table 4-5 The total intruded volume of hybrid cement composites

Sample name	Mesopores (Pores < 50nm)	Capillary pores (Pores b/n 50 & 100nm)	Large capillary voids (Pores >100nm)	Total intruded volume [mL/g]
CCF0.5	0.0436	0.0021	0.0150	0.0607
CCF1	0.0388	0.0014	0.0243	0.0646
CCF1.5	0.0374	0.0017	0.0186	0.0578
CCF2	0.0414	0.0022	0.0185	0.0621

From the result, CCF2 has the largest total intruded volume of 0.0646 from those the large voids more than 100 nm are clearly seen in the incremental graph, and this explains the decrease in the compressive and flexural strength in table 4.3. CCF0.5 and CCF2 both showed a high pore volume of mesopore, which shows that further hydration occurred in the sample compared to the remaining samples. In addition, the maximum capillary pores, which are responsible for the shrinkage to occur, were seen for CCF2 and CCF0.5 samples with 0.0022 and 0.0021 mL/g,

respectively. However, even though the CCF0.5 sample had the lowest pores of more than 100 nm, the strength was inferior compared with the remaining hybrid cement composite samples.

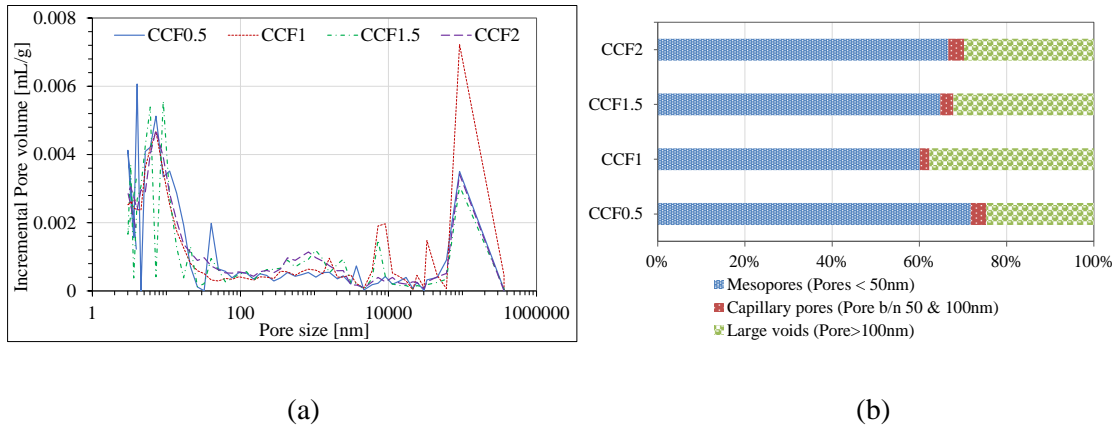


Figure 4-16 MIP result of the hybrid cement composites for shrinkage samples (a) incremental pore volume (b) cumulative pore volume in percentage by pore size

The total deformation of phase one and two combined is shown in figure 4.17 for the dry condition, which was measured for ten consecutive months. A maximum of 3880 $\mu\text{m}/\text{m}$ was seen by CCF0.5 specimens, which is a 12.7% increase compared to the lowest deformation of 3444 $\mu\text{m}/\text{m}$ by CCF2 specimen. Furthermore, by the increase of carbon fiber in the mix, the deformation of the specimens has also been reduced. The specimens with high capillary pores that are more than 50 nm pores have shown lower deformation except for CCF1. This could be due to the capillary pores initiate the shrinkage of the specimens, which help them to counteract the expansion deformation of the specimens during the microcracking. The micro-cracks are not only visible by the naked eye on the surface of the composites; some of the images are taken by a portable microscope are shown in figure 4.19a. The cracks shown are very thin hair cracks, mostly less than 0.1 mm, which are on the surface of the specimens. After putting the samples

in the outside environment, the expansion has increased by about 1200 $\mu\text{m/m}$ to 1560 $\mu\text{m/m}$ as shown in figure 4.19 for the dry condition.

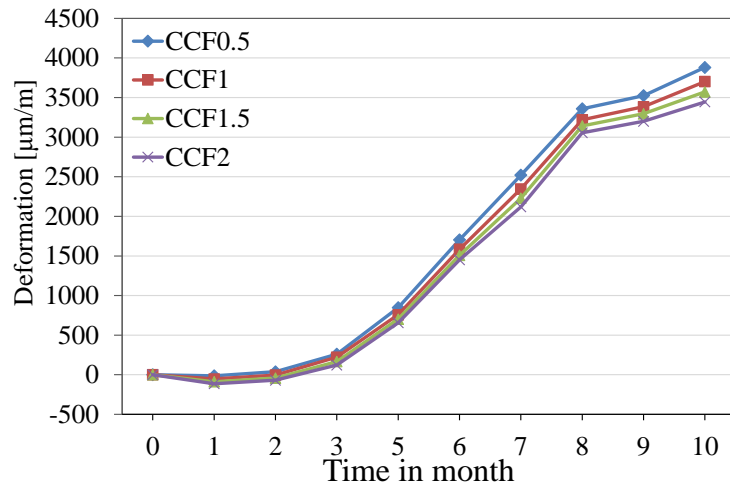
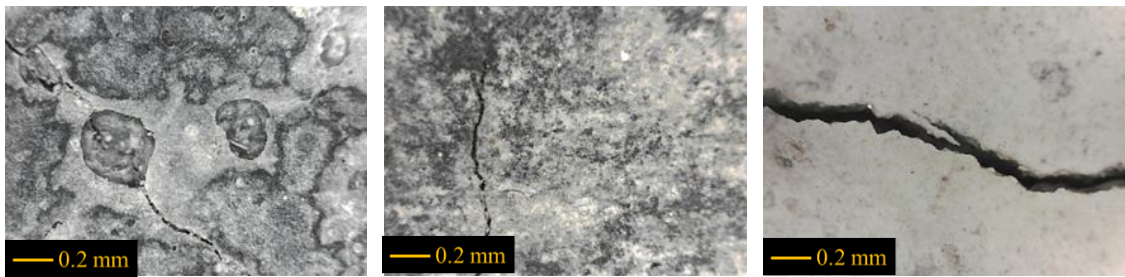
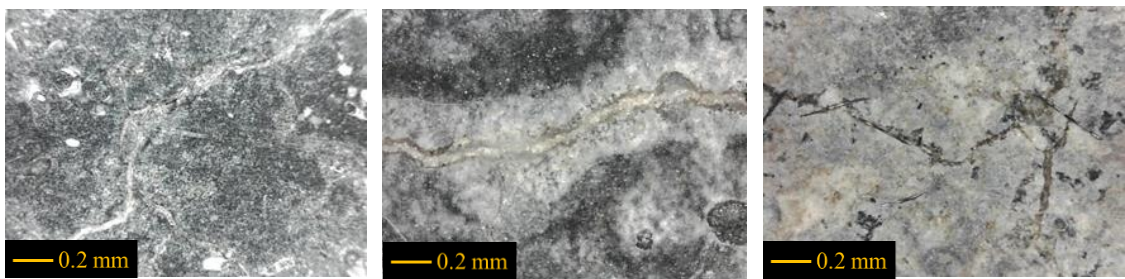


Figure 4-17 Total deformations of phase one and two

However, after completing the air exposure, the samples were cured inside water for a month. This is done to check the healing capabilities of the hybrid cement composite specimens. From the result, the expanded specimens were healed, further hydrated, and decreased their deformation by shrinkage, which could be due to further hydration or carbonation effect. The maximum shrinkage was seen for CCF2 specimens lowering the deformation by about 84 % compared to the dry state expansion recorded during the 6-month dormant period. All the specimens CCF0.5, CCF1, and CCF1.5 were also shown a shrinkage while healing around 32.09 %, 60.1%, and 36.3%, respectively, compared to the measurement made before curing in the water for a month. Figure 4.18b shows more clearly the healing by a portable microscope, as shown in the figure, most of the cracks were healed by water curing after one month.



(a)



(b)

Figure 4-18 Pictures of microcrack (a) cracks during phase two cycle (b) After healing on phase 3

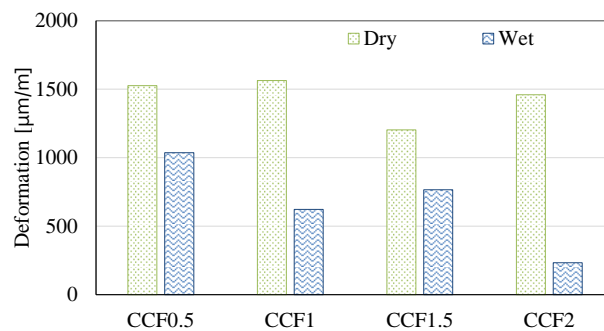


Figure 4-19 Deformation after end of phase two of the hybrid cement composite in phase three (dormant period) during air curing for 6 months

4.4 Discussion

The main goal of this chapter is to get a reliable CNT based cement composite sensor. To do it, the first ground or base for the study was to enhance the mechanical characteristics of the cement composite. It is a well-known fact that by adding sand on the paste composite, the mechanical strength can be improved. However, the addition of fine aggregates like sand would have a negative effect on the conductivity of the CNT cement composite (Coppola et al., 2011). Note that the addition of fine aggregates could also enhance the conductivity by creating a pore in the ITZ area and increasing the conductivity indirectly (Chung, 2018). To counteract on the effect, pitch-based carbon fiber was added to the CNT/cement composite besides the sand. This was done (addition of carbon fiber) for two reasons; (1) is that the carbon fiber can enhance the conductivity network inside the cement matrix and help to by-pass the effect of fine aggregate due to their longer size which is in millimeters, in this study 10 mm long carbon fiber were used (Park et al, 2018). And the second reason (2) is the cost of pitch-based carbon fiber compared to its relative types of fibers is economical and highly conductive (Park et al, 2018). By combining the carbon fiber with the CNT, a hybrid cement composite was manufactured as a mortar composite by introducing fine aggregates to the mix. Overall, by doing so, the strength of the sample has drastically increased from the previous study made in chapter 3, which is mortar without fiber having 37 MPa, and by adding about 2% carbon fiber in the mix, the strength has increased significantly, 64 MPa. As the amount of carbon fiber increased in the mix, compressive strength has also increased for most of the mixtures (Zuo et al., 2015). The same was also observed on the flexural and dynamic Young's modulus. In a previous study made by Tafesse., 2017, on a pure CNT cement composite the CNT has shown an adverse effect on the mechanical strength of paste mixtures as the amount of CNT increased. This could be attributed to the slight

agglomerations of the CNT due to their high Vander walls force creating weak points for crack nucleation inside the cement matrix (Tafesse., 2017). This was also observed in this study by a reduction in strength of CNT containing specimens compared to the plain samples. However, the addition of carbon fiber has reinforced the cement matrix and increased mechanical strength by further making the mortar denser. In addition, the electrical conductivity of the hybrid cement composite was very steady, and also resistivity has decreased further by the carbon fiber introduction (Zuo et al., 2012; Park et al., 2018). Please note that much of the conductivity is from the distribution of CNT inside the cement matrix. Besides, the carbon fiber has increased the conductivity network inside the cement matrix due to the high aspect ratio having a length of 10 mm, which will help the carbon fiber to act as a bridge between the CNT particles (Park et al., 2018). Moreover, carbon fibers could help in dispersing the CNT following aliment of the carbon fiber by binding the CNTs to the hydration products that are already bonded to the surface of the carbon fiber (Lee et al., 2017). This gives the CNT network to disperse and have a pattern inside the cement matrix, which ultimately contributes to the stability and increase in conductive.

Once the desired level of mechanical strength was achieved, the hybrid cement composites were further tested for the dimensional stability test using the dry shrinkage as stress and strain-inducing mechanism. This is done by immersing the samples inside the water and drying it in the oven under 50 °C temperature in a cyclic manner, as discussed earlier in this chapter for both phase one and two. During these cycles, a perfect stress-strain was recorded, which was confirmed by the mass loss results. By the end of both phases, the total deformation of specimens was decreased as the amount of carbon fiber increased, respectively (Tafesse et al., 2018), which

was also confirmed on the mechanical properties. This helped the CCF2 specimens to be superior in mechanical strength and to show a lower deformation compared to the remaining samples.

Even though the metal electrodes capability to detach from the surrounding mortar paste was already studied in chapter 3. However, in this study, a clear illustration of the effect debonding on the stress-strain measurement of the samples was seen in comparison with that the silver paste painted on the side of the composite. The results were seen to be stable for the silver electrodes and quite low in resistivity. However, unlike the silver paste, the electrodes initial resistivity was high even before the cycle started. This shows the first week initial bonding between the electrode and the matrix was not good, which even gets worse as the cycle continues by increasing the resistivity drastically even at the very initial phase (Lee et al., 2019). For this cause, the silver paste was used for the rest of the studies in this dissertation.

The relationship between the FCR and deformation by the stress-strain cycle is an indication of the hybrid cement composite sensing capability. In these continuous cycles, almost all the samples have shown an interesting result in both phases. Especially, CCF2 showed the highest coefficient of determination in both phases. This is due to the addition of fibers have a positive impact on the mechanical strength and deformation, which will indirectly help the conductive network to be stable throughout the cycle. Gauge factor is a common evaluation unit for the sensitivity of any strain sensor. Sensors made of metal have around 2-5 GF, and single crystal silicon and polysilicon-based sensors have -125 to 200 and ± 30 GF, respectively. For this case, the GF sensitivity was high around 60 to 170, with an R^2 value of 0.7089 and 0.9366, respectively, which shows a linear relationship with the strain of the hybrid cement composites. This is supported by Lee et al., 2017 studies, they used a broad amount of carbon fiber

concentration in a different mixture in order to get the best sensing composite. Based on the multiple experiments conducted by applying three stages of axial force, which increases intensity on every stage using compressive load it indicates that to get an acceptable sensing capability, the amount of carbon fiber should be at list above 0.1% (Lee et al., 2017). However, in this study rather than evaluating the performance of a 28 days samples based on load-based experiment (compressive cycle, tensile cycle or flexural cycle) with in a short period of time, a slender sample were put under cyclic conditions of wetting and drying that can more or less reflect the real conditions. The first phase shows the initial reaction of the hybrid cement composite samples for about 2 months, which showed a higher coefficient of determination and phase two showed the durability effect of the hybrid cement composite for the next 6 months under a stress-strain cycle showing a fair coefficient of determination. In overall, the carbon fiber role is major in controlling both the dimensional stability and the resistivity through time(durability) for attaining a reliable sensor. Future studies should focus on the amount of the carbon fiber threshold and its effect on the composite and the mix proportions should be done considering packing density theory.

The total porosity of the CCF2 specimen is relatively higher than the other specimens except for CCF1. On the other hand, the majority of the porosity around 65% on average from the total porosity is attributed to mesopores ($< 50\text{nm}$), which are mostly found on hydration products that also show a higher degree of hydration reaction. Note that this was seen in all samples including CCF2. In general, this small size pores have an insignificant effect on the mechanical strength of the specimens as shown on the result above. However, this small size pores have their own contribution for the conductive network since the electrolytic free electrons from the hydration

products could be found in this pore and it could facilitate the conductive network furthermore (Yoo et al., 2017; Park et al., 2018). Overall, the dimensional stability of the paste-CNT/cement composite is as high as 5600 $\mu\text{m}/\text{m}$ for the exact same amount of CNT without any cycle, as shown in previous studies of Tafesse et al., 2018 (Tafesse et al., 2018). However, in this study, even with the cyclic condition, the maximum deformation achieved is 5400 $\mu\text{m}/\text{m}$, which is by far a lower considering the drying and wetting cycle. This result was achieved by the addition of carbon fiber and sand inside the cement composite mixture.

Table 4-6 Comparison of the hybrid cement composite sensing capability results with previous literature reviews

Reference	Test mechanism	W/C ratio	CNT content (%)	Carbon fiber content (%)	R ²	GF
Phase 1	Shrinkage (Drying & wetting)	0.4	0.5	0.5	0.7245	60.8
				1	0.7089	66.7
				1.5	0.9366	170.2
				2	0.9091	168.5
Phase 2	Shrinkage (Drying & wetting)	0.4	0.5	0.5	0.4833	150.7
				1	0.7414	101.54
				1.5	0.6738	226.06
				2	0.8786	151.03
Azhari, 2008	Compression (loading & unloading)	0.4	1	15	0.9528	327751
Lee et al., 2017	Compression (loading & unloading)	0.35	0.15	0.35	0.2464	32.1
			0.25	0.25	0.4273	79.5
			0.35	0.15	-0.682	74.2
			0.5	0.1	0.9274	160.3

4.5 Conclusion

From the reliability study by stress-strain sensing of CNT-CFs hybrid cement composite on the dimensional stability is concluded by drawing the following conclusions.

- The mechanical strength has shown a significant increase while the carbon fiber increase in the mixture, and on the other hand, a decrease for a specimen with CNT only were seen by comparing with the plain samples.
- Besides the piezoresistive properties of the hybrid cement composite, a slight capacitive property was also observed on the composites.
- The comparison between the silver and stainless-steel electrode was unmatched even from the beginning to the end of the first phase. The steel electrodes were showing huge fluctuations and higher resistivity. Instead, the silver paste electrode showed the exact reverse, which is a steady and low resistivity.
- The first two shrinkage cycle phases were done having maximum stress and strain of around -1700 $\mu\text{m}/\text{m}$ and 2300 $\mu\text{m}/\text{m}$. and the shrinkage cycles match with the mass loss results. In addition, the total shrinkage recorded was around 5400 $\mu\text{m}/\text{m}$, which is very low compared to other studies. Furthermore, the CCF2 samples showed the lowest deformation of all the samples.
- During the sensing capability study of the hybrid cement composite, most of the hybrid composites have shown an R^2 of above 0.71 and 0.48 for phases one and two, respectively. The most noteworthy relationship was seen for CCF2, R^2 of 0.9, and 0.87 for both phases, consecutively.
- Based on a visual inspection made on the cracked hybrid cement composite specimens, the samples were shown to heal within one month. This was confirmed by shrinkage reduction after wetting the samples.

Chapter 5. Chloride profiling and conductivity relation of CNT-CFs hybrid cement composite following the rapid chloride penetration test and monitoring evaluation

5.1 Introduction

In this chapter, the effect of chloride concentration inside the hybrid cement composite compared to its conductivity is tested using a unique way. The samples were exposed to a slightly adopted rapid chloride penetration test method. After the test, the samples were sliced perpendicular to the chloride penetration direction, and each slice was investigated based on the actual chloride content in the slice and the conductivity of the slice itself. The procedure followed in this paper makes this article one of its kind, to the best of the author's knowledge. In addition, the degree of hydration and porosity of each slice was also investigated. Furthermore, hybrid cement composites were also embedded inside reinforced concrete to see the practical effects of the sensors.

5.2 Materials and method

5.2.1 Materials and mix proportions

The materials used for this study are the exact same materials, including the mixing procedure mentioned in chapter 4 of this dissertation. On the other hand, the mix proportions used to cast the hybrid cement composite were selected from the reliability study, which shows the steadiest conductivity and dimensional stability. In this case, the mix with 2% CFs content was chosen to be investigated for further experimental studies in chloride profiling. Since, the rapid chloride penetration test usually uses high voltage to pass the chloride ions from the cathode electrode to the anode electrode through the hybrid cement composite specimen the temperature will rise due

to the electrical conductive properties of the composite, as stated in Joule's first law and equation 5.1 below (Kim et al., 2019).

$$H = V^2T/R \dots\dots\dots 5.1$$

Where H is the heat produced, V is the voltage applied, R is the resistance of the specimen, and T is the time it takes to pass through the specimen.

In addition, the CNT content has a direct effect on the temperature of the specimen due to its high thermal conductivity the effect will even raise more (Wang et al., 2004). To reduce the effect of temperature in the mix an additional mixture was used this time only half the CNT content (0.3% CNT) of the original mixture (0.6% CNT) was used. On the other hand, the mix used to embed the hybrid cement composite have water to cement ratio of 0.45 and cement to sand ratio being 1:2 by weight.

Table 5-1 Mix proportion of chloride profiling samples and embedding mortars

Category	Mix-name	cement	Water	Sand	Silica fume	Percentage (%)		
						SP	CNT	CFs
Chloride profiling	CCF2	1	0.4	1	0.1	0.9	0.6	2
	C3CF2						0.3	
Embedding mortar	Plain Samples	1	0.45	2	-	0.4	-	-

5.2.2 Experimental methodology

5.2.2.1 Chloride profiling of hybrid cement composite

Chloride profiling is carried out after selecting the most durable and better conductive mixture through the preliminary and shrinkage results. For these tests, two types of mixtures were used,

0.3% and 0.6% CNT content, both mixtures having the same water-cement ratio and the carbon fiber content of 0.4 and 2%, respectively. The reduction in the amount of CNT from 0.6% to 0.3% was aimed to check the effects due to the increase in temperature by the CNT present (Kim, 2019). Prior to profiling, the chloride penetration test was done on a cubic sample having 5 cm dimensions in all directions in accordance with ASTM C1202 using 50 mm thick specimens. In order to fit the test for a mortar level specimen, the amount of voltage applied was reduced from the standard 60 Volt to 10 Volt, while increasing the time for the test that was given to be 6 hours to 24 hours. Keeping the other standards aligned with the regular procedures, including the 3% NaCl solution in one container and 0.3 M NaOH solution in the other container.

Figure 5.1 shows the setup of custom-made rapid chloride penetration test that fits smaller specimens of the hybrid cement composite. Once the specimens were penetrated by the chloride ion, the samples were divided equally into four-portion parallel to the chloride penetration direction, and each portion was used for a different purpose. Again, each of the portions was sliced by 5mm thickness in a perpendicular direction from the chloride penetration. To examine the penetration depth of chloride ion in the hybrid cement composite AgNO_3 was sprayed on the sliced samples, and a simple visual inspection was done. In addition, the sliced samples were grinded into powder to evaluate the concentration of Cl^- content on each slice using ion chromatography method. The electrical resistivity of each slice was measured as well in order to compare with the concentration of chlorides in the slices. Furthermore, the degree of hydration, porosity, and loss on ignition for each slice was also measured for a better understanding.

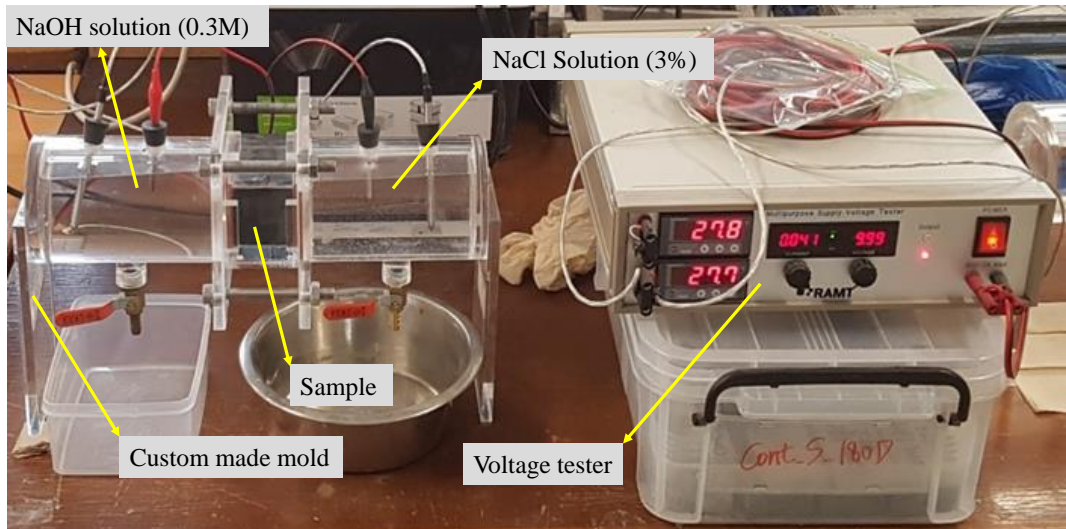


Figure 5-1 Custom made rapid chloride penetration testing instrument setup

5.2.2.2 Embedded hybrid cement composite

In addition to chloride profiling, the hybrid cement composite was embedded inside a reinforced mortar specimen to reciprocate the real-world scenario in the experiment. Two rectangular 12 cm × 80 cm × 180 cm (W × H × L) mortar specimens were reinforced using 2 ϕ 10mm bars from the opposite side of the sensors, and all except one face of the mortar is coated with an average of 2 mm thickness epoxy layer to prevent any lateral diffusion of chloride ions from the side. 16 sensors were embedded inside each mortar samples following a sequential pattern, as shown in figure 5.2. There are four rows of sensors in each, and every row contains four sensors, and the rows follow one another in line to the other without one blocking other. The nearest and distant sensors to the exposed outer surface are 1cm and 4 cm, respectively. The samples were cured for 28 days inside pure water at room temperature. After water curing a different cycle starts, the samples were immersed for one week inside a 10 % chloride solution and then let them dry in air for one week each step following the other in a repetitive manner. Data collection was

done after every two wet and two dry cycles for each case using both AC and DC measurements. Furthermore, to profile the mortar specimens for chloride ingress, additional samples were prepared with the same dimension but without the embedded sensors and follow the same immersion and drying cycle. These specimens were drilled up to 4cm to profile the mortar during the 6th and 12th cycles.

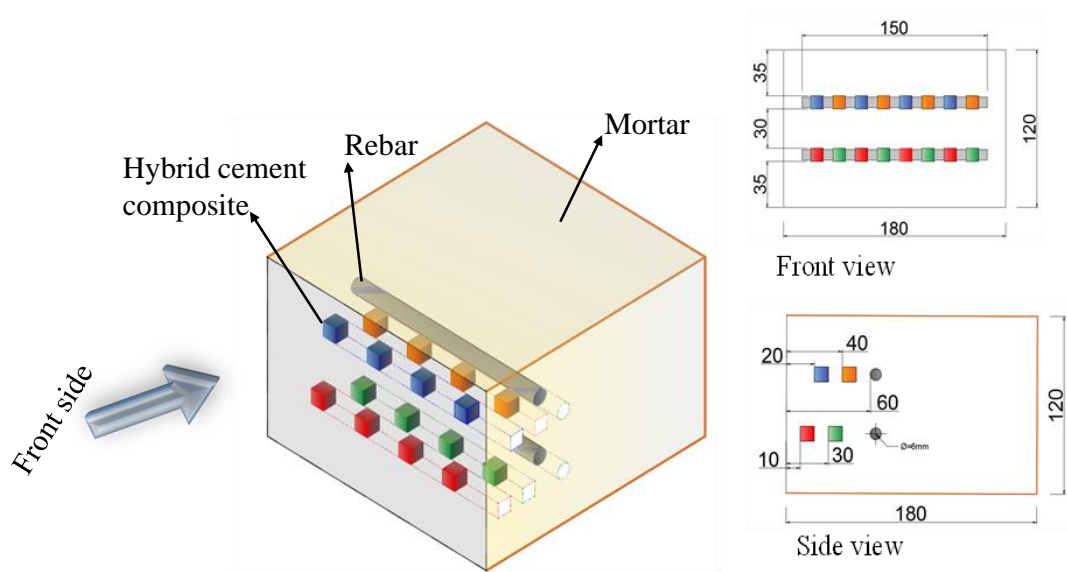


Figure 5-2 Schematic diagram showing the embedded sensors inside a reinforced mortar for chloride monitoring

5.3 Result and discussion

5.3.1 Chloride profiling of hybrid cement composite













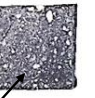




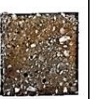
As shown in figure 5.1, the rapid chloride migration was done by custom-made instruments. The main goal of the experiment is to have a result in a short period of time before conducting the main chloride immersion technique, which could take years before a valuable result are seen. However, by conducting the rapid chloride migration test, the samples can be penetrated within



hours, which involve artificial acceleration of the process by using electrical voltage. In this study, the CCF2 hybrid cement composite sample was selected based on the studies done in chapter 4 due to its reliability. In addition, C3CF2 was prepared considering the adverse effect of temperature on CNT based mixtures during high voltage application. To avoid unwanted heat raise during the experiment, half the CNT content (0.3% CNT- content) was used compared to the original reliable mixture (0.6% CNT- content). Note that not only the CNT content was reduced but also the applied voltage was also decreased from 60 V to 10 V during the experiment for both mixtures to control the temperature.

5.3.1.1 AgNO₃ spray method

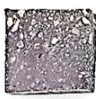

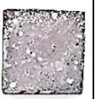








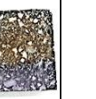



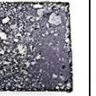
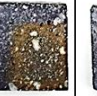
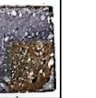
After the test, the samples were sliced in a 5 mm thickness following the chloride ingress direction. The first test was done by spraying silver nitrate (AgNO₃) 0.1M solution on the sliced samples as recommended by ASTM C1202 to check the depth of chloride penetration. The application of AgNO₃ on chloride penetrated samples lead to the formation of AgCl, which is white precipitation signifying the existence of chlorides on the samples. If none of the chlorides penetrated the samples, the brown color would be seen on the surface, showing a free zone from chloride. As shown in Figure 5.3, both samples were penetrated by the chloride. However, the temperature has a great effect on the specimens as expected, even though both mixtures have the same mix design except the amount of CNT content and both passing through the same experimental procedures the result was different. The chloride penetration depth based on this test for C3CF6 was about 10 mm to 15mm top, as shown in figure 5.3(a). On the other hand, Figure 5.3(b) shows the CCF2 depth of penetration, which is almost throughout the full depth were the last two depths (25 mm & 30 mm) were partially affected. This could be due to the

high-temperature rise of the specimens were subjected to a microcrack affecting the chloride ingress to go simply through the specimens. Additional experiments were taken to cross-check the result from AgNO_3 spraying using ion chromatography.

Sample No. (C3CF2)	Chloride penetration Depth	Profiling depth (mm)					
		5	10	15	20	25	30
1	Up to 5 mm						
2	Up to 10 mm						
3	Up to 5 mm						

 Chloride penetrated (white part)
  Chloride free (Brown part)

(a)

Sample No. (CCF2)	Chloride penetration Depth	Profiling depth (mm)					
		5	10	15	20	25	30
1	Up to 25 mm						
2	Up to 25 mm						
3	Up to 20 mm						

(b)

Figure 5-3 Hybrid cement composite samples sprayed by AgNO_3 based on the profiling depth after the rapid chloride penetration test (a) C3CF2 (b) CCF2

5.3.1.2 Ion chromatograph

To get more meaning full data than proving evidence of chloride presence based on visual inspection like AgNO_3 spry, an ion chromatography test was conducted. This is done to examine and quantify the chloride concentration on each layer or depth by taking powders based on parts per million (ppm) of the hardened cement composite. It is worth mentioning that the test is done twice to avoid any errors during the experiment or powder selection processes by using two different apparatus. Furthermore, the result presented here is the average of the two experiments done in different laboratories. Table. 8 shows the amount of chloride concentration on each depth.

Table 5-2 Chloride concentration of the hardened hybrid cement composite based on ion-chromatography

Depth (mm)	5	10	15	20	25	30
0.3% CNT sample(ppm)	1046.77	1144.04	417.32	497.65	130.80	48.16
Loss on ignition (%)	11.90	10.20	11.90	9.52	10.42	8.51
0.6% CNT sample (ppm)	1602.16	1653.89	1677.29	1425.47	1263.77	593.62
Loss on ignition (%)	11.76	11.11	12.90	13.51	12.82	10.71

The results of the experiments were aligned with the previous results made by visual inspection in the pictures shown above. The concentration of the C3CF6 samples was mostly high at the initial depth of the specimens 5 mm and 10 mm, which is 1046 ppm and 1144 ppm, respectively. Compared to their respective specimens (CCF2), even at the initial phase, the concentration is much lower by around 34.6 %, and 30.8 % and the remaining depths were mostly lower than 500 ppm interms of the chloride concentration. On the other hand, CCF2 specimens have shown a much higher and a relatively consistent number of concentration between 1602 ppm to 1263

ppm for most of the profiled depth except the final 30 mm depth having a lower concentration of chloride, 593.62 ppm. The loss of ignition results have shown diverse results and the relation with the chloride concentration on each profiling depth is low. This could be due to the higher percentage of carbon fiber by mass in the hardened hybrid cement composite affecting the loss of ignition easily by the fiber concentration. The relationship between the conductivity and the chloride concentration will be discussed in the coming sections.

5.3.1.3 Porosity

In order to check the effect of chloride penetration on the porosity of the specimens, the total and incremental pore volume of the specimens were taken using MIP. Table. 5.3 shows the total intruded volume of the specimens. From the result, the total intruded volume of CCF2 before chloride penetration is as shown in the previous chapter (0.0621), which is much lower than the intruded volume after chloride penetration, which is in average 0.1159. The increase in total intruded volume is over 80 % due to chloride ingress in the hybrid composite. This effect is mainly attributed to the large capillary pores or pore sizes of more than 100 nm by comparing the results with none-chloride samples. On the other hand, the capillary pores and mesopores have a negligible effect by comparison, as shown in figure 5.4 (b). This indicates the effect of the temperature during the experiment was too high and has influenced the porosity and has created microcracks.

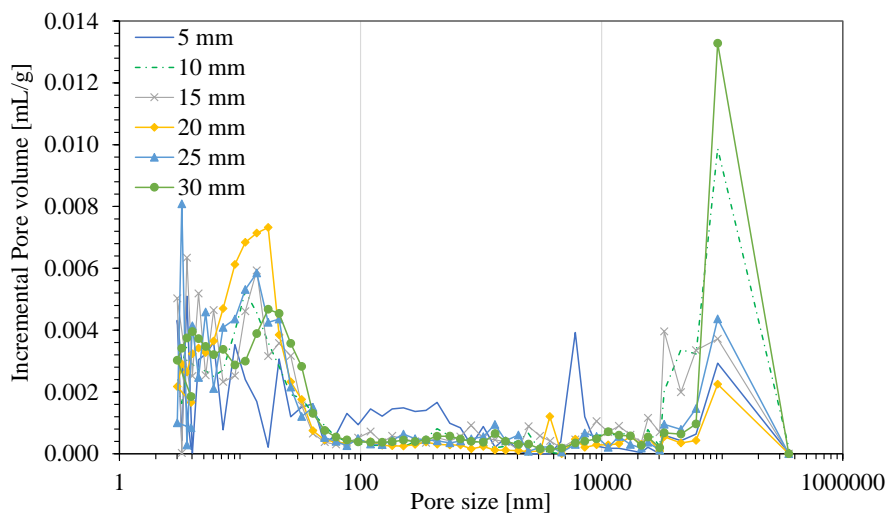
The same experiment was conducted on the C3CF2. From the result, except for the 5 mm sample that should a slight decrease on mesopores from the average 65% ,the remaining samples total intrusion was fairly equal. On average, it is around 0.0811mL/g. By relating it with the chloride-free CCF2 samples, the total intrusion, which is 0.0621 the porosity of C3CF2 has increased by

30.5% by chloride ingress. Comparing it to the 80% chloride ingressed CCF2 samples, the amount is relatively low. Furthermore, the incremental pore volume in figure 5.4 (a) shows a very dispersed results despite the chloride penetration depth direction. In general, the above discussion shows the amount of CNT in the experiment has a major role and will affect the rapid chloride test, and future studies should take a note from the above results. Note that even though the temperature has its own effect on the samples but since the chloride concentrations were known by ion chromatography and the effect of the temperature was uniform throughout the depth of the specimen, in overall, the resistivity data won't be affected for both specimens. This was confirmed further by analysing the relation ship between the porosity and the chloride concentration as shown in figure 5.5. The result indicates that the total intruded volume in the hybrid cement composite has no direct relation to the amount of chloride penetrated the specimen this was true for both samples. Eventhough the samples have shown microcracks especailly for CCF2 samples by increase in large voids but it was difficult to say there was a direct relation. This also extend to the resistivity effect due to porsity there was no relation especailly for the C3CF2 samples.

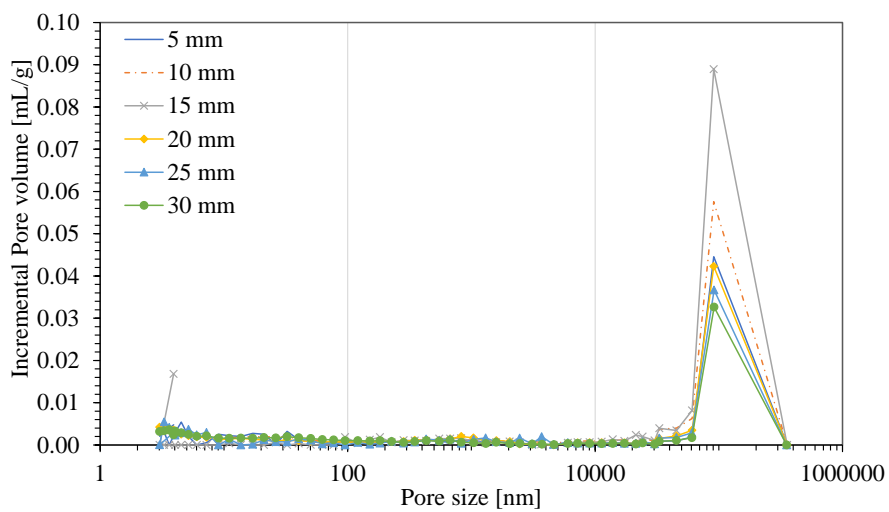
Table 5-3 Total intruded volume of the hybrid cement composite samples with chloride ingress

Sample name	Depth	Mesopores (Pores < 50nm)	Capillary pores (Pore b/n 50 & 100nm)	Large voids (Pore>100nm)	Total intruded volume [mL/g]
C3CF2	5	0.0359	0.0032	0.0249	0.0640
	10	0.0497	0.0022	0.0295	0.0815
	15	0.0556	0.0016	0.0284	0.0855
	20	0.0637	0.0016	0.0114	0.0768
	25	0.0566	0.0017	0.0182	0.0765
	30	0.0564	0.0021	0.0266	0.0852
CCF2	5	0.0374	0.0027	0.0641	0.1042
	10	0.0392	0.0037	0.0960	0.1389

	15	0.0181	0.0019	0.1300	0.1500
	20	0.0370	0.0031	0.0698	0.1098
	25	0.0326	0.0019	0.0630	0.0975
	30	0.0390	0.0050	0.0507	0.0947



(a)



(b)

Figure 5-4 Pore size distribution of chloride ingress samples following the profiling depth for (a) C3CF2 samples and (b) CCF2 samples

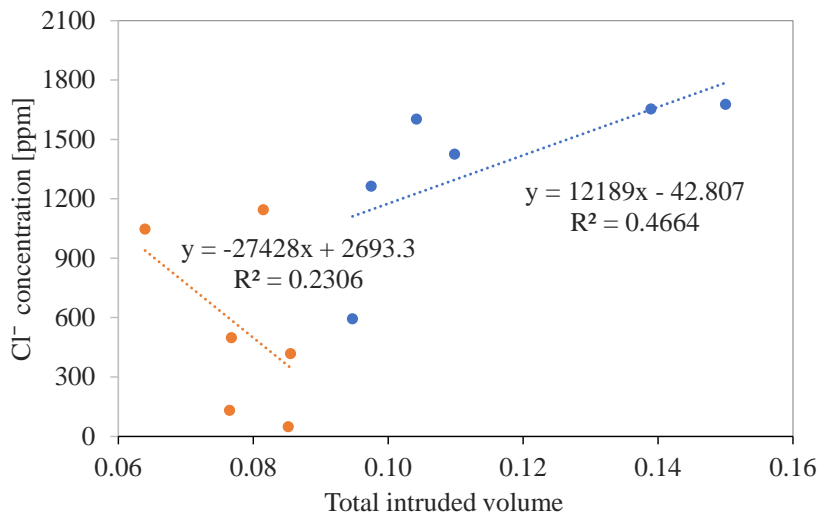


Figure 5-5 Relationship of the total intruded volume and chloride concentration in the hybrid cement composite

5.3.1.4 Profiling depth relation to W_{ne}/b ratio

The non-evaporated water to binder ratio (W_{ne}/B) was compared with the chloride penetration direction by profiling the sample by depth as shown in figure 5.6 This experiment were done previously by tafesse et al., 2019 for paste samples with non-chloride samples or samples free from chloride, and the result showed that a difference of less than 5% between both mixtures (C3CF2 and CCF2). On the other hand, on this experiment, a mortar based mixture was used and the difference between both mixtures was a minimum and maximum of 10.8 % and 40.2 %, respectively. In addition, both results showed a consistent increase in hydration as the depth of the specimen increases, especially for CCF2 samples. This could be due to binding of the

chloride in to Fridal's salt chemicaly at the initial depth, which will increase the evaporable water.

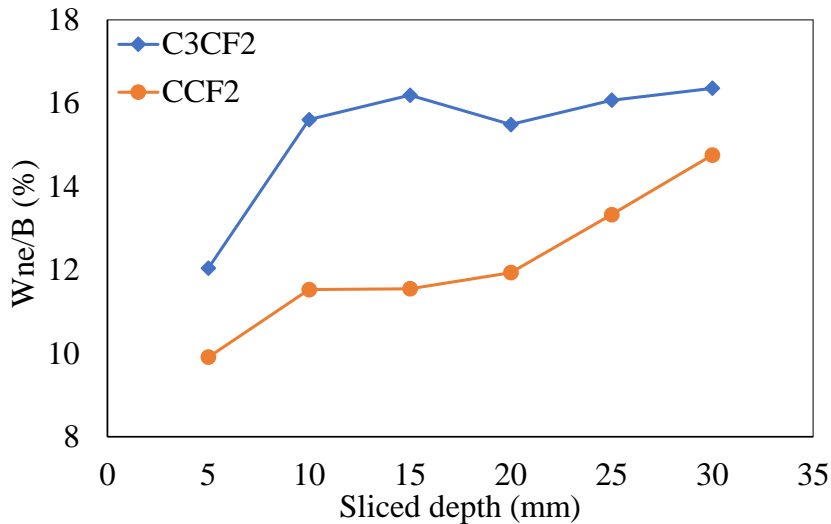


Figure 5-6 Non-evaporated water-to-cement ratio (Wne/C) of the hybrid cement composite based on the profiling depth of the chloride ingress samples

5.3.1.4 Resistivity and chloride concentration relation

To analyze the sensing capability of the hybrid cement composite specimens to the chloride ingress, the sliced samples were not only measured for the Cl^- concentration, but also the resistivity of each sliced sample was measured. Figure 5.7 shows the relation of the chloride concentration with the resistivity clearly. For instance, C3CF2 samples have low chloride ingress, which was also signified by a low resistivity result, especially as the depth of the specimen increased. On the other hand, at the front side where the chloride concentration is high, the resistivity was high as well. The same is true for CCF2 samples where the concentration of chloride is above 500 ppm almost for all samples, which was also implied by a high resistivity mostly in kilohms. In addition, figure 5.8 showed an exponential relationship between the

concentration of chloride and the resistivity were the R^2 value is 0.6776 and 0.5499 for C3CF2 and CCF2 specimens, respectively. This result have showed even under the influence of the temperature and the microcrack the hybrid cement composite can be still used as a reliable means of chloride sensing. The above data can be improved highly by avoiding the surrounding effects and if the chlorides were allowed to be ingress inside the composite without any voltage application only through time.

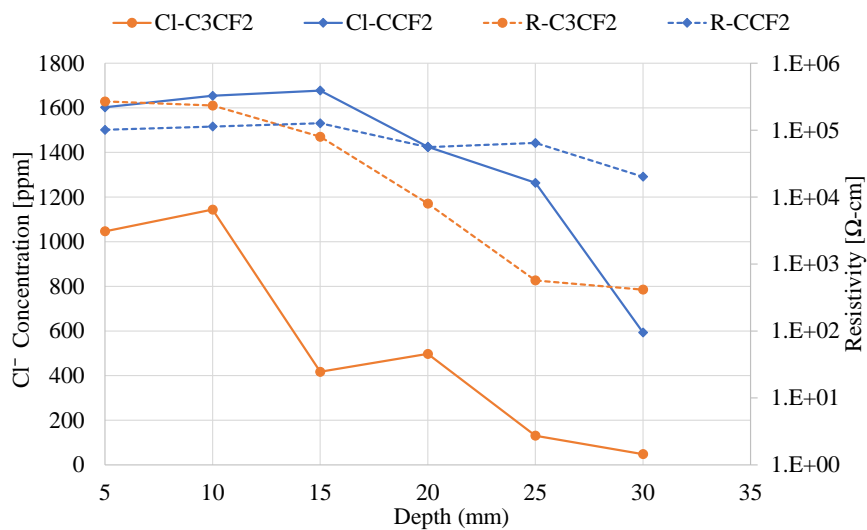


Figure 5-7 Chloride concentration and resistivity result of the hybrid cement composite by the profiling depth

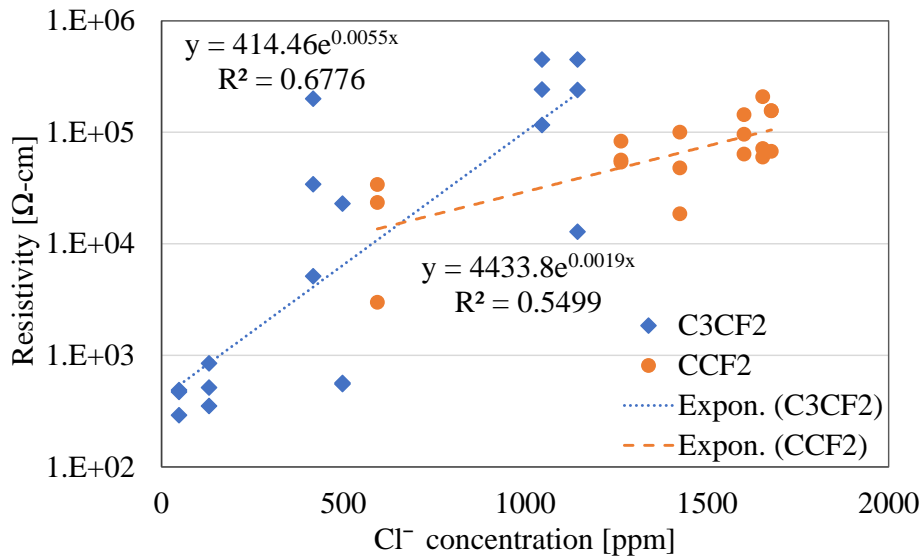


Figure 5-8 Chloride concentration and resistivity relationship of the hybrid cement composite sensing capability

5.3.2 Mortar embedded hybrid cement composite sensors

5.3.3.1 Ion chromatograph

Figure 5.9 shows the chloride concentration in ppm based on the depth of the specimens. Three reinforced mortar specimens were fabricated without embedding the hybrid sensors inside the mortar. However, all three samples were subjected to all the conditions, which the mortar specimen with embedded sensors experienced. This was done in order to drill the samples without affecting the sensors. For the accuracy and homogeneity of the test throughout the cross-sectional area, each of the specimens was drilled in 3 different places and profiled in 5 mm difference at a maximum depth of 40 mm.

The ion chromatography result shows a lower concentration of chloride in general. The initial 5 mm and 10 mm showed a higher concentration of chloride around 600 mg/kg to 800 mg/kg. Except for sample 3, which showed oddly higher concentration in 10 mm depth that is around

1200 mg/kg. Below this depth, the concentration of chloride is mostly less than 600 mg/kg, and this gets lower while the depth increased having a minimum of 80 mg/kg approximately. In addition, in the previous section of rapid chloride penetration, the response of resistivity was low for most of the cases having low chloride concentration below 600 mg/kg.

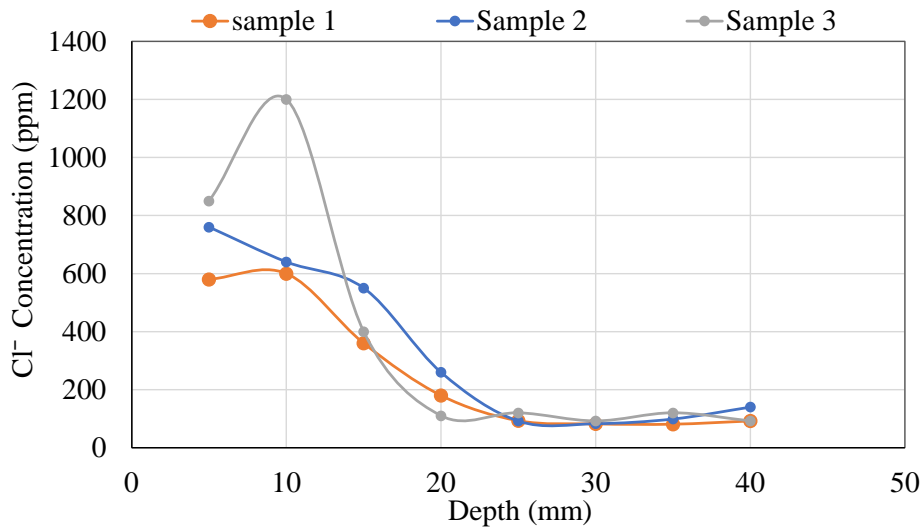


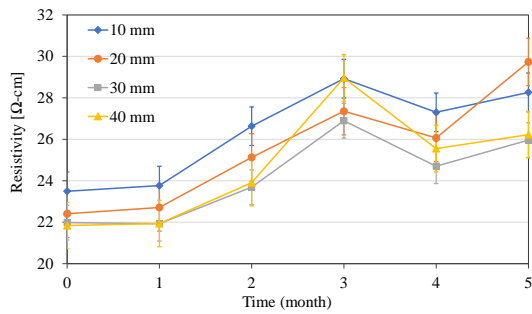
Figure 5-9 Chloride concentration of each profiling depth of the hybrid cement composites based on ion-chromatography test result

Furthermore, the specimens are not yet at there full penetration depth, which is currently six months for all specimens. Until now, the chloride has reached at 10 mm depth where the sensors can pick the change; however, 10 mm is just the first sensors front side, which might take some time for the first sensors row to pick the change. Please note that this is a time taking experiment, which usually takes a year or two for specimens with 0.5 water to cement ratio to reach the full depth of the sensors.

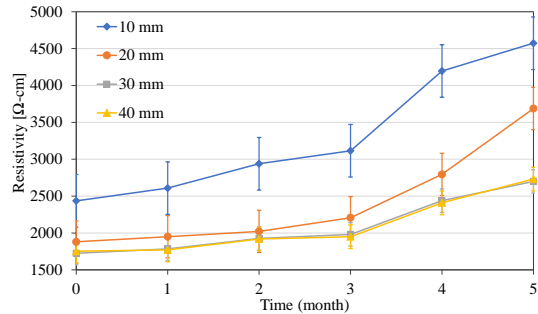
5.3.3.2 Resistivity and chloride concentration relation

Even though, the chloride concentration that have reached the sensors is very low to be picked by the sensors but here are some of the initial stages that are showing the capability of the hybrid cement composite sensors seen in the rapid chloride penetration test done earlier. Figure 5.10 a and b shows the resistivity of 10 mm, 20 mm, 30mm, and 40 mm depth sensors change in 6 month period including the initial measurement before immersing the specimens inside the chloride solution. The most overwhelming and noteworthy to take note of is that of all the 32 embedded sensors inside the mortar samples, not a single sensors have failed to do. This shows the high reliability and sustainability of the sensors during the 6-month cycle. On top of that, Since the chloride concentration that reached the sensors is low, the change was very low as well. In general, while comparing the initial resistivity with the last resistivity measurement taken, a slight and negligible increase was seen in the result clearly.

On the other hand, a measurement was taken on a row of 4 sensors, which are connected in series. They are measured as a single circuit, as shown in Figure 5.2. The series combination of 4 sensors as a single unit of measurement has given a more clear result on the initial stages. Figure 5.10 (b) shows an increase in resistivity on each depth in general. The most change in resistivity was seen consecutively for 10 mm and 20 mm specimens having a change of 2137 Ω -cm and 1807 Ω -cm, which is roughly two-fold of the initial measurement. For the 30 mm and 40 mm depth of the row sensors, the resistivity has increased as well by half the initial measurement during the last measurement. In addition, the rise in resistivity seen in both graphs was smooth and consistent in time, even if the numbers were quite small to make a conclusion.

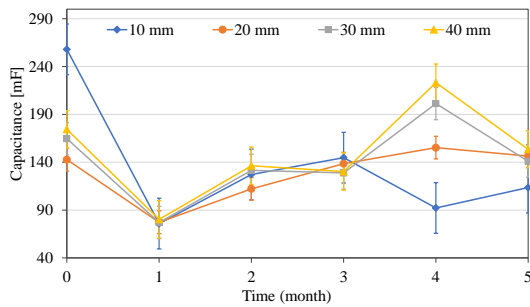


(a)

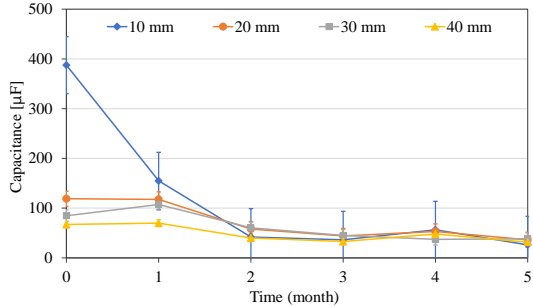


(b)

Figure 5-10 Embedded sensors change of resistivity for chloride monitoring (a) individual sensors result (b) seriously connected sensors result



(a)



(b)

Figure 5-11 Embedded sensors change of capacitance for chloride monitoring (a) individual sensors result (b) seriously connected sensors result

5.3.3.3 Capacitance and chloride concentration relation

This experiment was conducted based on the result of the phase angle seen in the preliminary study of this dissertation. It was seen that the hybrid cement composite has a capacitive sensor property as well. And due to the heterogeneous nature of the concrete, the pores and microcracks might act as a dielectric inside the hybrid composite initiating the capacitance. The infiltration

of substances like water and chloride in the pore structures of the composite or the microcracks could lead to a decrease in the capacitance. In figure 5.11 (a), the results of individual sensors average based on their depth is shown. During the first month of curing the specimens inside a chloride solution, the capacitance has decreased the most from its initial value before curing. However, after that the individual sensors result were shown to increase slightly. Furthermore, during in a row measurement of sensors the same results were obtained like the individual sensors a decrease at the initial age. However, the capacitance further decreased consistently in the later ages, even though the decrease is very small and negligible.

5.3.3 BSE-SEM, EDX, and EPMA analysis

In order to check if the chloride have penetrated the sample the following analysis were taken by immersing the sensor for 3 months in a 10% NaCl solution. The sample were prepared by cutting the specimen in mid-section using a high precision diamond saw. Figure 5.12 and figure 5.13 show the BSE-SEM, EDX, and EPMA mapping images of the CCF2 sample cross-sections. From the result, both hydrated and unhydrated products contain Ca-ion with a slight amount of Si and Al ion. The amount of Al-ion increases on the unhydrated products and the fine aggregate, the same is true for Si and Na, while a negligible amount of S and Fe ion were seen, in general. O-ions were seen all over the area inside the perimeter having higher concentration on fine aggregates. On the other hand, the C-ions were detected on both figures in a scattered pattern throughout the area having higher concentration in most spots in the area, but mostly the carbon fibers were visible. Another data was also seen on the BSE images, that the microcracks observed are uniformly distributed throughout the sample, as shown in appendix c. This will facilitate the chloride intrusion in the composite but, based on the mapping of the Cl-ion it is

clear that Cl^- diffusion had taken place in a slight amount. Meanwhile, the EDX also showed a similar result, giving a concentration of 1.72% from the total mass, as shown in figure 5.12.

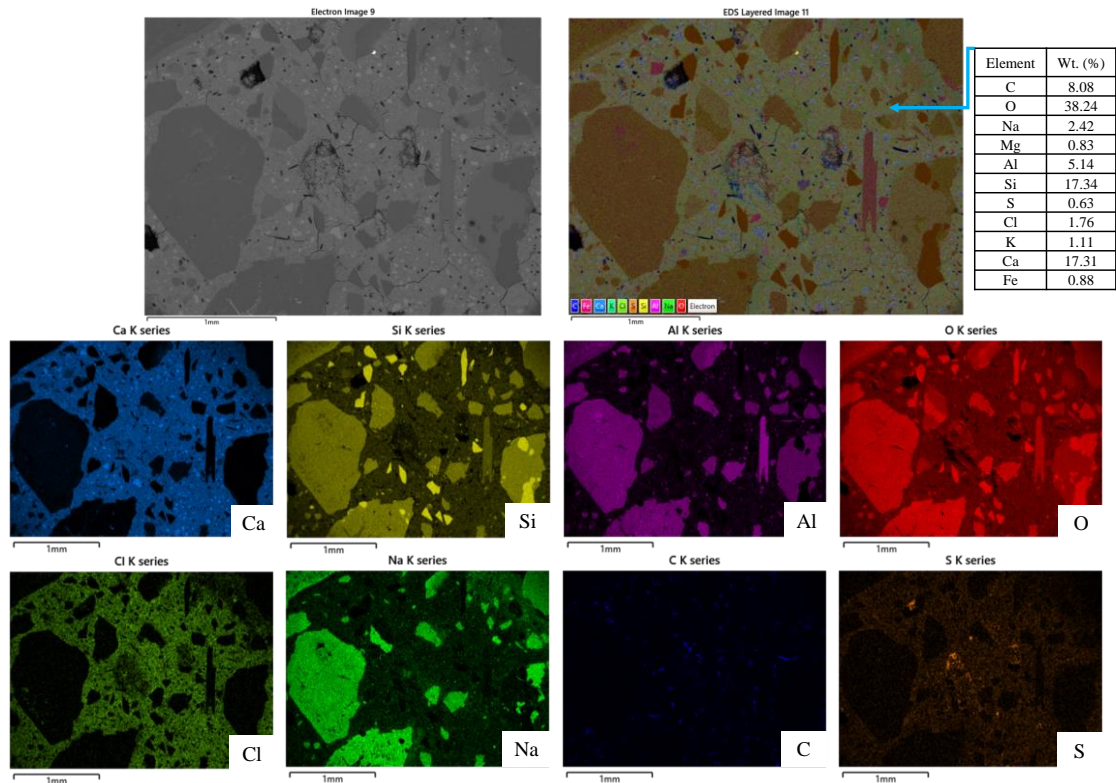


Figure 5-12 BSE-SEM, EDX mapping and element composition of CCF2 hybrid cement composite immersed in chloride for 90 days

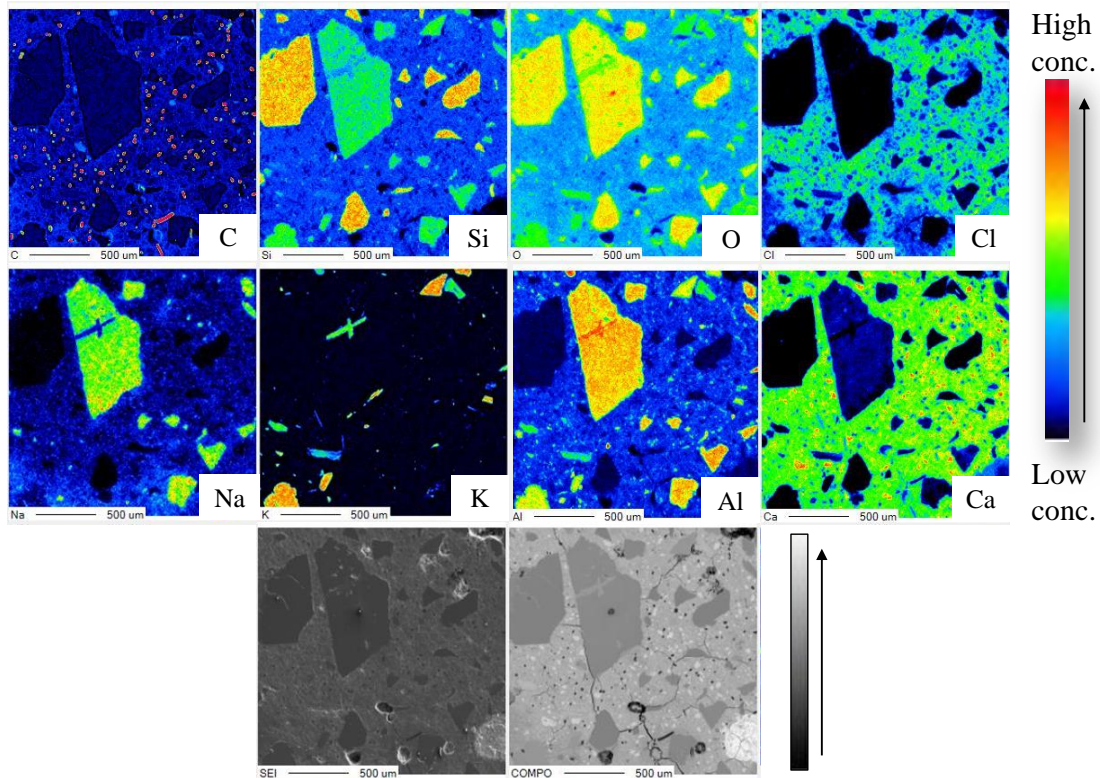


Figure 5-13 BSE-SEM and EPMA image mapping of CCF2 hybrid cement composite immersed in chloride for 90 days

The Cl-ion were also seen in the EMPA mapping all over the hydration products with a more or less constant intensity and images were taken on different levels to analyses the concentration by depth at each point, as shown in figure 5.14. Even though, the brightness is not that much, which shows that the chloride would not have any effect on the hybrid cement composite but the slight concentration that intruded the composite were distributed fairly all over the area of the hybrid cement composite. Furthermore, since the chlorides were intruded from all sides the uniformity was expected on the sides, however, observing the same result on the most center part would have a substantial implication on the sensing ability of the composite. The uniform

distribution of Cl-ion would help the chloride sensing ability by affecting the conductivity not only on the surface but also throughout the sample conductivity network, which will give a more reliable data.

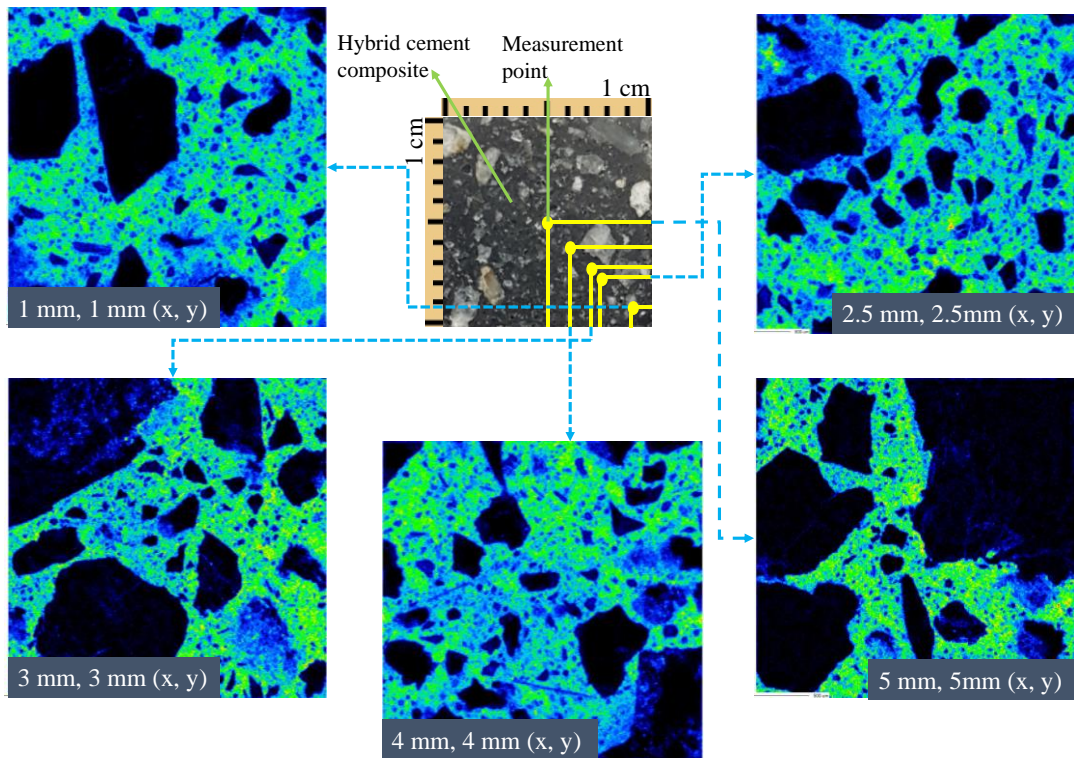


Figure 5-14 Chloride depth mapping in different levels using EMPA image of CCF2 hybrid cement composite immersed in chloride for 90 days

5.4 Discussion

This chapter follows a different approach from most of the studies made earlier to monitor the chloride penetration on a concrete. In this study, the chloride ion was forced to ingress the hybrid cement composite sensor using a customized rapid chloride penetration method. Using this method for cement composites with conductive materials like steel, CNT, or carbon fiber is not

suitable. However, in order to fit the ASTM C1202 standard, the whole setup was redesigned, and the amount of the voltage was also regulated to 10 Volt from 30 Volt to reduce the heat evolution. Furthermore, as a control sample, C3CF2 was used by reducing the amount of CNT by half from the original CCF2 samples. In addition, Knowing how the composite conduct electricity will help to analyze the reaction of the hybrid cement composite for chloride ingress. The ingress of chloride ion and binding to the hydration products would reduce and block the existing highly conductive network of carbon fiber and CNT, which is much conductive than water and chloride solution conductivity. The results also indicate an increase in resistivity as the chloride amount in the matrix increased. Furthermore, as the chloride amount increase in the cement matrix, it would create cracks, which further decrease the conductivity.

After the test, the samples were profiled in a 5 mm thickness perpendicular to the chloride penetration direction. Different approaches were taken in order to analyze the depth of the chloride in the specimen accurately. This is because it is a fundamental step before analyzing the relationship between the conductivity and the penetration depth. Initially, a simple visual inspection was done to check the penetration depth using AgNO_3 . In addition, the total chloride was analyzed using the crashed powder of each profiled depth of chloride penetration in the ion chromatography test, which gives the exact concentration in ppm. Both results have shown a similar result having 10 mm and 25 mm chloride penetration depth for C3CF2 and CCF2

Furthermore, the loss of ignition, non-evaporated water to binder ratio, and porosity were measured with the intention of investigating the chloride effect by chloride penetration depth systematically. However, the loss of ignition was affected by the amount of carbon fiber inside the hardened hybrid cement composite. The high temperature for the ignition that is around 1000

$^{\circ}\text{C}$ will lead the carbon fiber to oxidation at about 400°C 9. However, the non-evaporated water to binder ratio was conducted using a 100°C . The result showed a consistent increase in W_{ne}/B ratio for both specimens as the depth of the specimen increases, especially for CCF2 samples. This could be due to chloride binding and formation of Friedal's salt formation on the initial depth (Kim., 2013). The following statement can be seen by the total intruded volume decrease at 5mm and 10mm while showing the maximum intruded volume at 15 mm and decreased again for the remaining depth. This was seen on both C3CF2 and CCF2 samples. In addition, the total intruded volume increased by 80% due to the chloride ingress for CCF2 samples. However, this is not solely contributed to the chloride ingress rather the effect of the temperature was also another factor for creating microcracks. The formation of microcracks was proven through visual inspection, in addition, the drastic increase of large pores($>100\text{nm}$) in the intruded volume was also another proof compared to the C3CF2 specimens having a regular porosity distribution throughout the depth. From the result, it was clear that the rapid chloride penetration test was sensitive for conductive fillers inside the composite (Stanish et al., 2001; Ahmad and Kumar, 2013). However, since the effect was uniform through the depth of CCF2 samples, the conductivity was not affected by the microcracks. In addition, there were no relations between the porosity and chloride concentration, which gives an advantage to analysis the chloride concentration data in terms of the resistivity with minor effects. Note that microcracks were slight or insignificant for C3CF2, which showed a better relationship than the CCF2 having 0.68 coefficient of determination. The following results can confirm that the results can be further improved more by lowering the voltage to reduce the resistance that creates heat evolution (Dalla et al., 2019).

The same is done for the reinforced specimens cured under 10% NaCl for six months. Three samples were tested for ion chromatography by digging three holes in each sample and averaging all. All most all of the profiled depth showed chloride concentration below 600 ppm except for the initial depth, 5 mm. It was clear from the above test, the rapid chloride penetration test, for the chloride samples to achieve major changes in resistivity the chloride concentration should be at list above 600 ppm. Based on this, the embedded samples are yet to sense the chlorides since there is a low concentration. However, based on a series method of measurement, the initial 10 mm row of sensors have picked on the chloride intrusion by an increase in resistivity and a decrease in capacitance.

Moreover, to check if the chloride is intruding the hybrid cement composite, the sample was sectioned in the mid by half, and then on the edge side, the chloride concentration was observed using BSE-SEM and EDX. It was proved that the chloride had penetrated the samples most exterior parts. This was also confirmed clearly through EPMA mapping. It was interesting to find out that the chloride was not only present on the outer part, but also through different point observations, the chloride was found fairly dispersed throughout the composite form the most exterior to the most interior part of the hybrid cement composite. This could be for two reasons, one is that due to the pore connectivity inside the matrix, even though it was not observed in the porosity relationship result and the other is the periodical measurement of resistance might help the ions to be distributed, however, this needs further research to conclude.

5.5 Conclusion

The following conclusions are drawn from the profiling of CNT-CFs hybrid cement composite for sensing capability study using a rapid chloride penetration method, including chloride monitoring study embedding the hybrid cement composite inside a reinforced mortar.

- The chloride depth analysis made using AgNO_3 and ion chromatography has shown more or less very close results. From the results, the majority of chloride concentration was detected at about 10 mm for C3CF2 specimens, and the chloride depth goes as far as 25 mm for CCF2. It is worth mentioning that both the visual inspection and chemical analysis have given similar chloride penetration depth.
- From the pore analysis, more than 80% of the total intruded volume increase as the chloride ingress in the hybrid composite majorly due to pore sizes over 100nm. On the other hand, the capillary pores and mesopores have negligible effects in comparison. This is especially true for CCF2 samples. This indicates the appearance of microcracks in the CCF2 samples during chloride penetration.
- The non-evaporable water to binder ratio has for increased as the depth of chloride ingress increased, showing the effect of the chloride binding on the hybrid cement composite.
- The effect of CNT concentration on the specimens during chloride penetration were seen in the experiments clearly. Even though both C3CF2 and CCF2 were conducted under the same condition, the chloride penetration depth was completely different. This is mainly due to the effect of temperature rise during current flow through the resistive

hybrid cement composite specimens, and it is also responsible for facilitating the microcracks observed in the porosity result.

- During the relationship study for the sensing capability of chloride using hybrid cement composite, the resistivity the have increased as the chloride concentration increased. The sensing capability of the hybrid cement composite R^2 value for C3CF2 and CCF2 were 0.68 and 0.55, respectively. Even though the R^2 value is fair, but the microcracks occurred during the experiment due to high temperature have influenced it to be low.
- Embedded samples change in resistivity have shown a slight increase in resistivity through time. However, since the age of the samples is six months, the samples could change through time. This is true for the capacitance as well. On the other hand, sensors measured in a serious connection by row should clear results on the initial chloride penetration by depth on both the resistivity and capacitance by increasing and decreasing continuously in time.

Chapter 6. Multiple CNT-CFs hybrid cement composite sensors embedded in reinforced mortar for crack and moisture monitoring

6.1 Introduction

As discussed in section 1.1 of this paper, we can understand that most sensors are limited to a specific purpose. However, in this chapter, the capability of hybrid cement composite sensors multifunctional properties will be tasted in terms of crack and moisture. Note that for chloride, the study was discussed in chapter 5. Specifically, the crack sample detection and location, including their healing abilities, will be discussed in detail in this section. However, only an introductory study is done on moisture to show the capability in the area.

6.2 Materials and method

6.2.1 Materials and mix proportions

The same materials and mix proportions will be used in this study, as shown in chapter 5, including the procedure of mixing mentioned in chapter 4. Table 6.1 shows the mix proportions in the chapter.

6.2.2 Experimental methodology

6.2.2.1 Moisture sample

To investigate the moisture, four hybrid cement composite sensors with a cubic dimension ($1\text{ cm} \times 1\text{ cm} \times 1\text{ cm}$) were embedded inside a rectangular mortar specimen of $120\text{ cm} \times 110\text{ cm} \times 140\text{ cm}$ ($W \times H \times L$) as shown in figure 6.1. Each embedded sensor has equal distance from each other in a circular pattern having a small circular inlet in the center, 4 cm depth and 1.5 cm diameter, to measure the moisture level of the inside concrete. Measurement of the relative

humidity was taken using a Vaisala HNP40S probe and a Vaisala HN40 indicator. Before embedding, the sensors were cured inside water for 91 plus days, and after embedding the mortar was cured for another 91 days inside water. Initial measurements were taken at wet and dry state then the samples were placed inside water in a humidity chamber of 80%. This was done to get a higher humidity level inside the mortar specimens. On the other hand, to lower the relative humidity in the mortar silica gel was used due to their high moisture absorption capability. This process was done to decrease the relative humidity progressively from higher relative humidity range to the lower gradually while monitoring the change in the electrical properties continuously.

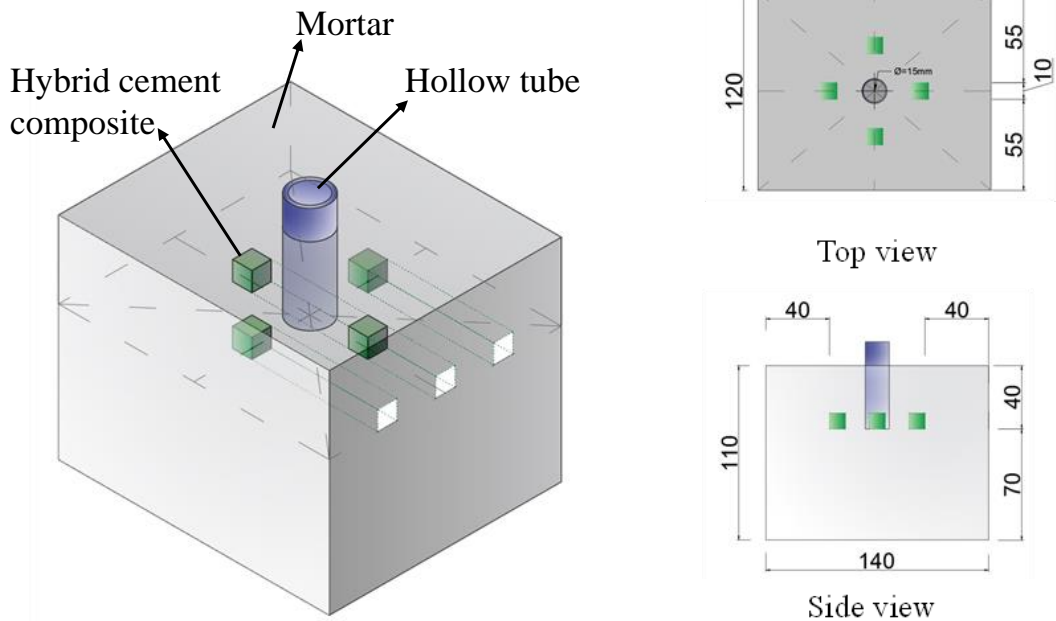


Figure 6-1 Schematic diagram of moisture samples showing the embedded sensors inside a mortar

6.2.2.2 Crack samples

For the crack sample preparation, $2.5 \times 2.5 \times 30$ cm (W \times H \times L) hybrid cement composite specimens were prepared and embedded inside a reinforced mortar specimen with 1 $\phi 10$ mm bar, as shown in Figure 6.2. For each of the rectangular $130 \times 130 \times 340$ (W \times H \times L) mortar specimens, six hybrid composite sensors were embedded inside, three exposed to the lower surface in the tension side and three on the compression side having 30 mm cover from the top surface. Before embedding the hybrid, cement composite was cured inside water for 28 days. After curing, the samples were air-dried to brush silver paste and attach a wire on both ends of the composite and to make the connection of the wire, and composite firm epoxy was applied

on top. Before applying any type of force on the reinforced mortar samples, it was cured for 91 days until it gets its full maturity. Then the samples were tested for three-point flexural bending while monitoring the resistivity of the hybrid cement composites inside the mortar specimen. Furthermore, the samples were left for one month, one in air and one inside water to check the self-healing properties on the conductivity of the cracked samples measuring both AC and DC data.

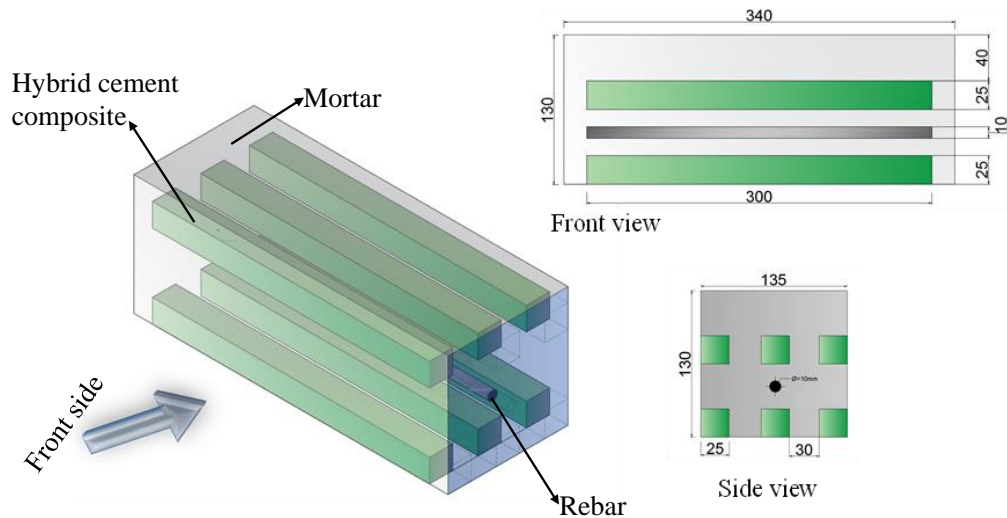


Figure 6-2 Schematic diagram of crack samples showing the embedded sensors inside a reinforced mortar

6.3 Result and discussion

6.3.1 Moisture monitoring

The relative humidity measurement is conducted to show the capability of the CNT cement composite sensing ability beyond the common studies like chloride and crack sensing. Note that this is not a detailed study of moisture sensing and monitoring. In this study, the aim is to show the relationship between the CNT cement composite resistivity and the relative humidity, as

shown in figure 6.3. From the study, the sensors measurement has should a coefficient of determination about 0.7906 with a linear relationship. On the other hand, the mortar measurement between the sensors was fluctuating; however, the result was still straight forward with a coefficient of determination of 0.4197.

In the upcoming studies made on this dissertation of saturated and dried specimens, the benchmark for the change in resistivity was 55 Ω -cm. Any specimen having a resistivity below the benchmark point the resistivity will increase by moisture, and the opposite is true for specimens having initial resistivity above 55 Ω -cm the resistive will decrease as the samples get wet. However, the same things were not observed in this study in both cases, the resistivity have increased as the humidity decreases. This effect is very low in a range of between 40 Ω -cm to 45 Ω -cm for the sensor measurement. This makes it difficult to make a boundary on this small range. However, it is possible to do so, if the samples accuracy and stability can be pushed further from current ± 0.5 Ω -cm precision to a very high ± 0.001 Ω -cm sensitivity. In most literature reviews the CNT cement composite fluctuation is very high, as high as ± 10 Ω -cm to ± 100 Ω -cm on measurements made on the single specimen at different times. In addition, the depth of the sensors used to monitor the moisture were 1cm, this have to be improved by increasing the depth of the hybrid cement composite to get a better result and use the samples as an electrode for the surrounding mortar sample measurement. Please note that this study is a relationship study, not the sensing capability of the hybrid cement composites. The sensing capability is very low, due to the small range between the fully dry sample and saturated sample. In addition, the fluctuation or low sensitivity have their contribution to the sensing capability.

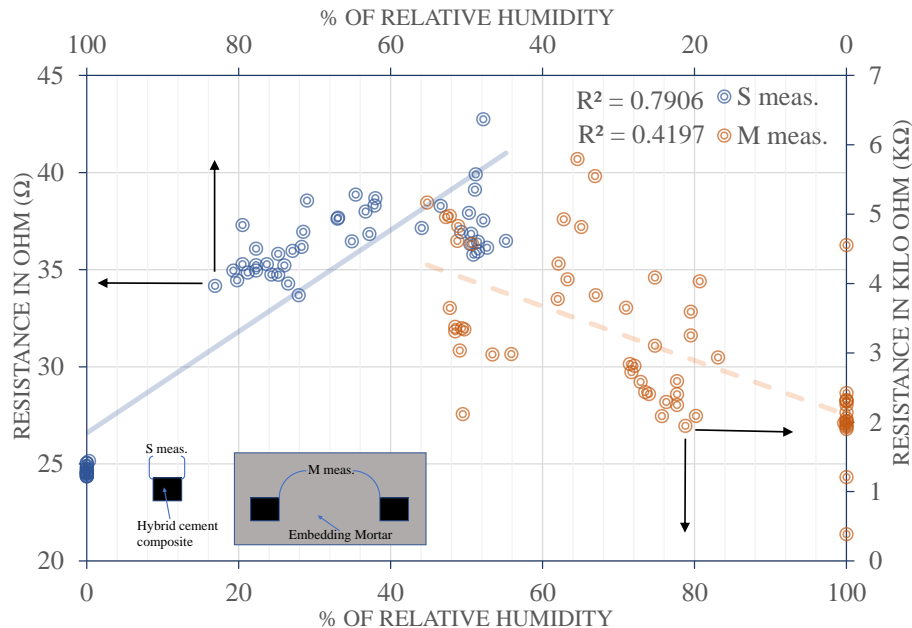


Figure 6-3 Relative humidity and resistance relationship of the hybrid cement composite embedded in reinforced mortar for moisture monitoring

6.3.2 Crack monitoring

The goal of this study, crack monitoring, is not only to show the capability of the hybrid cement composite to detect crack but also to make sure that the sensor is a reliable, durable and above all, sustainable, which can be reliable even after large and multiple cracks were detected. In addition, the sensors would be able to locate the primary position of the crack, including the width of the crack. Furthermore, the effects of moisture and microcracks, which are difficulties in most cement-based composite sensor studies by creating fluctuations on the resistivity data. However, in this study, their effect was kept to the minimum so that the monitoring would not be affected easily.

Note that the measurement methods used throughout the study are shown in figure 6.4. four different kinds of measurement were used: the first is measuring only the hybrid cement

composite, which is sensor measurement [S meas.] from one end to the other. The second is horizontal measurement [H meas.], measuring the conductivity of the surrounding mortar, which is between the two hybrid cement composite sensors used as an electrode. The third and fourth are basically similar to horizontal measurement on their approach but are made in a vertical [V meas.] and cross over [X meas.] directions, as shown in figure 6.4.

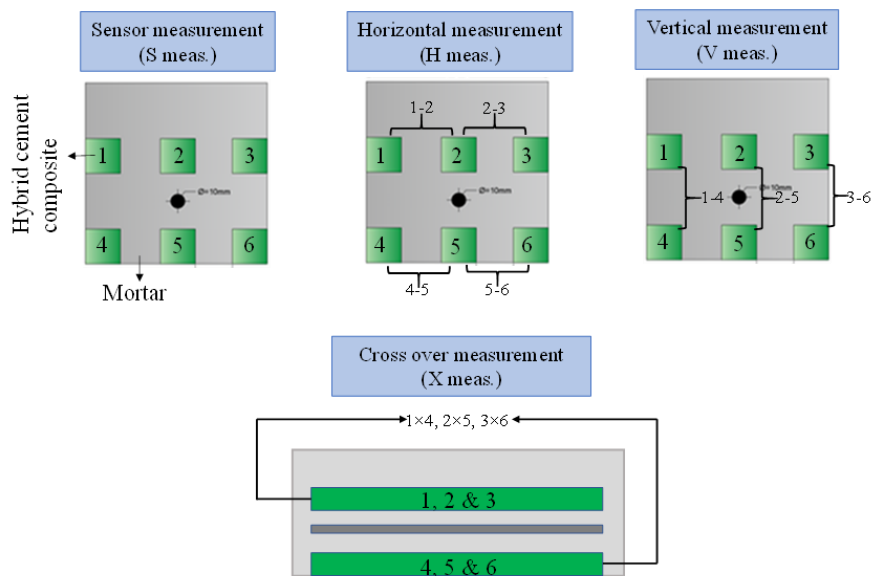


Figure 6-4 Measurement directions of the hybrid cement composite and the mortar between the hybrid cement composites

6.3.2.1 Before cracking (Initial resistivity)

The initial resistivity has been measured in order to check the effect of moisture before cracking the samples. Figure 6.5 shows the change in resistivity by the number of the sensors embedded in the reinforced mortar while in SSD and dry conditions. This was conducted in order to check the effect of moisture and its relation with the initial conductivity of the composite. The measurement was taken in many ways: the first is by directly measuring the hybrid cement

composite sensor embedded inside the reinforced mortar [S meas.], the second and third measurement was done by using the embedded hybrid sensors as an electrode horizontally and vertically, respectively as shown in figure. 6.4 [H meas. & V meas.]. The results from the experiment show that most of the measurements with resistivity above 55 Ω -cm were affected by water inside the reinforced mortar, increasing the conductivity up to 32%. On the other hand, all initial resistivity measurements below 55 Ω -cm showed a decrease in conductivity by the effect of moisture. Note that the effect of the moisture on the sensors were very low that most of the conductivity loss is below 5% with an R^2 of 0.073 showing very low relationship, unlike the vertical and horizontal measurements with an R^2 of 0.614, which is an identical value for both measurements.

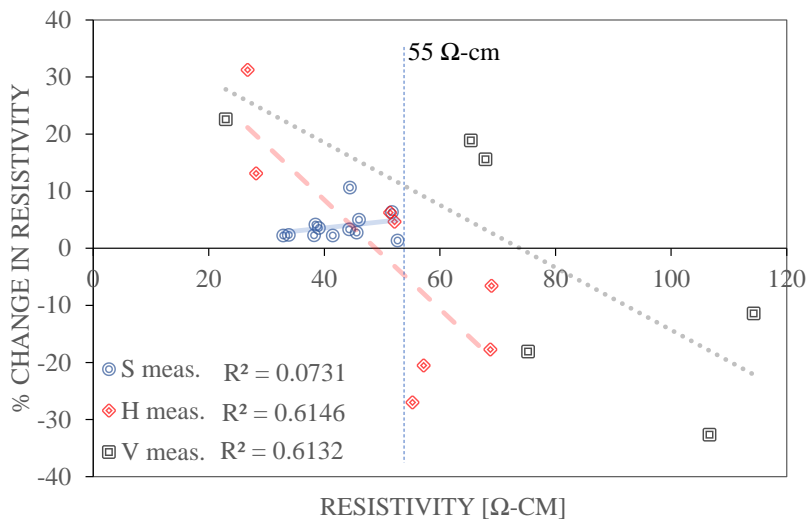


Figure 6-5 Initial resistivity relationship measurement of crack specimens due to change in moisture



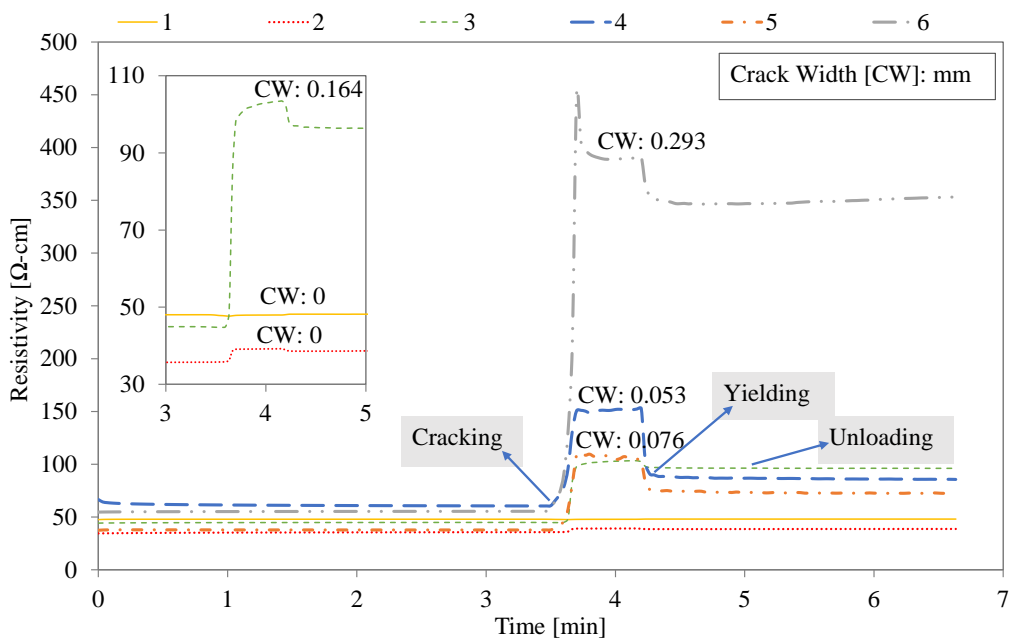
Figure 6-6 Three-point bending test setup and crack propagation directions

6.3.2.2 During cracking (bending test)

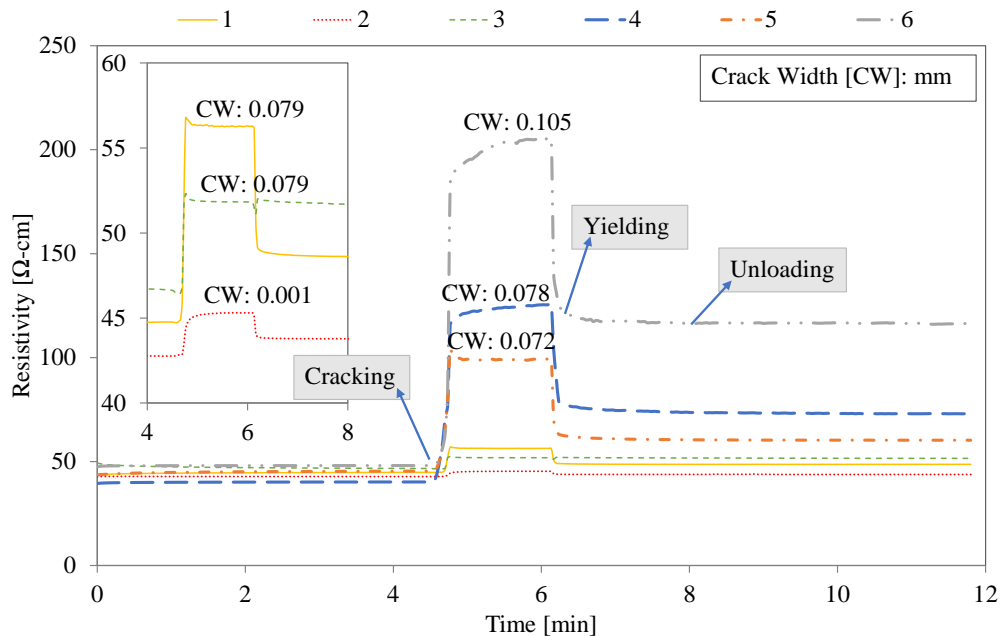
After the initial resistivity measurement, the samples were placed in a three-point bending test, as shown in figure 6.6. During cracking, the resistivity of all the six embedded sensors in the reinforced mortar was measured on a real-time basis simultaneously. After the crack, multiple shear and flexural cracks were seen in the specimens in different locations. These cracks were also investigated by measuring the horizontal and vertical resistivity measurement by using the sensors as an electrode.

Figure 6.7 presents the sensors resistivity measurement while the samples were under crack. As shown from the graph, the resistivity was smooth before the crack happened. This shows the reliability of the sensors to not fluctuate under certain loads. Furthermore, even after the cracks, the conductivity of the sensors were not lost completely or were very high to the extent of that monitoring was not possible anymore, rather the sensors were working with a remarkable performance having only a reasonable resistivity increase due to the cracks. These results are

shown in figure 6.7 a and b with their corresponding width of the crack. For cracks with close to zero width of crack the overall increase in resistivity was very low and in some sample no change at all were recorded. And for the cracks with significant crack width, the resistivity has spiked high during the cracking time and slightly decrease in time and attained a constant resistivity in time after the cracks occurred. For cracks with crack width from 0.05 to 0.3, the resistivity has shown an increase from 100 Ω -cm up to 700 Ω -cm, respectively.



(a)



(b)

Figure 6-7 Real time monitoring of the resistivity change of sensors during a three-point bending test for crack monitoring

Furthermore, the resistivity percentage increase graph in relation to the crack width has shown a tangible result, as shown in figure 6.8, with an R^2 value of 0.825. The crack width has shown a linear relationship with the increase in resistivity due to the crack. This result indicates not only the crack width but also could locate the primary crack area by the number of the sensors location in the reinforced mortar. However, since the number of specimens used in this experiment is low (12 embedded sensors), a further experiment is required in the future with more sensors in order to get even a higher coefficient of determination and to understand the effects of cracks with their respective resistivity increase range.

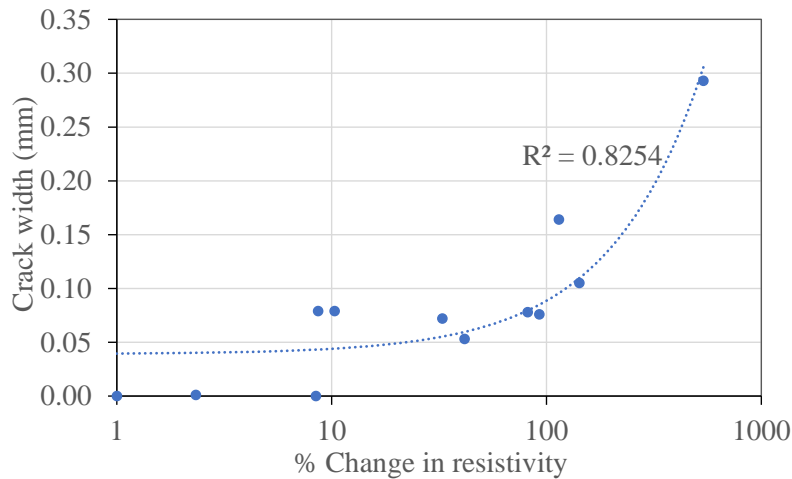


Figure 6-8 Crack width Vs change of resistivity relationship of the hybrid cement composite during cracking

6.3.2.3 After cracking

The vertical, horizontal and cross over measurements of resistivity have also supported the cracking of the specimens by further investigating the dry and wet conditions of the specimens before and after the crack. This result was collected using the embedded hybrid cement composites as an electrode between the concrete. One composite sensor is 3 cm apart from the next sensor, both vertically and horizontally. Following the measurement, figure 6.10 shows the results of both measurements indicating a location of pure mortar that is in between the hybrid cement composite sensors. Even though it was difficult to extract the crack width data between the sensors due to the multiple cracks and many surface fractures, however, a visual inspection was carried out in order to understand the observed data in figure 6.10 a and b.

From the result, it was seen an increase in conductivity when the sample was in a wet condition for most of the cases with resistivity above 55 Ω -cm. The resistivity value for most of the measurements before crack either in dry or wet conditions is below 100 Ω -cm, which is very

conductive and stable. In addition, on locations where no cracks were observed, the fluctuation is slight and insignificant, as shown in figure 6.10 (b) on sample 2. This supports the data measured using only the sensors and the visual observation made on the cracks. It is worth to mention that the numerical data of these results and pictures on all sides of the specimens including the crack width observed are all included as supplementary data in appendix D.

However, once the crack is introduced through the bending test to the specimens, the dry state resistivity has increased significantly, showing the crack occurrence in the designated area in addition to the data spike increase seen while direct monitoring. And after saturating the cracked samples, the resistivity has shown a drastic decrease in resistivity due to water intrusion between the cracks, which will affect the monitoring for cases like underwater monitoring. However, it was possible to identify the cracks even under full saturation by using cross over measurement. During the initial cross over measurement before crack there was no conductivity between the hybrid composites but after the crack due to moisture diffusion through the crack the specimens have started to conduct each other. This result will indicate a crack has occurred and furthermore, it specifies that the crack has also reached the second sensors by indicating the depth of the crack.

Furthermore, before cracking the effect of drying and wetting, the sensors were shown in figure 6.5, having a coefficient of determination 0.0731, which was quite low and insignificant. On top of that, the percentage change is below 5%. Note that the percentage is a resistivity increase by the moisture intrusion, not a reduction in resistivity. This means the effect of moisture on the hybrid cement composite is insignificant, or there was almost no effect on the hybrid cement composite, and also it shows that the sample is intact with no cracks. However, after the samples were subjected to cracks, the result on dry state and wet condition have been changed drastically

based on the crack width, as shown in figure 6.9. The changes have reached up to a maximum of about 80% in an opposite way from the original samples, which means the intrusion of water inside the hybrid cement composite decreases the resistivity of the composite. This indicates the occurrence of cracks in the sample with the respective magnitude of the crack in a change of resistivity by the water. The coefficient of determination has changed to 0.0731 to 0.699 after the samples have cracked.

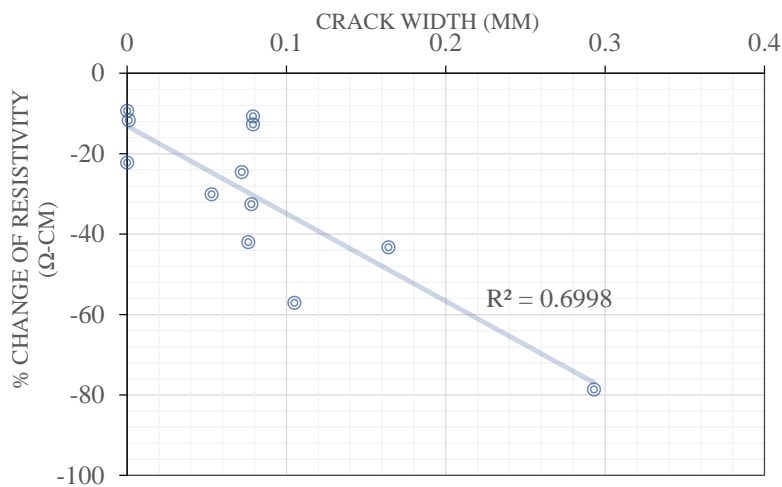
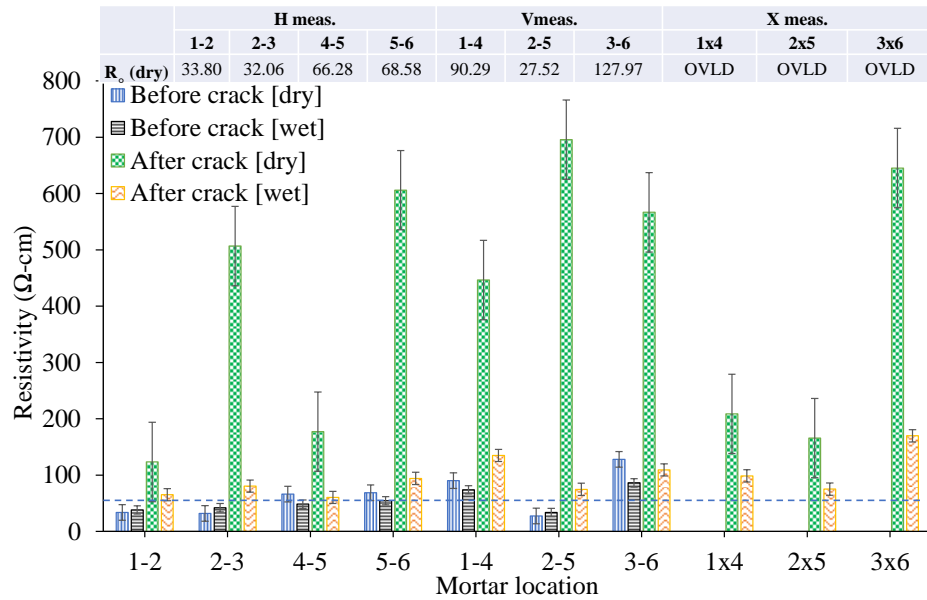
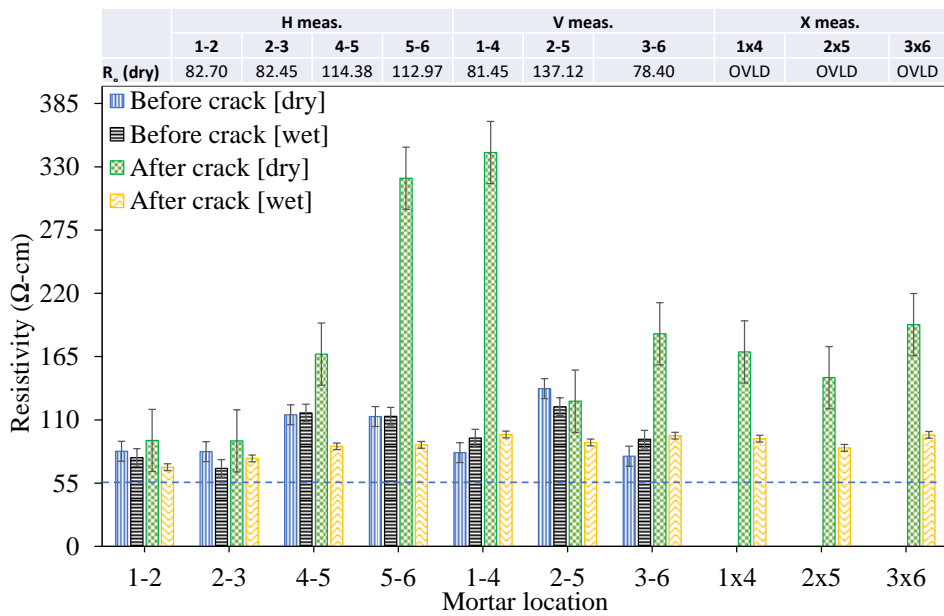


Figure 6-9 Relationship graph of the change on resistivity and crack width based on the effect of moisture



(a)



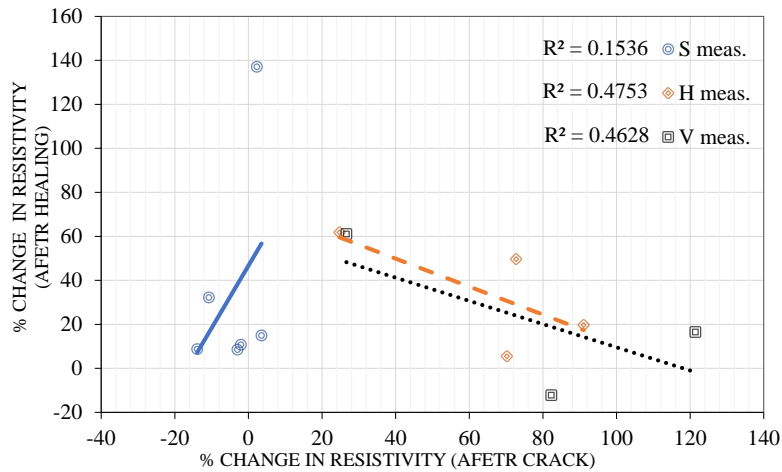
(b)

Figure 6-10 Resistivity measurement of the surrounding mortar using the hybrid cement composite as an electrode: (a) Sample 1 (b) Sample 2

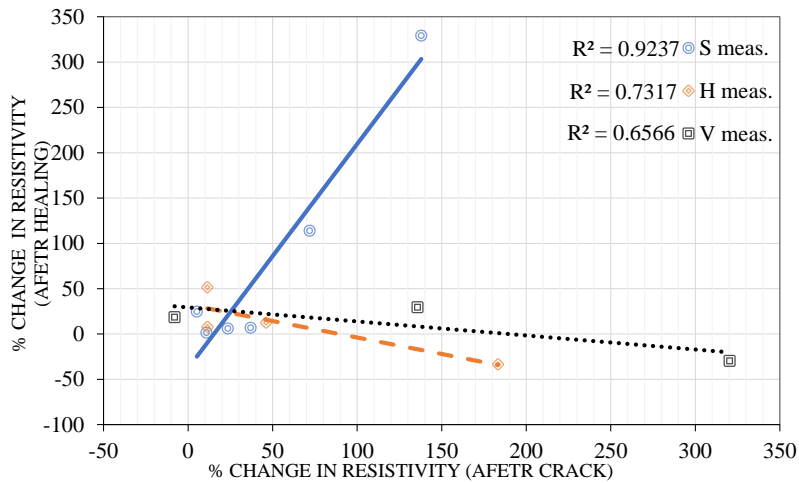
6.3.2.4 Crack Healing

After two months of water curing and air drying, the specimens were measured to check on the healing properties of the hybrid cement composite. The sample cured by air has shown a much better relationship compared to the one cured inside water, as shown in figure 6.11. The sensors measurement has shown a similar pattern for both curing conditions. For a higher initial crack, which indicates a large crack width, the healing response was by an increase in the resistivity. And the reverse was also true for low initial crack resistivity change, the healing change was not significant, or it has no effect on the conductivity of the sample.

Furthermore, during the mortar measurement, which is the vertical and horizontal measurement, the lower the initial crack change the higher the resistivity after healing compared to the result showed by higher initial cracks were a low resistivity change after the healing period. Note that even though the result is consistent for both conditions but the change in resistivity seen on the mortar samples is quite low, especially for the air-dried samples. Based on the visual inspection made on the samples after the healing period, the water cured samples have shown a better healing capability than the air-cured samples. In overall, the healing of both the hybrid composite and the surrounding mortar has a very slight effect on the conductivity for both cases. This could be due to the higher initial conductivity of the hybrid cement composite before and after crack.



(a)



(b)

Figure 6-11 Relationship of the change in resistivity after crack and after healing (a) specimen placed underwater (SSD) (b) specimen placed in the air (Dry)

6.4 Discussion

In this chapter, a detailed study was made to show the multifunctionality of the hybrid cement composite sensors. Especially, the multi-crack and chloride monitoring using numerous sensors in a single reinforced mortar sample, which is first in its kind, including moisture monitoring just to show the capability as shown in figure 6.12. The sensors were not only measured as a single resistive composite but also the sensors were used as an electrode to measure the resistivity of the embedded mortar between the two electrodes at a distance of 3 cm both vertically and horizontally. The most incredible thing is that the resistance between the hybrid cement composite electrodes was very low, a maximum measurement was 450 Ω , and the minimum goes as low as 100 Ω . This needs further detailed investigation on the electrochemical and potential difference study to make concluding remarks on how the current is passing through the insulative surrounding mortar and to analyze what factors contribute to high current passage. Details and full analysis of the following results will be published in an upcoming journal. The following results are very new and would contribute to a new way of approaches in the field. Based on the author's best knowledge, the following results have never been published anywhere else

The crack samples were prepared in order to conduct a three-point flexural strength test for artificial crack creation. The initial moisture effect was investigated before cracking and also after cracking. The hybrid cement composite samples have shown low relation to the moisture. This could be due to the high stable conductivity network inside the cement matrix, mainly attributed to the carbon fiber length. However, the moisture relation that was low before cracking has increased dramatically from 0.07 to 0.7 coefficient of determination as a result of the crack formation and the conductivity network interruption, which indicate crack formation under the

saturated condition as well. On the other hand, while measuring the surrounding mortar (H meas. & V meas.) before cracking, the moisture effect was relatively high due to the insulating properties of the mortar, and the absorption of water by the mortar will increase the conductivity drastically, increasing the relationship.

During cracking the hybrid cement composites inside the reinforced mortar were monitored on a real-time base (S meas.). The result indicated an apparent upsurge in resistivity with respect to the crack width showing a high degree of relation in between with 0.825 coefficient of determination. Moreover, even after crack the samples did not lose their conductivity completely, rather there was a significant amount of conductivity, which could help to tell even after crack during yielding of the reinforcement inside mortar. This could have great application in emergency exit location before a structure fully collapsed by analyzing the resistivity even after crack, one can identify safe exit way until the structure fully collapses. However, the downside of this study is that the piezo-resistivity is quite low and should be improved to identify cracks before formation as the stress and strain increases on the specimen. Future studies should tackle these problems in order to predict cracks before formation as well.

After cracking the samples, a comparison was made to see the relationship between the crack width and the change in resistivity besides the monitoring done while the samples were under based on the moisture relationship from the initial dry state resistivity data (ground zero data) before embedding the samples, which were already discussed above. Furthermore, to check the crossover measurement was used to identify cracks inside saturated conditions. This would help for civil infrastructures, which are constructed under water or could frequently get saturated under heavy rain or flood. Under dry state, the V meas. and H meas. have given a great

indication of crack formation inside the surrounding reinforced mortar with direct measurement, including the S meas. All the measurements showed a direct increase in resistivity as the crack widens, which was confirmed through visual observation. Furthermore, the healing properties of the crack after cured in water and air were also investigated. In overall, the healing of both the hybrid composite and the surrounding mortar has a very slight effect on the conductivity of both cases (saturated curing and dry curing). This could be due to the higher initial conductivity of the hybrid cement composite before and after crack making the healing products conductivity effect negligible.

Unlike the crack monitoring study, the moisture study was done to show only the possibilities and to encourage future studies in this area. So, the study is only done as a kick-start for further studies and to show the multipurpose capability of the hybrid cement composite. In this study, the moisture result was compared with the change in the resistivity of the sensors having a coefficient of determination about 0.79, with only 18 Ω maximum variance. However, the relationship should be improved highly in order to commercialize the hybrid cement composite to the market as a sensor. This can be done by controlling the small range of fluctuation achieved in this research, pushing the fluctuation level furthermore to manipulate the small-scale changes accurately in a $\pm 0.1\Omega$ level to quantify the resistivity easily with the corresponding moisture level with an overall 3 to 5 Ω variance in between 40% to 100% relative humidity. On the other hand, the surrounding mortar measurement should low relationship. This could be improved by increasing the size of the sensors, especially the length, which needs detailed studies in the future to analyze the effect.

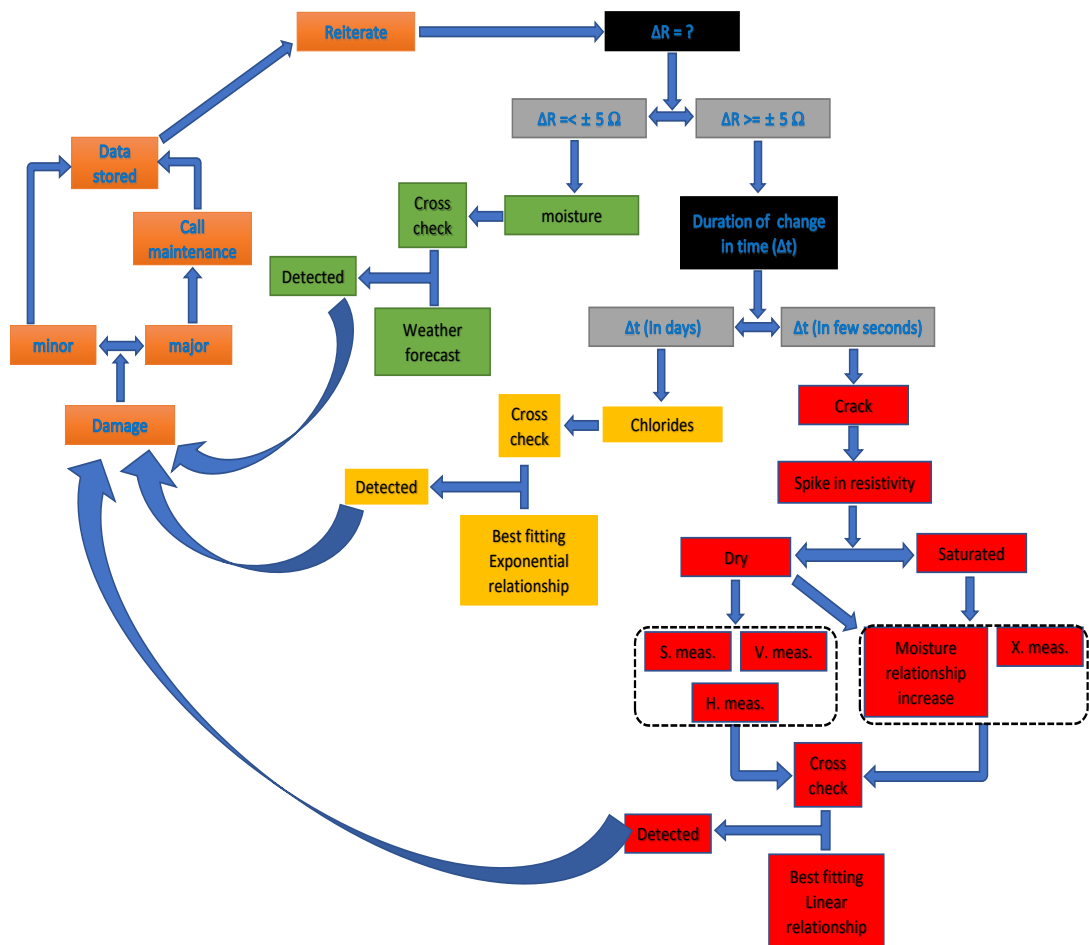


Figure 6-12 Flow chart showing the multi-functionality of the hybrid cement composite to detect crack, chloride, and moisture.

6.4 Conclusion

The following conclusions are drawn from the moisture and chloride monitoring using multiple hybrid cement composites inside a single reinforced mortar.

- The initial resistivity of the crack sensors was not affected by the moisture. However, the surrounding concrete showed a great interaction with the moisture and was easily affected by moisture, while measuring it using the composite sensors as an electrode.

After cracking the sensors exhibited a linear relationship with the saturation of the hybrid cement composite, this is due to the crack formation. The coefficient of determination has improved before and after the crack, 0.0731 and 0.699, respectively indicating crack formation. For the surrounding concrete, the percentage change (by drying and wetting) also gets high after the crack. Furthermore, by using the cross over measurement the cracks were identified even under complete water saturation.

- During cracking, the real-time change was captured while each hybrid cement composite sensors were cracked. A spike was seen in each individual sensor as the load reaches its maximum, and the width of the crack have been correlated directly with the change in resistivity before and after the crack with a coefficient of determination of 0.8254.
- After two months of water curing and air drying, the healing products were observed visually on the samples. From the result, the sample cured under water showed a high rebound after crack, and for the air-dried samples, a relatively low healing properties were observed. However, the overall result is not satisfactory due to the high conductivity of the hybrid cement composite even after crack. It makes it difficult for the healing effect to be significant.
- In general, this multi-crack study showed the capability to detect the width of the cracks in relation to the change in resistivity. The whole studies take more than 6 months, in this time, all the sensors were sound and reliable, not a single sensor has filed throughout the test. In addition, the rough location of the cracks can be done based on the position of the sensors, and using the sensors location the cracks between the sensors

were also identified by locating the crack areas including depth of crack. Unlike most studies, the effect of the microcracks and moisture was kept completely to the minimum with no significant effect.

- For the relative humidity study, the sensors resistance has shown a good relationship with the moisture having a coefficient of determination of 0.7906. And the change in resistance for the surrounding mortar was fluctuated highly due to its low initial conductivity. However, currently, the sensing capability of the hybrid cement composite for the moisture is low, and the fluctuations, which are 0.5 Ω -cm, need to be regulated to a minimum of 0.01 Ω -cm in future studies for a better performance of the sensors.

Chapter 7. Conclusions

7.1 Summary

The nano-science field in material engineering has gained a new way of approach in determining the future through carbon allotropes. Of this, the construction industry is one of them capitalizing on researches that could change the properties of previously known cement composite properties for good. In this dissertation, analytical and experimental studies were made to investigate the characteristics of multi-walled carbon nanotube as a functional filler inside the cement composite. To do so, initially, a pilot study was made to pin-point and recognize the adverse effects through experimental works and previous literature reviews. The pilot experiments were used as a baseline for the preliminary test made to enhance the mechanical and electrical properties of the CNT/cement composite by introducing carbon fiber to the mix, creating a hybrid cement composite. Furthermore, successive tests were done to minimize and avoid the adverse effects proven during the pilot experiments. In general, the main aim of this dissertation is to enhance the CNT/cement composite sensors, reliability, sensing capability, and multifunctionality using pitch-based carbon fiber.

The proposed hybrid cement composite eliminates most of the shortcomings that exist in current researches to develop reliable cement-based composite sensors. The following conclusions can be drawn from the studies made in this dissertation.

Unwanted electrical fluctuation of CNT/cement composite using CNT as a sole agent: Pilot experiment.

- A series of experiments were carried out, mixing and immersing of CNT/cement composites with NaCl particles and chloride solution, accelerated carbonation test to assess the carbonation effects, and effect of the rebar on the electrical behavior of the CNT/cement composite embedded in a mortar specimen. In this study, different experiments have been conducted to assess the possible causes of CNT/cement composite sensors to fluctuate. Of this, the ununiformed dispersion of CNT in a cement matrix could influence the electrical properties of the composite, microcracking leads to a partial disconnection CNT network affecting the electrical properties of CNT/cement composites and this was worsened on paste type composites, due to cement hydration in time the hydration products could be filled between CNT (tunnel blockage effect) creating fluctuations, based on the electrode type debonding can grow between the interface of the composite and electrode affecting measurement results, Interfacial void around composite sensor embedded in concrete or mortar specimens can induce the possibility for resistance fluctuation, and moisture contents in cement composite (also correlated with polarization and ion flow) have a strong influence on the electrical properties of CNT composites. In addition, the electrical properties of CNM/cement composite sensors may be changed by the damage of the sensor itself, which induced by freezing and thawing, acid, and other chemical attacks from outside or ASR.

Reliability of CNT-CFs hybrid cement composite on dimensional stability and electrical stress-strain sensing capability

- The reliability study by stress-strain sensing of CNT-CFs hybrid cement composite has shown significant improvements. Besides the piezoresistive properties of the hybrid cement composite, a slight capacitive property was also observed on the composites. The mechanical strength has shown a significant increase while the carbon fiber increase in the mixture. A comparison made between the silver and stainless-steel electrode was unmatched even from the beginning. The steel electrodes have shown a huge fluctuation and higher resistivity than the silver paste electrodes, which showed a steady and low resistivity throughout the test. During the shrinkage cycle, the hybrid cement composites have shown lower deformation without any major defects compared to other studies. Furthermore, the CCF2 samples showed the lowest deformation of all the samples. During the sensing capability study of the hybrid cement composite, most of the hybrid composites have shown an R^2 of above 0.71 and 0.48 for phase one and two, respectively. The most noteworthy relationship was seen for CCF2, R^2 of 0.9, and 0.87 for both phases, consecutively. Cracked hybrid cement composite specimens were seen to be healed within one-month water curing. (freeze-thaw)

Chloride profiling and conductivity relation of CNT-CFs hybrid cement composite following the rapid chloride penetration test and monitoring evaluation

- The chloride depth analysis made using AgNO_3 and ion chromatography has shown more or less very close results. From the pore analysis, more than 80% of the total intruded volume increases as the chloride ingress in the hybrid composite majorly due to pore sizes over 100nm, and especially this is true for CCF2 samples. This indicates the appearance of microcracks in the samples during chloride penetration. The degree

of hydration for both samples increased as the depth of chloride ingress increased despite the chloride content. The effect of CNT concentration on the specimens during chloride penetration was seen in the experiments clearly. Even though both C3CF2 and CCF2 were conducted under the same condition, the chloride penetration depth was completely different. This is mainly due to the effect of temperature rise during current flow through the resistive hybrid cement composite specimens, and it is also responsible for facilitating the microcracks observed in the porosity result. During the relationship study for the sensing capability of chloride using hybrid cement composite, the resistivity the have increased as the chloride concentration increased. The sensing capability of the hybrid cement composite R2 value for C3CF2 and CCF2 were 0.68 and 0.55. Even though the R2 value is fair, but the microcracks occurred during the experiment due to high temperature have influenced it to be low. Embedded samples change in resistivity have shown a slight increase in resistivity through time. On the other hand, sensors measured in a serious connection by raw showed clear results on the initial chloride penetration by depth on both the resistivity and capacitance by increasing and decreasing continuously in time.

Multiple CNT-CFs hybrid cement composite sensors embedded in reinforced mortar for crack and moisture monitoring

- The effect of moisture was insignificant for uncracked hybrid cement composite sensors; however, the surrounding concrete showed a great interaction with the moisture and was easily affected by moisture, while measuring it using the composite sensors as an electrode. On the other hand, after cracking the sensors exhibited a linear relationship

with the saturation of the hybrid cement composite sensors due to crack formations. During cracking, a spike was seen in each individual sensor as the load reaches its maximum, and the width of the crack has been correlated directly with the change in resistivity before and after the crack with a coefficient of determination of 0.7775. After two months of water curing and air drying, the healing products were observed visually on the samples. From the result, the sample cured under water showed a high rebound after crack, and for the air-dried samples, a relatively low healing properties were observed. However, the result was not satisfactory due to the high conductivity of the hybrid cement composite even after crack makes it difficult for the healing effect to be significant and noticeable. In addition, the location of the cracks can be located based on the position of the sensor, and using the location of the sensor, the cracks between the sensors were also investigated by locating the crack areas. Unlike most studies, the effect of the microcracks and moisture was kept completely to the minimum with no significant effect.

- For the relative humidity study, the sensors resistance has shown a good relationship with the moisture having a coefficient of determination of 0.7906. And the change in resistance for the surrounding mortar was fluctuated highly due to its low initial conductivity. However, currently, the sensing capability of the hybrid cement composite for the moisture is low and the fluctuations, which are $0.5 \Omega\text{-cm}$, need to be regulated to a minimum of $0.01\Omega\text{-cm}$ in future studies for a better performance of the sensors. On the other hand, the carbonation study has shown no change in resistivity, which can be contributed to the carbonation effect confidently. This could be due to the highly distributed conductive network using the CNT and carbon fiber networks,

making the electrolytes conductivity inside pores less significant compared to the previous study only on the CNT-based cement composite sensors without the carbon fiber.

7.2 Recommendations

These are some of the recommendations for using hybrid cement composite sensors.

- (i). Even though, the key for creating conductivity cement composite is CNT however, using CNT as a sole agent for the electrical conductivity would affect the stability due to weak conductivity network inside the cement matrix. This has been improved by using pitch-based carbon fiber inside the matrix and enhancing the conductive network, which will help in avoiding moisture and minor microcrack effects. Furthermore, it will boost the mechanical properties as well.
- (ii). Due to the dynamic and heterogeneous nature of concrete, achieving a low resistivity is quite essential in order to control the hybrid cement composite inside concrete structures for a long period of time. The reliability of the hybrid cement composition has been proven to be satisfactory in this study. In addition, even after cracking the samples maintain to conduct electricity, which shows its sustainability.
- (iii). To enhance the sensing capability of hybrid cement composite, rather than increasing the conductivity, it would be better to control the fluctuation rate even further from the current $\pm 2.5\%$ in this study to at list less than $\pm 1\%$. This will enhance the sensing capability and increase the coefficient of determination. Furthermore, this will open new opportunities by broadening the small ranges of change (like $0.05 \Omega\text{-cm}$) to significant data that can clearly indicate the moisture, carbonation or very minor microcracks.

7.3 Future studies

In this dissertation, the reliability and monitoring capability of multipurpose CNT-CF cement composite sensor for concrete structures

- (i). The reliability and sensing capability of the hybrid cement composite in this study have been made very carefully with a limited number of specimens. However, this should be assessed by mass testing and practical field tests.
- (ii). Most researchers claim the resistivity of their composite materials based on the samples they are testing at the moment. This can be true for homogenous materials like iron, gold, or silver. However, cement composite is a heterogeneous material, which has many constituents for its production, and its resistivity does not change linearly as the length of the cement composite specimen increases. For this reason, the author recommends for its standardization on future studies by using known length, width, and thickness for uniformity.
- (iii). In order to stabilize the conductivity measurements made on a single specimen, the accuracy should be a priority. To achieve that, the conductive network should be uniformly distributed, and the porosity of the specimens should also be controlled to reduce the reactance due to the capacitive properties of the composite using artificial admixtures.
- (iv). In this study, the hybrid cement composites have been used as an electrode, especially for crack and moisture monitoring to measure the surrounding mortar conductivity. This is a new approach in the area, which encourages vast future researches to be done for different applications.

(v). Overall, the following study target on crack monitoring is not only achieving a higher coefficient of determination, instead to show multiple ways of crack monitoring and data accusation from sensors to sensors communication as well. This could lead to enormous data collation from different sources, and by utilizing the vast information gathered, it is possible to increase the coefficient of determination furthermore with a high accuracy using Big data or/and data science on future studies. This would help our conclusion not to rely on a single data source or sensor.

References

- [1]. Ahmad, A., & Kumar, A. (2013). Chloride ion migration/diffusion through concrete and test methods. *International Journal of Advanced Scientific and Technical Research*, 6(3), 151-180.
- [2]. Al-Mufadi, F., & Sherif, H. A. (2019). Effect of Multiwalled Carbon Nanotubes on Sensing Crack Initiation and Ultimate Strength of Cement Nanocomposites. *Arabian Journal for Science and Engineering*, 44(2), 1403-1413.
- [3]. Angst, U., Elsener, B., Larsen, C. K., & Vennesland, Ø. (2009). Critical chloride content in reinforced concrete—a review. *Cement and concrete research*, 39(12), 1122-1138.
- [4]. ASTM, C. (2012). Standard test method for electrical indication of concrete's ability to resist chloride ion penetration. *STM International, West Conshohocken, PA, C1202–18*.
- [5]. ASTM, E2983. (2019). Standard guide for application of acoustic emission for structural health monitoring. *ASTM International, West Conshohocken, PA, 03(04)*.
- [6]. Azhari, F. (2008). Cement-based sensors for structural health monitoring. *Doctoral dissertation, University of British Columbia*.
- [7]. Azhari, F., & Banthia, N. (2010, June). Structural health monitoring using piezoresistive cementitious composites. In *Proceedings of the 2nd International Conference on Sustainable Construction Materials and Technologies*. Ancona, Italy.
- [8]. Azhari, F., & Banthia, N. (2012). Cement-based sensors with carbon fibers and carbon nanotubes for piezoresistive sensing. *Cement and Concrete Composites*, 34(7), 866-873.
- [9]. Azhari, F., & Banthia, N. (2017). Carbon Fiber-Reinforced Cementitious Composites for Tensile Strain Sensing. *ACI Materials Journal*, 114(1).
- [10]. Bamforth, P. B., Price, W. F., & Emerson, M. (1997). *International Review of Chloride Ingress Into Structural Concrete: A Trl Report (Trl 359)*. Thomas Telford.
- [11]. Bartels, K. A., Dynes, C. P., Lu, Y., & Kwun, H. (1999). Evaluation of concrete reinforcements using magnetostrictive sensors. In *Nondestructive Evaluation of Bridges and Highways III: International Society for Optics and Photonics*, 3587, 210-218.
- [12]. Bernholc J, Brenner D, Buongiorno Nardelli M, Meunier V, Roland C. Mechanical and electrical properties of nanotubes. *Annual Review of Materials Research*. 2002 Aug; 32(1):347-75.
- [13]. Boncel, S., & Koziol, K. K. (2014). Enhanced graphitization of c-CVD grown multi-wall carbon nanotube arrays assisted by removal of encapsulated iron-based phases under thermal treatment in argon. *Applied surface science*, 301, 488-491.
- [14]. Bowen, C. R., & Almond, D. P. (2006). Modelling the 'universal' dielectric response in heterogeneous materials using microstructural electrical networks. *Materials Science and Technology*, 22(6), 719-724.
- [15]. Cao, J., & Chung, D. D. L. (2003). Colloidal graphite as an admixture in cement and as a coating on cement for electromagnetic interference shielding. *Cement and Concrete Research*, 33(11), 1737-1740.

- [16]. Cao, J., & Chung, D. D. L. (2004). Electric polarization and depolarization in cement-based materials, studied by apparent electrical resistance measurement. *Cement and Concrete Research*, 34(3), 481-485.
- [17]. Chacko, R. M., Banthia, N., & Mufti, A. A. (2007). Carbon-fiber-reinforced cement-based sensors. *Canadian Journal of Civil Engineering*, 34(3), 284-290.
- [18]. Chang, C. F., & Chen, J. W. (2006). The experimental investigation of concrete carbonation depth. *Cement and Concrete Research*, 36(9), 1760-1767.
- [19]. Chen, G., Lei, J., Du, Y., & Chen, X. (2018). Synthesis of a novel polycarboxylate superplasticizer with carboxyl group as side chain terminal group to enhance its clay tolerance. *Journal of Wuhan University of Technology-Mater. Sci. Ed.*, 33(1), 226-232.
- [20]. Chen, G., Lei, J., Du, Y., Du, X., & Chen, X. (2018). A polycarboxylate as a superplasticizer for montmorillonite clay in cement: Adsorption and tolerance studies. *Arabian journal of chemistry*, 11(6), 747-755.
- [21]. Christensen, B. J., Coverdale, T., Olson, R. A., Ford, S. J., Garboczi, E. J., Jennings, H. M., & Mason, T. O. (1994). Impedance Spectroscopy of Hydrating Cement-Based Materials: Measurement, Interpretation, and Application. *Journal of the American Ceramic Society*, 77(11), 2789-2804.
- [22]. Chung, D. D. (2018). *Multifunctional cement-based materials*. CRC Press
- [23]. Chung, D. D. L. (2002). Piezoresistive cement-based materials for strain sensing. *Journal of Intelligent Material Systems and Structures*, 13(9), 599-609.
- [24]. Chung, D. D. L. (2004). Electrically conductive cement-based materials. *Advances in Cement Research*, 16(4), 167-176.
- [25]. Chung, D. D. L. (2012). Carbon materials for structural self-sensing, electromagnetic shielding and thermal interfacing. *Carbon*, 50(9), 3342-3353.
- [26]. Clemente, P. (2017). Seismic isolation: past, present and the importance of SHM for the future. *Journal of Civil Structural Health Monitoring*, 7(2), 217-231.
- [27]. Coppola, L., Buoso, A., & Corazza, F. (2011). Electrical properties of carbon nanotubes cement composites for monitoring stress conditions in concrete structures. In *Applied Mechanics and Materials. Trans Tech Publications Ltd*, 82, 118-123.
- [28]. Cseresnyés, I., Rajkai, K., & Vozáry, E. (2013). Role of phase angle measurement in electrical impedance spectroscopy. *International Agrophysics*, 27(4): 377-383.
- [29]. Cwirzen A, Habermehl-Cwirzen K, Penttala V. Surface decoration of carbon nanotubes and mechanical properties of cement/carbon nanotube composites. *Adv Cem Res* 2008;20(2):65–73.
- [30]. D'Alessandro, A., Rallini, M., Ubertini, F., Materazzi, A. L., & Kenny, J. M. (2016). Investigations on scalable fabrication procedures for self-sensing carbon nanotube cement-matrix composites for SHM applications. *Cement and Concrete Composites*, 65, 200-213.

- [31]. Dalla, P. T., Tragazikis, I. K., Exarchos, D. A., Dassios, K. G., Barkoula, N. M., & Matikas, T. E. (2019). Effect of carbon nanotubes on chloride penetration in cement mortars. *Applied Sciences*, 9(5), 1032.
- [32]. Davis, A., Mirsayar, M., & Hartl, D. (2019). Structural Health Monitoring by Magnetic Sensing in Concrete Structures via Embedded Shape Memory Alloy Components. In *MATEC Web of Conferences EDP Sciences*, 271, 01003.
- [33]. de Medeiros-Junior, R. A., de Lima, M. G., & de Medeiros, M. H. (2015). Service life of concrete structures considering the effects of temperature and relative humidity on chloride transport. *Environment, development and sustainability*, 17(5), 1103-1119.
- [34]. Del, C. C. M., Galao, O., Baeza, F. J., Zornoza, E., & Garcés, P. (2014). Mechanical properties and durability of CNT cement composites. *Materials*, 7(3), 1640-1651.
- [35]. Delatte, N. (Ed.). (2009). *Failure, distress and repair of concrete structures*. Elsevier.
- [36]. Fedorov, A., Lazarev, V., Makhrov, I., Pozhar, N., Anufriev, M., Pnev, A., & Karasik, V. (2015). Structural monitoring system with fiber bragg grating sensors: implementation and software solution. In *Journal of Physics: IOP Publishing Conference Series*, 594(1), 012049.
- [37]. Fukuda T, Arai F, Dong L. Assembly of nanodevices with carbon nanotubes through nanorobotic manipulations. *Proceedings of the IEEE*. 2003 Nov;91(11):1803-18.
- [38]. García-Macías, E., D'Alessandro, A., Castro-Triguero, R., Pérez-Mira, D., & Ubertini, F. (2017a). Micromechanics modeling of the electrical conductivity of carbon nanotube cement-matrix composites. *Composites Part B: Engineering*, 108, 451-469.
- [39]. García-Macías, E., D'Alessandro, A., Castro-Triguero, R., Pérez-Mira, D., & Ubertini, F. (2017b). Micromechanics modeling of the uniaxial strain-sensing property of carbon nanotube cement-matrix composites for SHM applications. *Composite Structures*, 163, 195-215.
- [40]. García-Macías, E., Downey, A., D'Alessandro, A., Castro-Triguero, R., Laflamme, S., & Ubertini, F. (2017c). Enhanced lumped circuit model for smart nanocomposite cement-based sensors under dynamic compressive loading conditions. *Sensors and Actuators A: Physical*, 260, 45-57.
- [41]. Geng, S., Wang, P., & Ding, T. (2011). Impedance characteristics and electrical modelling of multi-walled carbon nanotube/silicone rubber composites. *Composites Science and Technology*, 72(1), 36-40.
- [42]. Gu, P., Xu, Z., Xie, P., & Beaudoin, J. J. (1993). Application of AC impedance techniques in studies of porous cementitious materials:(I): influence of solid phase and pore solution on high frequency resistance. *Cement and Concrete Research*, 23(3), 531-540.
- [43]. Ham, S., & Popovics, J. S. (2015). Application of micro-electro-mechanical sensors contactless NDT of concrete structures. *Sensors*, 15(4), 9078-9096.
- [44]. Han, B., & Ou, J. (2007). Embedded piezoresistive cement-based stress/strain sensor. *Sensors and Actuators A: Physical*, 138(2), 294-298.

- [45]. Han, B., Sun, S., Ding, S., Zhang, L., Yu, X., & Ou, J. (2015). Review of nanocarbon-engineered multifunctional cementitious composites. *Composites Part A: Applied Science and Manufacturing*, 70, 69-81.
- [46]. Han, B., Yu, X., & Ou, J. (2010). Effect of water content on the piezoresistivity of MWNT/cement composites. *Journal of materials science*, 45(14), 3714-3719.
- [47]. Han, B., Zhang, K., Yu, X., Kwon, E., & Ou, J. (2011). Fabrication of piezoresistive CNT/CNF cementitious composites with superplasticizer as dispersant. *Journal of Materials in Civil Engineering*, 24(6), 658-665.
- [48]. Han, B., Zhang, K., Yu, X., Kwon, E., & Ou, J. (2012). Electrical characteristics and pressure-sensitive response measurements of carboxyl MWNT/cement composites. *Cement and Concrete Composites*, 34(6), 794-800.
- [49]. Hawreen, A., Bogas, J. A., & Dias, A. P. S. (2018). On the mechanical and shrinkage behavior of cement mortars reinforced with carbon nanotubes. *Construction and Building Materials*, 168, 459-470.
- [50]. He, X., & Shi, X. (2008). Chloride permeability and microstructure of Portland cement mortars incorporating nanomaterials. *Transportation Research Record*, 2070(1), 13-21.
- [51]. Hoheneder, J., Flores-Vivian, I., Lin, Z., Zilberman, P., & Sobolev, K. (2015). The performance of stress-sensing smart fiber reinforced composites in moist and sodium chloride environments. *Composites Part B: Engineering*, 73, 89-95.
- [52]. Hu, B., Kundu, T., Grill, W., Liu, B., & Toufigh, V. (2013). Embedded piezoelectric sensors for health monitoring of concrete structures. *ACI Materials Journal*, 110(2), 149.
- [53]. Hunkeler, F. (1996). The resistivity of pore water solution—a decisive parameter of rebar corrosion and repair methods. *Construction and Building Materials*, 10(5), 381-389.
- [54]. Jang, S. H., Hochstein, D. P., Kawashima, S., & Yin, H. (2017). Experiments and micromechanical modeling of electrical conductivity of carbon nanotube/cement composites with moisture. *Cement and Concrete Composites*, 77, 49-59.
- [55]. Jennings, H. M., Bullard, J. W., Thomas, J. J., Andrade, J. E., Chen, J. J., & Scherer, G. W. (2008). Characterization and modeling of pores and surfaces in cement paste. *Journal of Advanced Concrete Technology*, 6(1), 5-29.
- [56]. Jianlin, L., Qiuyi, L., Shunjian, C., Lu, L., Dongshuai, H., & Chunwei, Z. (2017). Piezoresistive properties of cement composites reinforced by functionalized carbon nanotubes using photo-assisted Fenton. *Smart Materials and Structures*, 26(3), 035025.
- [57]. Jin, M., Jiang, L., Lu, M., & Bai, S. (2017). Monitoring chloride ion penetration in concrete structure based on the conductivity of graphene/cement composite. *Construction and Building Materials*, 136, 394-404.
- [58]. Jun, Y., Jeong, Y., Oh, J. E., Park, J., Ha, J. H., & Sohn, S. G. (2015). Influence of the structural modification of polycarboxylate copolymer with a low dispersing ability on the set-retarding of Portland cement. *KSCE Journal of Civil Engineering*, 19(6), 1787-1794.

- [59]. Kavitha, S., Daniel, R. J., & Sumangala, K. (2012). Design and analysis of bulk micromachined piezoresistive MEMS accelerometer for concrete SHM applications. *Sensors & Transducers*, 144(9), 62.
- [60]. Khazem, D. A., Kwun, H., Kim, S. Y., & Dynes, C. (2001). Long-range inspection of suspender ropes in suspension bridges using the magnetostrictive sensor technology. In *in Proceedings of the 3rd International Workshop on Structural Health Monitoring: The Demands and Challenges*.
- [61]. Kim HK, Nam IW, Lee HK. Enhanced effect of carbon nanotube on mechanical and electrical properties of cement composites by incorporation of silica fume. *Composite Structures*. 2014 Jan 1;107:60-9.
- [62]. Kim HK. Chloride penetration monitoring in reinforced concrete structure using carbon nanotube/cement composite. *Construction and Building Materials*. 2015 Oct 15;96:29-36.
- [63]. Kim, G. M., Naeem, F., Kim, H. K., & Lee, H. K. (2016a). Heating and heat-dependent mechanical characteristics of CNT-embedded cementitious composites. *Composite Structures*, 136, 162-170.
- [64]. Kim, G. M., Nam, I. W., Yang, B., Yoon, H. N., Lee, H. K., & Park, S. (2019). Carbon nanotube (CNT) incorporated cementitious composites for functional construction materials: The state of the art. *Composite Structures*, 111244.
- [65]. Kim, G. M., Yang, B. J., Ryu, G. U., & Lee, H. K. (2016b). The electrically conductive carbon nanotube (CNT)/cement composites for accelerated curing and thermal cracking reduction. *Composite Structures*, 158, 20-29.
- [66]. Kim, H. K. (2015). Chloride penetration monitoring in reinforced concrete structure using carbon nanotube/cement composite. *Construction and Building Materials*, 96, 29-36.
- [67]. Kim, H. K., Nam, I. W., & Lee, H. K. (2014d). Enhanced effect of carbon nanotube on mechanical and electrical properties of cement composites by incorporation of silica fume. *Composite Structures*, 107, 60-69.
- [68]. Kim, H. K., Park, I. S., & Lee, H. K. (2014). Improved piezoresistive sensitivity and stability of CNT/cement mortar composites with low water–binder ratio. *Composite Structures*, 116, 713-719.
- [69]. Kim, H. K., Park, I. S., & Lee, H. K. (2014). Improved piezoresistive sensitivity and stability of CNT/cement mortar composites with low water–binder ratio. *Composite Structures*, 116, 713-719.
- [70]. Kim, H. K., Park, I. S., & Lee, H. K. (2014c). Improved piezoresistive sensitivity and stability of CNT/cement mortar composites with low water–binder ratio. *Composite Structures*, 116, 713-719.
- [71]. Kim, H., Park, Y., Choi, D., Chu, W. S., Ahn, S. H., Chun, D. M., & Lee, C. S. (2018). Kinetic spraying of silver nanowire blended graphite powder to fabricate transparent conductive electrode and their application in electrochromic device. *Applied Surface Science*, 456, 19-24.

- [72]. Ko, J. M., & Ni, Y. Q. (2005). Technology developments in structural health monitoring of large-scale bridges. *Engineering structures*, 27(12), 1715-1725.
- [73]. Konsta-Gdoutos MS, Metaxa ZS, Shah SP. Highly dispersed carbon nanotube reinforced cement based materials. *Cement Concr Res* 2010;40(7):1052–9.
- [74]. Konsta-Gdoutos, M. S., & Aza, C. A. (2014). Self sensing carbon nanotube (CNT) and nanofiber (CNF) cementitious composites for real time damage assessment in smart structures. *Cement and Concrete Composites*, 53, 162-169.
- [75]. Lau, K. T., Chan, C. C., Zhou, L. M., & Jin, W. (2001). Strain monitoring in composite-strengthened concrete structures using optical fibre sensors. *Composites part B: engineering*, 32(1), 33-45.
- [76]. Laukaitis, A., Kerienė, J., Kligys, M., Mikulskis, D., & Lekūnaitė, L. (2012). Influence of mechanically treated carbon fibre additives on structure formation and properties of autoclaved aerated concrete. *Construction and building materials*, 26(1), 362-371.
- [77]. Le, J. L., Du, H., & Dai Pang, S. (2014). Use of 2D Graphene Nanoplatelets (GNP) in cement composites for structural health evaluation. *Composites Part B: Engineering*, 67, 555-563.
- [78]. Lee, H. K., Nam, I. W., Tafesse, M., & Kim, H. K. (2019). Fluctuation of electrical properties of carbon-based nanomaterials/cement composites: Case studies and parametric modeling. *Cement and Concrete Composites*, 102, 55-70.
- [79]. Lee, S. J., & Park, J. M. (2017). An experimental study on the structural behaviors of HIRC beams using nickel-titanium SMA wires. *In Key Engineering Materials Trans Tech Publications*, 730, 423-428.
- [80]. Lee, S. J., You, I., Zi, G., & Yoo, D. Y. (2017). Experimental investigation of the piezoresistive properties of cement composites with hybrid carbon fibers and nanotubes. *Sensors*, 17(11), 2516.
- [81]. Lelusz, M. (2014). Carbon nanotubes influence on the compressive strength of cement composites. *Czasopismo Techniczne*.
- [82]. Leng, J., & Asundi, A. (2003). Structural health monitoring of smart composite materials by using EFPI and FBG sensors. *Sensors and Actuators A: Physical*, 103(3), 330-340.
- [83]. Li GY, Wang PM, Zhao X. Mechanical behavior and microstructure of cement composites incorporating surface-treated multi-walled carbon nanotubes. *Carbon* 2005;43(6):1239–45.
- [84]. Li, G. Y., Wang, P. M., & Zhao, X. (2007). Pressure-sensitive properties and microstructure of carbon nanotube reinforced cement composites. *Cement and Concrete Composites*, 29(5), 377-382.
- [85]. Li, H., Xiao, H. G., & Ou, J. P. (2006). Effect of compressive strain on electrical resistivity of carbon black-filled cement-based composites. *Cement and Concrete Composites*, 28(9), 824-828.

- [86]. Li, H., Xiao, H., & Ou, J. (2008). Electrical property of cement-based composites filled with carbon black under long-term wet and loading condition. *Composites Science and Technology*, 68(9), 2114-2119.
- [87]. Lim MJ, Lee HK, Nam IW, Kim HK. Carbon nanotube/cement composites for crack monitoring of concrete structures. *Composite Structures*. 2017 Nov 15;180:741-50.
- [88]. Lin, S. H. (1990). Chloride diffusion in a porous concrete slab. *Corrosion*, 46(12), 964-967.
- [89]. Loyola, B. R., Zhao, Y., Loh, K. J., & La Saponara, V. (2012). The electrical response of carbon nanotube-based thin film sensors subjected to mechanical and environmental effects. *Smart Materials and Structures*, 22(2), 025010.
- [90]. Lynch JP, Loh KJ. A summary review of wireless sensors and sensor networks for structural health monitoring. *Shock and Vibration Digest*. 2006 Mar 1;38(2):91-130.
- [91]. Lynch, J. P., & Loh, K. J. (2006). A summary review of wireless sensors and sensor networks for structural health monitoring. *Shock and Vibration Digest*, 38(2), 91-130.
- [92]. Lynch, J. P., Partridge, A., Law, K. H., Kenny, T. W., Kiremidjian, A. S., & Carryer, E. (2003). Design of piezoresistive MEMS-based accelerometer for integration with wireless sensing unit for structural monitoring. *Journal of Aerospace Engineering*, 16(3), 108-114.
- [93]. Mahdikhani, M., & Bayati, Z. (2008). Application and development of fiber optic sensors in civil engineering. In *The 14th World Conference on Earthquake Engineering*, 12-17.
- [94]. Marchand, J., Pigeon, M., & Setzer, M. J. (1996). *Freeze-thaw durability of concrete*. CRC Press.
- [95]. McCarter, W. J., Starrs, G., & Chrisp, T. M. (2000). Electrical conductivity, diffusion, and permeability of Portland cement-based mortars. *Cement and Concrete Research*, 30(9), 1395-1400.
- [96]. Miloud, B. (2005). Permeability and porosity characteristics of steel fiber reinforced concrete. *Asian Journal of Civil Engineering*, 6(4), 317-330.
- [97]. Mindess, S. (Ed.). (2019). *Developments in the Formulation and Reinforcement of Concrete*. Woodhead Publishing.
- [98]. Mosavinejad, S. G., Barandoust, J., Ghanizadeh, A., & Sigari, M. (2018). Crack detection of a HPCFRCC thin plate using electrical resistivity method. *Construction and Building Materials*, 193, 255-267.
- [99]. Naeem F, Lee HK, Kim HK, Nam IW. Flexural stress and crack sensing capabilities of MWNT/cement composites. *Composite Structures*. 2017 Sep 1;175:86-100.
- [100]. Naeem, F., Lee, H. K., Kim, H. K., & Nam, I. W. (2017). Flexural stress and crack sensing capabilities of MWNT/cement composites. *Composite Structures*, 175, 86-100.

- [101]. Nam, I. W., Kim, H. K., & Lee, H. K. (2012). Influence of silica fume additions on electromagnetic interference shielding effectiveness of multi-walled carbon nanotube/cement composites. *Construction and Building Materials*, 30, 480-487.
- [102]. Nam, I. W., Lee, H. K., & Jang, J. H. (2011). Electromagnetic interference shielding/absorbing characteristics of CNT-embedded epoxy composites. *Composites Part A: Applied Science and Manufacturing*, 42(9), 1110-1118.
- [103]. Nguyen, V. H., & Shim, J. J. (2015). Green synthesis and characterization of carbon nanotubes/polyaniline nanocomposites. *Journal of Spectroscopy*, 2015.
- [104]. Norhasri, M. M., Hamidah, M. S., & Fadzil, A. M. (2017). Applications of using nano material in concrete: A review. *Construction and Building Materials*, 133, 91-97.
- [105]. NT BUILD 492. (1999). Concrete, mortar and cement-based repair materials: Chloride migration coefficient from non-steady-state migration experiments. *Nordtest method*.
- [106]. Olivera, J., González, M., Varga, R., Zhukov, A., & Anaya, J. J. (2014). An embedded stress sensor for concrete SHM based on amorphous ferromagnetic microwires. *Sensors*, 14(11), 19963-19978.
- [107]. Ong YT, Ahmad AL, Zein SH, Tan SH. A review on carbon nanotubes in an environmental protection and green engineering perspective. *Brazilian Journal of Chemical Engineering*. 2010 Jun;27(2):227-42.
- [108]. Oppenheim, I. J., Garrett, Jr, J. H., & Gabriel, K. J. (2000). Potential MEMS applications in civil engineering. *In Space*, 2000, 495-501.
- [109]. Pan, Z., He, L., Qiu, L., Korayem, A. H., Li, G., Zhu, J. W., Collins, F., Li, D., Duan, W.H., & Wang, M. C. (2015). Mechanical properties and microstructure of a graphene oxide–cement composite. *Cement and Concrete Composites*, 58, 140-147.
- [110]. Papadakis, V. G. (2000). Effect of supplementary cementing materials on concrete resistance against carbonation and chloride ingress. *Cement and concrete research*, 30(2), 291-299.
- [111]. Park, H. M., Kim, G. M., Lee, S. Y., Jeon, H., Kim, S. Y., Kim, M., ... & Yang, B. J. (2018). Electrical resistivity reduction with pitch-based carbon fiber into multi-walled carbon nanotube (MWCNT)-embedded cement composites. *Construction and Building Materials*, 165, 484-493.
- [112]. Parveen, S., Rana, S., & Fanguero, R. (2013). A review on nanomaterial dispersion, microstructure, and mechanical properties of carbon nanotube and nanofiber reinforced cementitious composites. *Journal of Nanomaterials*, 80, 3271-3283.
- [113]. Polder, R., Andrade, C., Elsener, B., Vennesland, Ø., Gulikers, J., Weidert, R., & Raupach, M. (2000). Test methods for on-site measurement of resistivity of concrete. *Materials and Structures*, 33(10), 603-611.
- [114]. Powers, T. C. (1968). The thermodynamics of volume change and creep. *Matériaux et Construction*, 1(6), 487-507.

- [115]. Qian, S., Jiang, H., Ding, B., Wang, Y., Zheng, C., & Guo, Z. (2017, March). Synthesis and performances of polycarboxylate superplasticizer with clay-inerting and high slump retention capability. In *IOP Conference Series: Materials Science and Engineering* 182(1) p. 012033.
- [116]. Rainieri C, Fabbrocino G, Song Y, Shanov V. CNT composites for SHM: A literature review. In International workshop: smart materials, structures & NDT in aerospace 2011 Nov (pp. 2-4).
- [117]. Rainieri, C., Fabbrocino, G., Song, Y., & Shanov, V. (2011, November). CNT composites for SHM: a literature review. In *International workshop: smart materials, structures & NDT in aerospace* (pp. 2-4).
- [118]. Rajabzadeh, A., Heusdens, R., Hendriks, R. C., & Groves, R. M. (2019). A method for determining the length of FBG sensors accurately. *IEEE photonics technology letters*, 31(2), 197-200.
- [119]. Reales, O. A. M., & Toledo Filho, R. D. (2017). A review on the chemical, mechanical and microstructural characterization of carbon nanotubes-cement based composites. *Construction and Building Materials*, 154, 697-710.
- [120]. Rhoades, J. D. (1996). Salinity: Electrical conductivity and total dissolved solids. *Methods of Soil Analysis Part 3—Chemical Methods*, 417-435.
- [121]. Ribeiro, R. R., & Lameiras, R. D. M. (2019). Evaluation of low-cost MEMS accelerometers for SHM: frequency and damping identification of civil structures. *Latin American Journal of Solids and Structures*, 16(7).
- [122]. Roberts, M. H. (1962). Effect of calcium chloride on the durability of pre-tensioned wire in prestressed concrete. *Magazine of Concrete Research*, 14(42), 143-154.
- [123]. Saafi, M. (2009). Wireless and embedded carbon nanotube networks for damage detection in concrete structures. *Nanotechnology*, 20(39), 395502.
- [124]. Saafi, M., & Romine, P. (2004). Embedded MEMS for health monitoring and management of civil infrastructure. In *Smart Structures and Materials 2004: Sensors and Smart Structures Technologies for Civil, Mechanical, and Aerospace Systems*: International Society for Optics and Photonics, 5391, 331-343.
- [125]. Safedian, M., & Ramezani-pour, A. A. (2013). Assessment of service life models for determination of chloride penetration into silica fume concrete in the severe marine environmental condition. *Construction and Building Materials*, 48, 287-294.
- [126]. Sanchez, F., & Ince, C. (2009). Microstructure and macroscopic properties of hybrid carbon nanofiber/silica fume cement composites. *Composites science and technology*, 69(7-8), 1310-1318.
- [127]. Sanchez F, Sobolev K. Nanotechnology in concrete—a review. *Construction and building materials*. 2010 Nov 1;24(11):2060-71.
- [128]. Shen, B., Yang, X., & Li, Z. (2006). A cement-based piezoelectric sensor for civil engineering structure. *Materials and Structures*, 39(1), 37-42.

- [129]. Siad, H., Lachemi, M., Sahmaran, M., Mesbah, H. A., & Hossain, K. A. (2018). Advanced engineered cementitious composites with combined self-sensing and self-healing functionalities. *Construction and Building Materials*, 176, 313-322.
- [130]. Simmons, J. G. (1963). Generalized formula for the electric tunnel effect between similar electrodes separated by a thin insulating film. *Journal of applied physics*, 34(6), 1793-1803.
- [131]. Skakalova, V., Kaiser, A. B., Dettlaff-Weglikowska, U., Hrnčarikova, K., & Roth, S. (2005). Effect of chemical treatment on electrical conductivity, infrared absorption, and Raman spectra of single-walled carbon nanotubes. *The Journal of Physical Chemistry B*, 109(15), 7174-7181.
- [132]. Son, Y.J. (201). A study on the physical properties of mortar containing conductive materials. Master thesis, Hanseo University.
- [133]. Song, C., & Choi, S. (2017). Moisture-dependent piezoresistive responses of CNT-embedded cementitious composites. *Composite Structures*, 170, 103-110.
- [134]. Song, G., Wang, C., & Wang, B. (2017). Structural health monitoring (SHM) of civil structures.
- [135]. Stanish, K. D., Hooton, R. D., & Thomas, M. D. (2001). *Testing the Chloride Penetration Resistance of Concrete: A Literature Review* (No. FHWA Contract DTFH61-97-R-00022). United States. Federal Highway Administration.
- [136]. Sulapha, P., Wong, S. F., Wee, T. H., & Swaddiwudhipong, S. (2003). Carbonation of concrete containing mineral admixtures. *Journal of materials in civil engineering*, 15(2), 134-143.
- [137]. Tafesse M, Kim HK. The role of carbon nanotube on hydration kinetics and shrinkage of cement composite. *Composites Part B: Engineering*. 2019 Jul 15;169:55-64.
- [138]. Tafesse, M, Kim, H.K. (2016). Experimental study on shrinkage and hydration kinetics of high-performance concrete by utilizing CNT, The 10th Asian-Australasian Conference on Composite Materials (ACCM-10), October 16 -19, 2016, Bexcoin Busan, Korea
- [139]. Taheri, S. (2019). A review on five key sensors for monitoring of concrete structures. *Construction and Building Materials*, 204, 492-509.
- [140]. Tyson BM. Carbon nanotube and nanofiber reinforcement for improving the flexural strength and fracture toughness of Portland cement paste Doctoral dissertation Texas A & M University; 2012.
- [141]. Uva, G., Porco, F., Fiore, A., & Porco, G. (2014). Structural monitoring using fiber optic sensors of a pre-stressed concrete viaduct during construction phases. *Case Studies in Nondestructive Testing and Evaluation*, 2, 27-37.
- [142]. Wang, S., Wen, S., & Chung, D. D. L. (2004). Resistance heating using electrically conductive cements. *Advances in cement research*, 16(4), 161-166.

- [143]. Wansom, S., Kidner, N. J., Woo, L. Y., & Mason, T. O. (2006). AC-impedance response of multi-walled carbon nanotube/cement composites. *Cement and Concrete Composites*, 28(6), 509-519.
- [144]. Wei, J., Cheng, F., & Yuan, H. (2012). Electrical resistance and microstructure of latex modified carbon fiber reinforced cement composites. *Journal of Wuhan University of Technology-Mater. Sci. Ed.*, 27(4), 746-749.
- [145]. Wei, J., Fan, Y., Zhao, L., Xue, F., Hao, L., & Zhang, Q. (2018). Thermoelectric properties of carbon nanotube reinforced cement-based composites fabricated by compression shear. *Ceramics International*, 44(6), 5829-5833.
- [146]. Wei, J., Zhang, Q., Zhao, L., Hao, L., & Nie, Z. (2017). Effect of moisture on the thermoelectric properties in expanded graphite/carbon fiber cement composites. *Ceramics International*, 43(14), 10763-10769.
- [147]. Wu, F., & Chang, F. K. (2006). Debond detection using embedded piezoelectric elements in reinforced concrete structures-part I: experiment. *Structural Health Monitoring*, 5(1), 5-15.
- [148]. Yao, Y., Tung, S. T. E., & Glisic, B. (2014). Crack detection and characterization techniques—An overview. *Structural Control and Health Monitoring*, 21(12), 1387-1413.
- [149]. Yoo, D. Y., You, I., Zi, G., & Lee, S. J. (2019). Effects of carbon nanomaterial type and amount on self-sensing capacity of cement paste. *Measurement*, 134, 750-761.
- [150]. Yuan, F. G. (Ed.). (2016). *Structural health monitoring (SHM) in aerospace structures*. Woodhead Publishing.
- [151]. Yuan, Q., Shi, C., De Schutter, G., Audenaert, K., & Deng, D. (2009). Chloride binding of cement-based materials subjected to external chloride environment—a review. *Construction and Building Materials*, 23(1), 1-13.
- [152]. Zhu, W., Bartos, P. J., & Porro, A. (2004). Application of nanotechnology in construction. *Materials and Structures*, 37(9), 649-658.
- [153]. Zuo, J., Yao, W., & Wu, K. (2015). Seebeck effect and mechanical properties of carbon nanotube-carbon fiber/cement nanocomposites. *Fullerenes, Nanotubes and Carbon Nanostructures*, 23(5), 383-391.
- [154]. Zuo, J., Yao, W., Liu, X., & Qin, J. (2012). Sensing properties of carbon nanotube-carbon fiber/cement nanocomposites. *Journal of Testing and Evaluation*, 40(5), 838-843.

Appendix

Appendix A. Glossary of electrical terms and definitions

Basic Law of AC and DC (Ohm's Law)

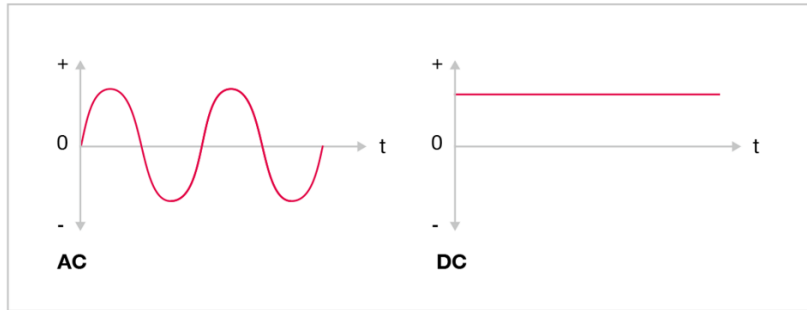
One of the basic laws in electrical engineering is ohms law, which dictate the empirical relationship between the voltage, current and resistance as shown in equation 1 and 2. The voltage is the electrical potential difference between two terminals, and the amount of electrical charge that past across the terminal is referred to us a current, and the ease or opposition that is faced by the current to flow through a conductive material is the electrical resistance.

$$V = IR$$

$$V = IZ$$

Where: V is voltage of in volt (v), I is the current measured in ampere (A), R and Z are the resistance and impedance, respectively of the material both having the same unit ohm (Ω)

The ohms law has an effect on both direct current (DC) and alternating current (AC) circuit. DC is a current flow in one direction having a magnitude at a zero or no frequency. While in case of AC the resistance would have not only magnitude like DC but also has an alternating direction were current flows, which indicates the addition of the phase angle (ϕ) that can be expressed in terms of time for a designated frequency. Over all, the resistance in case of AC is called impedance (Z) both R and Z will be discussed in detail in the next section.



Resistivity (p)

Resistivity is the resistance of a material by normalizing the geometry in order to avoid the effect of the material volume. In short, resistivity is the inverse of conductivity. Electrical resistivity plays a critical role in comparing and selecting a material for different purposes and it is denoted by phi (p).

$$\rho = R \frac{A}{L}$$

Where: R is the resistance in Ω , L is the length in meter (m), A is the area in meter square (m^2) and p is the resistivity in ohm meter (Ωm)

Polarization (P)

By definition, it is a shift of positive and negative electric charges of ions or molecules in opposite direction within a dielectric material induced by an external electric field. This will create a slight potential difference in the material that will generate its own potential, which will be opposite to the applied external voltage. The opposing potential will increase the resistivity of material with time making the data collection problematic and tricky. In order to reduce the effect of polarization while measuring resistivity a 4-point DC measurement can be used or AC

measurement can also be an alternative, in addition, increasing the conductivity of the material that will be measured will reduce the polarization.

Impedance (Z)

It is an extension of DC resistance plus reactance, which is a vector quantity with both magnitude and phase change. Impedance is the ease or opposition of an AC current to flow through a conductive material at a specified frequency and it is denoted by ohm (Ω).

$$Z = R + jX;$$

$$R = |Z| \sin \theta + |Z| \cos \theta$$

Where, R is the resistivity in Ω , X is the reactance in Ω , j is an imaginary unit, θ is the phase angle shift in degrees ($^\circ$), and Z is the impedance in Ω .

Frequency (f)

The number of waves that can pass through a fixed place during a given period of time is called frequency. The effect of frequency has an impact on the AC measurement and none or zero for DC measurement. During resistance measurement using AC the reactance is highly affected by the change in the frequency, which implies a capacitance or inductive reactance. In order to lower the reactance effect, the materials should be classified as a capacitive or inductive before measurement of resistance is done to minimize the reactance to get a relatively constant resistance value by using high or low frequencies, respectively.

Phase angle (θ)

A phase angel is a shift by current or voltage sine waves in degrees ($^{\circ}$), were one lag and one is ahead of the other. Note that although they reach their trough or crest at a different time, however, both oscillate under a similar frequency. The phase shift under impedance measurement indicates a negative value when the current is leading the voltage, which shows that the material being measured has a capacitive reactance. The same is true; when voltage leads the current, the reactance will show a more inductive value, which is positive.

$$\theta = \tan^{-1} \frac{X_L + X_C}{R}$$

Where θ is the phase angle in degrees ($^{\circ}$), R is the resistance in ohms (Ω), X_L is the inductive reactance in ohms (Ω), X_C is the capacitive reactance in ohms (Ω).

Reactance

Reactance can be divided into two to, capacitive and inductive reactance. The reason why the capacitance and inductance are created in the reactance is due to the lead or lag of the current, which would be explained in detail under the phase angle section. A negative value is more capacitive reactance, and positive is more of inductive reactance since both arise by the presence of capacitance and inductance within the material being measured.

$$X = X_L + X_C$$

$$X_L = \omega L = 2\pi fL$$

$$X_C = -\frac{1}{\omega C} = -\frac{1}{2\pi fC}$$

Where; ω is the angular frequency in radians per second (rad/s), f is frequency in hertz (Hz), C is the capacitance in farads(f), L inductance in henrys (H) and X , X_L and X_C are reactance, inductive reactance and capacitive reactance, respectively all in ohms (Ω).

Appendix B. Supplementary data of chapter 4

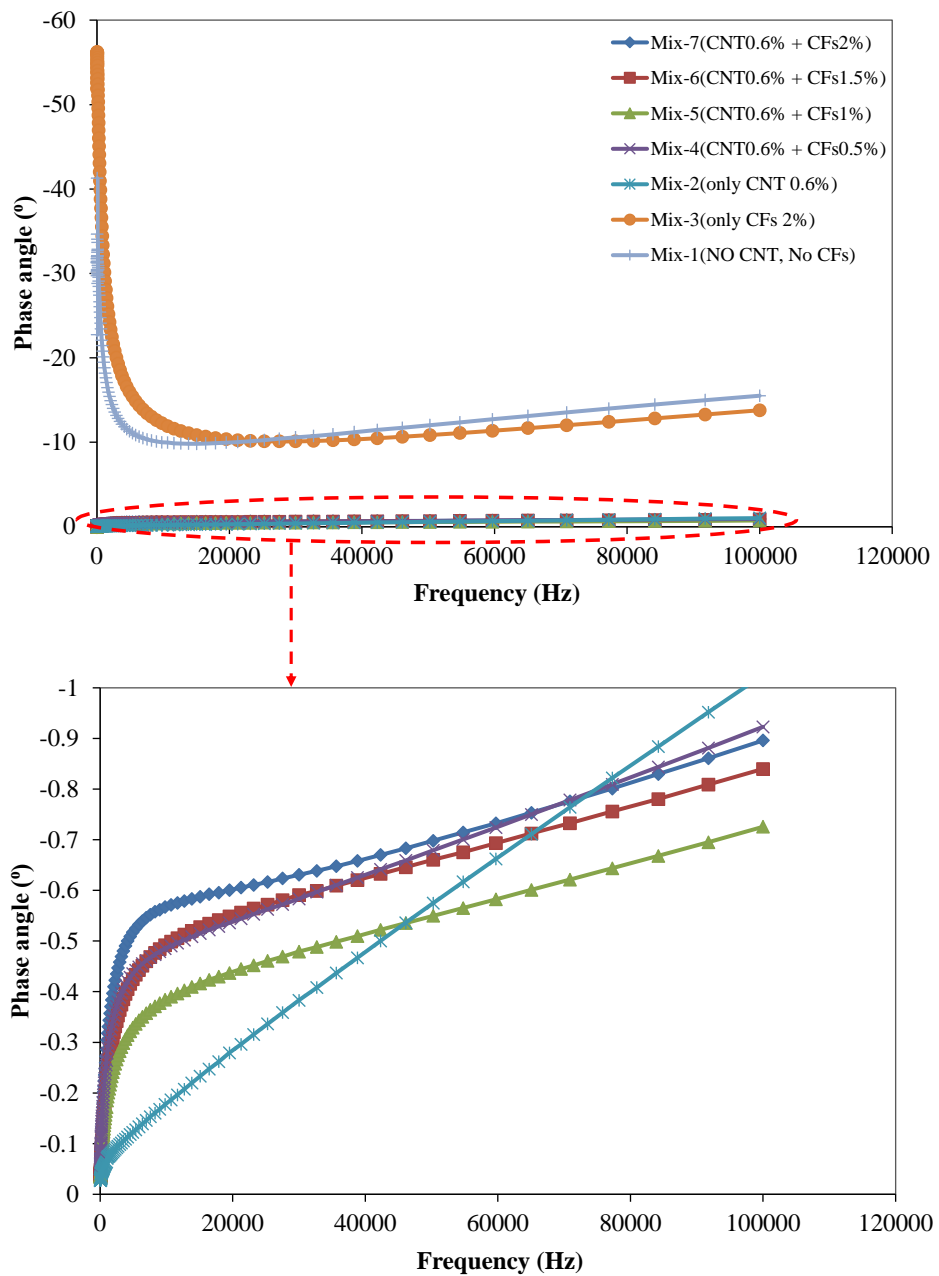


Figure B-1 Phase angle Vs frequency value for new samples at dry state

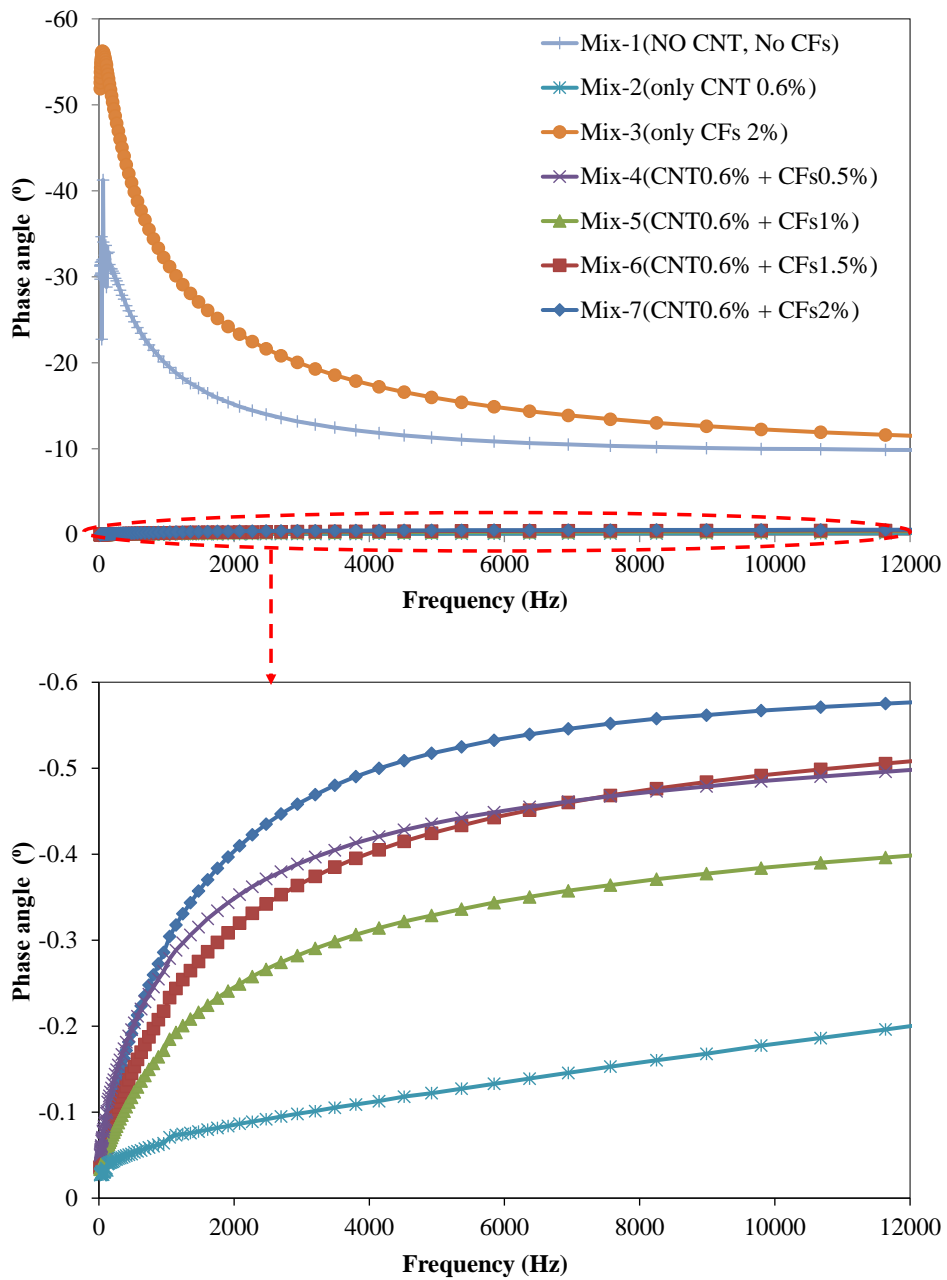


Figure B-2 Phase angle Vs frequency value for new samples at SSD state

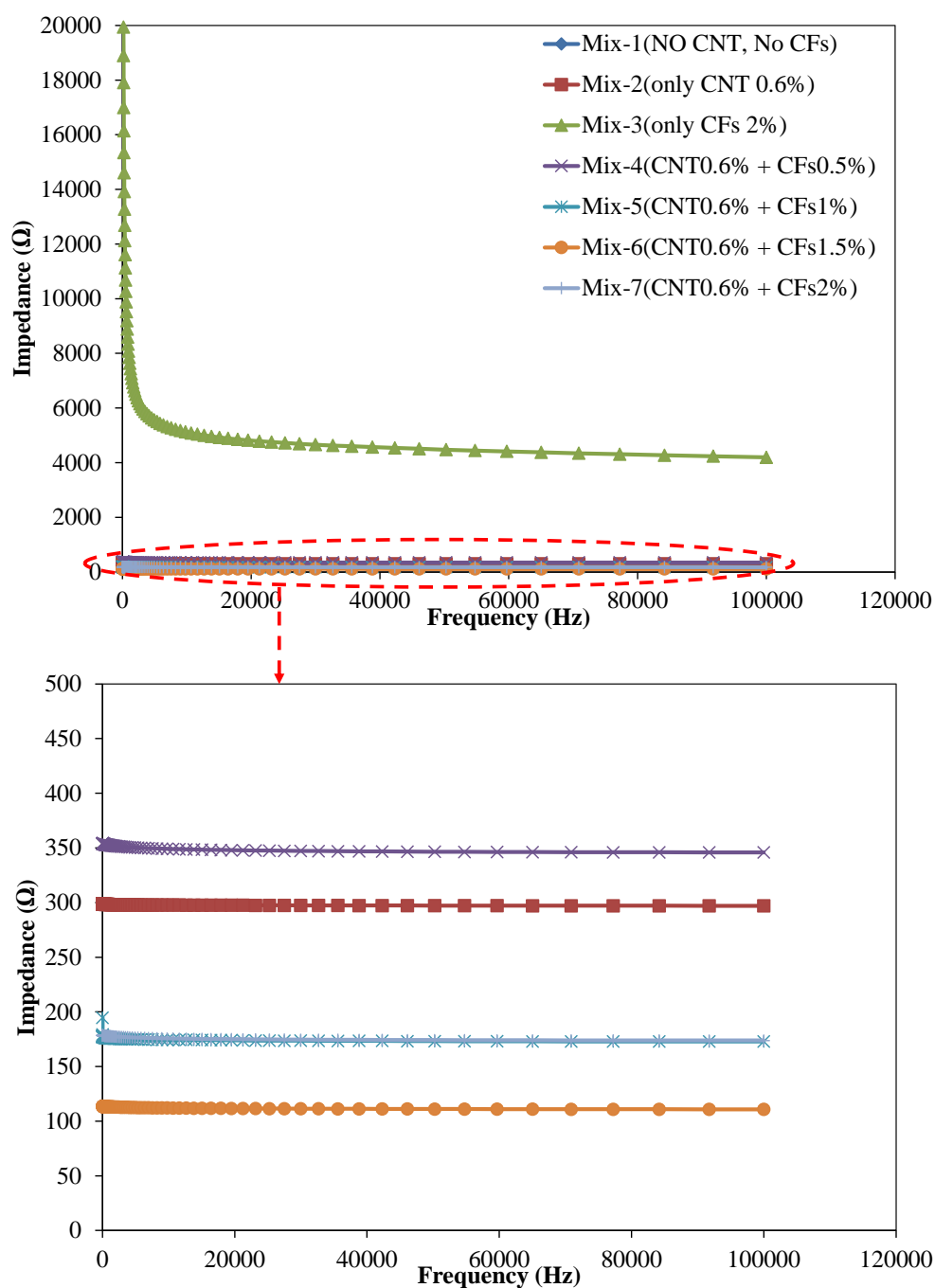


Figure B-3 Impedance Vs frequency value for new samples at dry state

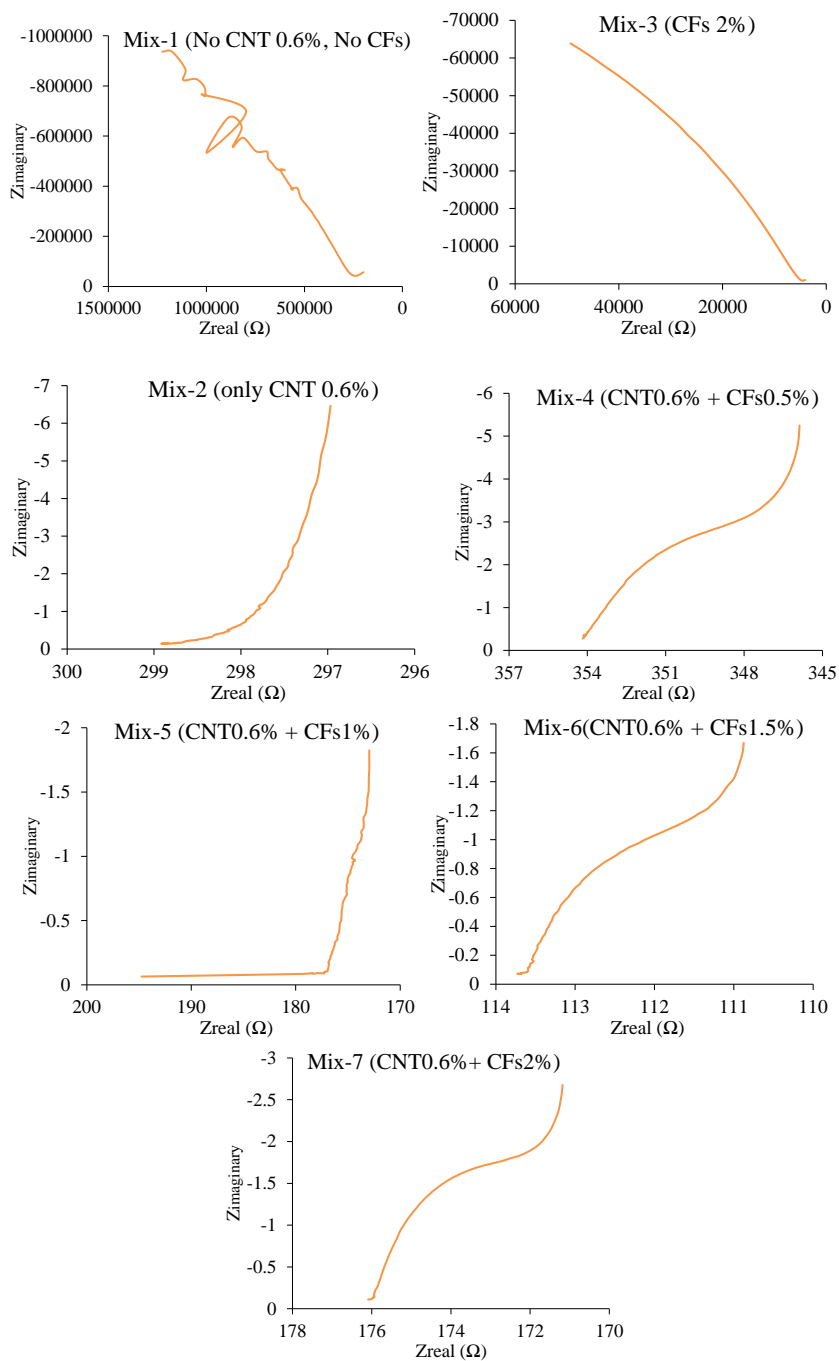


Figure B-4 Real Vs imaginary Impedance measurement values for new samples at dry state

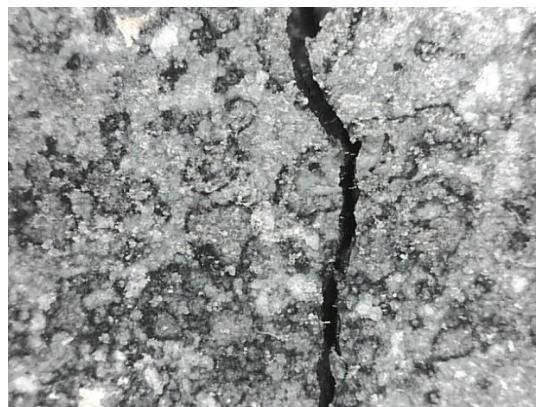
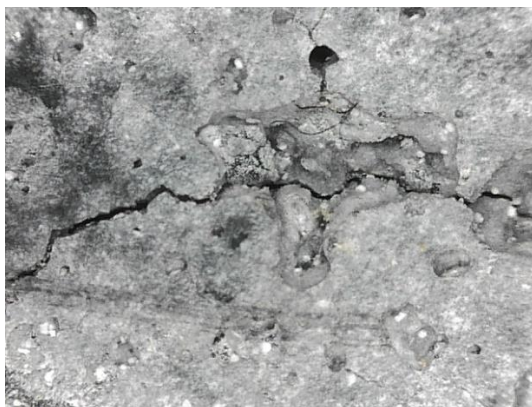


Figure B-5 Images taken after phase 2 and phase 3 during cracking and healing

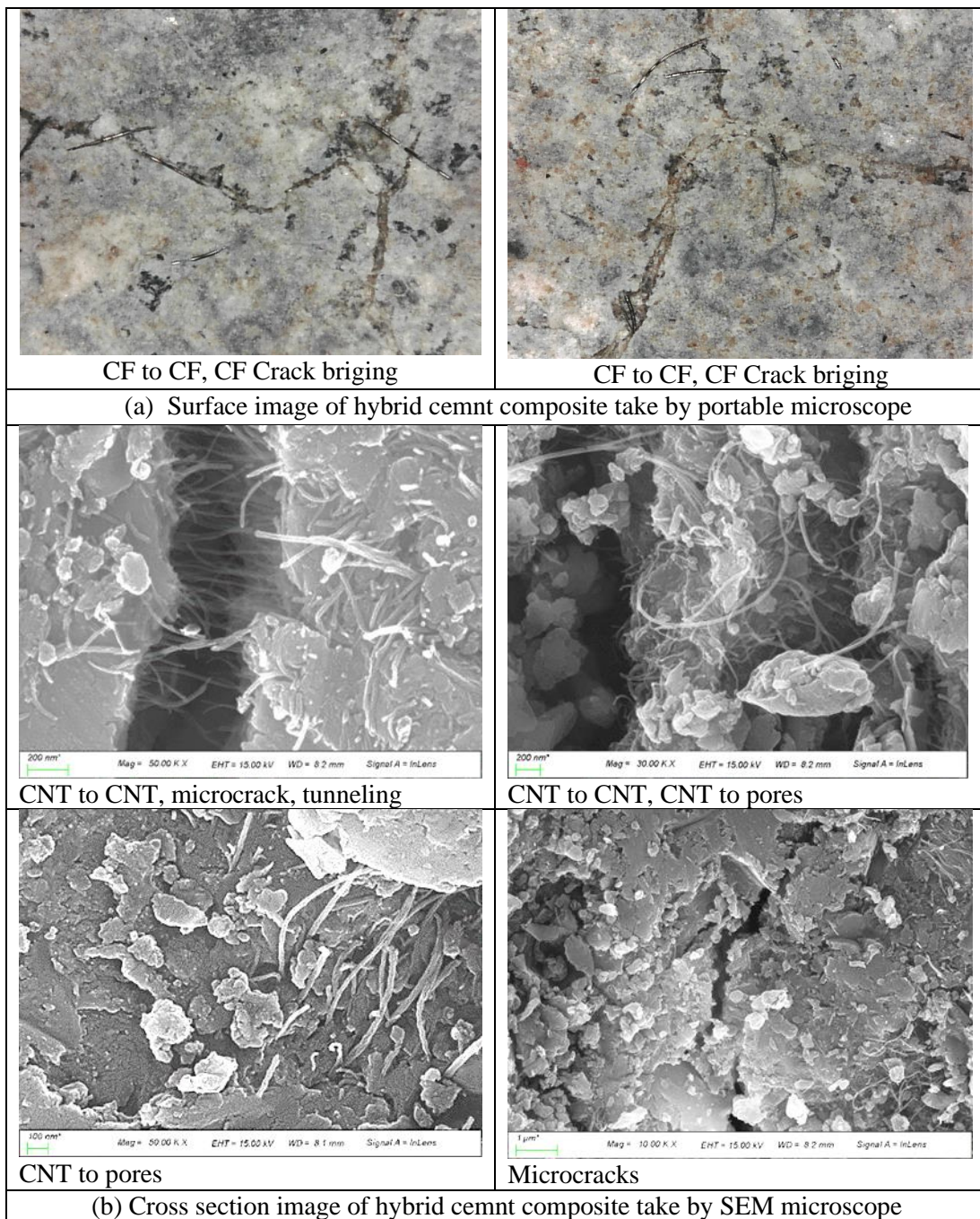


Figure B-6 SEM images for the hybrid cement composite (CCF2)

Appendix C. Supplementary data of chapter 5

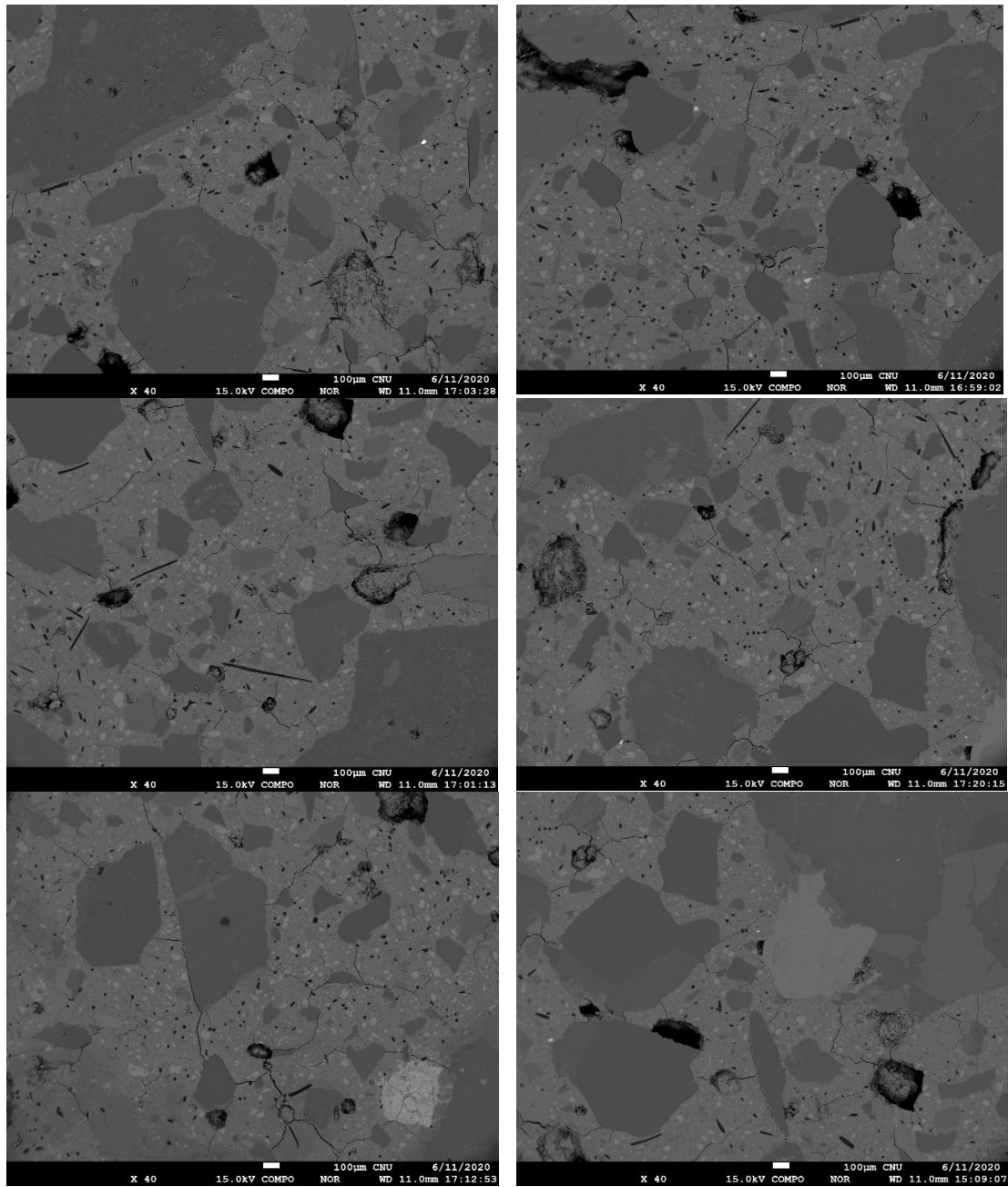
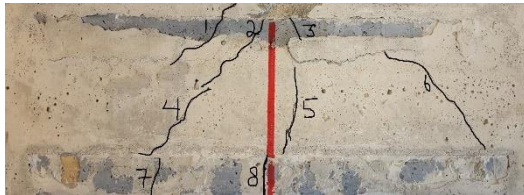


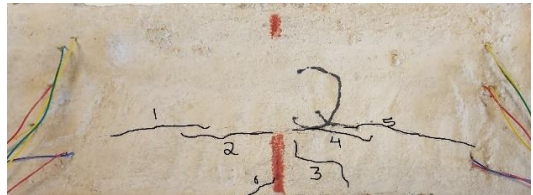
Figure C-1 Backscattering images for the hybrid cement composite (CCF2)

Appendix D. Supplementary data of chapter 6

Sample 1



Front side



Top side

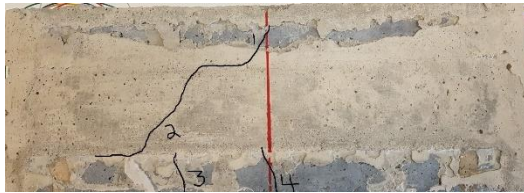


Back side



Bottom side

Sample 2



Front side



Top side



Back side



Bottom side

Figure D-1 Crack patterns of specimens cracked under three-point bending test

Table D-1 Flexural crack widths measured by portable microscope

Sample	Crack No.	Front side			Bottom side			Back side			Top side		
		max	ave	min	max	ave	min	max	ave	min	max	ave	min
1	1	0.0075	0.051	0.018	0.05	0.04	0.038	0.037	0.034	0.018	0.102	0.095	0.079
	2	0.164	0.151	0.108	0.293	0.249	0.186				0.098		0.077
	3	0.072	0.048	0.04	0.088	0.073	0.053				0.081	0.048	0.01
	4	0.1	0.074	0.07	0.109	0.107	0.105				0.065		0.05
	5	0.137	0.125	0.112	0.174	0.169	0.165				0.11		0.082
	6	0.11	0.107	0.095	0.065	0.052	0.04				0.105	0.105	0.063
	7	0.066	0.039	0.028	0.076	0.069	0.059						
	8	0.262	0.262	0.248	0.053	0.034	0.029						
2	1	0.079	0.077		0.102	0.089	0.087	0.079	0.077	0.076			
	2	0.059	0.058	0.056	0.072	0.058	0.056	0.047	0.039	0.034			
	3	0.105	0.1	0.056	0.046	0.046	0.046	0.059	0.046				
	4	0.082	0.045	0.037	0.078	0.075	0.062						
	5				0.053	0.047	0.033						

Table D-2 Resistivity measurement before, during and after cracking of the sensors

Sample No.	Test condition	Sensor number	Initial conductivity			During cracking					After cracking		
			Dry	$\Delta\%$	SSD	Initial	$\Delta\%$	Spike	$\Delta\%$	After	Dry	$\Delta\%$	wet
2	Under compression	1	44.3	3.3	45.8	48.0	-0.2	47.9	0.5	48.2	49.5	-9.4	44.8
		2	33.9	2.3	34.7	35.8	9.7	39.2	-1.1	38.8	38.4	-22.2	29.8
		3	46.0	5.0	48.3	44.9	130.1	103.3	-6.9	96.2	88.2	-43.3	50.0
	Under tension	4	52.7	1.4	53.4	60.5	152.4	152.7	-43.9	85.6	68.2	-30.1	47.6
		5	32.9	2.2	33.6	37.8	194.3	111.1	-34.5	72.8	56.3	-42.0	32.6
		6	51.7	6.3	55.0	55.5	713.1	451.0	-21.7	353.3	263.5	-78.7	56.2
3	Under compression	1	41.4	2.2	42.4	44.8	26.4	56.6	-14.1	48.6	51.2	-10.7	45.7
		2	38.2	2.2	39.1	42.8	5.9	45.3	-3.4	43.8	42.4	-11.7	37.4
		3	45.6	2.7	46.8	46.7	11.0	51.8	-0.6	51.5	48.0	-12.7	41.8
	Under tension	4	38.5	4.1	40.1	40.2	213.1	125.8	-42.0	73.0	66.1	-32.6	44.6
		5	39.0	3.5	40.4	45.4	129.1	104.0	-42.1	60.3	53.5	-24.6	40.3
		6	44.4	10.6	49.1	48.0	328.2	205.6	-43.5	116.2	105.7	-57.1	45.3

Table D-3 Resistivity measurement before and after cracking of the surrounding reinforced mortar sample

Sample No.	measurement direction	Sensor number	Initial conductivity (IC)			After cracking		
			Dry	$\Delta\%$	SSD	Dry	$\Delta\%$	wet
2	Horizontal measurement	12	112.66	13.11557	127.436	411.106	-47.2	216.871
		23	106.85	31.25877	140.25	1689	-84.1	267.993
		45	220.921	-27.0074	161.256	590.4	-65.9	201.115
		56	228.613	-20.5465	181.641	2020	-84.5	313.704
	Vertical measurement	14	300.96	-18.1007	246.484	1488	-69.8	449.304
		25	91.738	22.57734	112.45	2319	-89.3	248.985
		36	426.568	-32.6588	287.256	1889	-80.7	363.715
	Cross over measurement	14				695.65	-52.8	328.678
		25				552.25	-54.7	250.223
		36				2151	-73.7	565.718
3	Horizontal measurement	12	275.667	-6.56916	257.558	307.18	-25.2	229.711
		23	274.841	-17.7379	226.09	306.1	-16.7	255.106
		45	381.269	1.427076	386.71	557.2	-48.0	289.985
		56	376.571	0.172345	377.22	1067	-72.4	294.518
	Vertical measurement	14	271.505	15.57172	313.783	1141.3	-71.6	324.182
		25	457.06	-11.421	404.859	420.587	-28.4	301.337
		36	261.322	18.88896	310.683	616.02	-47.9	321.061
	Cross over measurement	14				563.45	-44.6	312.02
		25				488.98	-41.6	285.511
		36				642.56	-49.7	323.352

Table D-4 Resistivity measurement before and after crack healing

Measurement direction	Sensor number	Sample 1 (SSD condition)					Sample 1 (Dry condition)				
		before cracking	Δ%	after cracking	Δ%	After healing	before cracking	Δ%	after cracking	Δ%	After healing
Sensors measurements	1	45.8	-2.0	44.8	10.8	49.7	41.4	23.5	51.2	6.1	54.3
	2	34.7	-13.9	29.8	8.8	32.4	38.2	10.9	42.4	1.4	43.0
	3	48.3	3.5	50.0	15.0	57.5	45.6	5.2	48.0	24.6	59.8
	4	53.4	-10.8	47.6	32.2	63.0	38.5	71.9	66.1	113.9	141.5
	5	33.6	-3.0	32.6	8.5	35.4	39.0	37.0	53.5	6.9	57.2
	6	55.0	2.3	56.2	137.1	133.3	44.4	137.9	105.7	329.2	453.5
Horizontal measurements	12	31.9	70.2	54.2	5.5	57.2	68.9	11.4	76.8	7.7	82.7
	23	35.1	91.1	67.0	19.7	80.2	68.7	11.4	76.5	51.5	116.0
	45	40.3	24.7	50.3	61.8	81.4	95.3	46.1	139.3	12.6	156.9
	56	45.4	72.7	78.4	49.7	117.4	94.1	183.3	266.8	-33.4	177.5
Vertical measurements	14	61.6	82.3	112.3	-12.2	98.6	67.9	320.4	285.3	-29.6	200.9
	25	28.1	121.4	62.2	16.5	72.5	114.3	-8.0	105.1	18.6	124.7
	36	71.8	26.6	90.9	61.1	146.5	65.3	135.7	154.0	29.6	199.5

Acknowledgment

First and foremost, I would like to thank The Almighty God for His grace and love, which made me complete. May He help me to give what is already His to Him. This dissertation is dedicated to Him, The Almighty, who He is Love Himself.

I would like to honor my advisor, Professor Hyeong-Ki Kim (Ph.D.) for all the countless hours that he spends on me since 2015, during my Masters, PhD, and all the research works we have done together. It was my pleasure to work for him under his valuable supervision and constructive comments. I am very thankful for all the things I have received from him without any restrictions. Thank you, professor, much love!

I also would like to extend my appreciation to my dissertation advisors and all the committee members, Prof. Chang-Geun Cho, Prof. Hee Young Lee, Prof. Beomjoo Yang, Prof. Bang Yeon Lee, for their constructive comments and reviews. And I would like to express my special thanks to Prof. Beomjoo Yang for supporting valuable materials for the experimental work.

Parts of this work could not be full without the contribution of these three co-workers and friends. Dr. Hyo-Kyoung Lee, Selamu Yihune Abate, and Abel Shiferaw Alemu, thank you for all the help I received without any hesitation throughout this research work. I would like to assure you that your helping hands have made a significant contribution to the quality of the dissertation. Thank you so much!

For all my lab members, including Lim Minju, Song Mi-rae, Jeon Sang-min, Jong-jin Baek, SangJun LEE, Jaesung Ahn, Seogyong Gu, Jeong eun Kim, Gebremicael Liyew, Minwuye Mesfin and Ju-Youn Moon I would like to thank you all from the bottom of my heart.

Sincere appreciation is due to Dr. Mesfin Getu, Dr. Daniel Yesheawork, Dr. Biruk Tesfaye, Meron Wubshet, Mohamed Jemal, Zekiya Bedru, Goytom Afera, and Sofanit Wubshet for their limitless help. By paving my way through their advice, making life too easy for me. I could not thank them enough.

Finally, I would like to thank my gifts from God: families, relatives, and friends. You all are the reason who I am. I could not be full without you all. Let my God keep you always on my side and help me to be on your side too. Special thanks to all my Ethiopian friends in Korea, Belay, Haymanot, Dr. Suraj, Dr. Awwal, Vnoth, Najira, Yonatan, Bizu, Tomi, Hamersan, Elsa, and Almirah, who has been with me through thick and thin. I am so grateful to know you all, and you guys are so fun to be around I could not forget you all, much love!

I acknowledge that this research was supported by a Grant (NRF; No. 2017R1D1A1B03034055) from the National Research Foundation of Korea funded by the Ministry of Education, Science, and Technology.

Curriculum Vitae

Million Tafesse Bedso

Department of Architectural Engineering
Chosun University
309 Pilumun-daero, Dong-gu, Gwangju 61452, South Korea

Education:

Ph.D.(candidate) Sept 2017- present

Department of Architectural Engineering, Chosun University, Gwangju, South Korea.

M.Sc. Sept 2015 – Aug 2017

Department of Architectural Engineering, Chosun University, Gwangju, South Korea.

B.Sc. Sept 2009 - Aug 2014

Department of Civil Engineering, Hawassa University, Hawassa, Ethiopia.

Scholarship Awards:

PhD student scholarship, Chosun University

MS student scholarship, Chosun University

BS student scholarship, Hawassa University

Publication:

International journal papers

- [1]. **Tafesse, M[†]**, Lee, N. K[†], Alemu, A. S., Kim, H. K*. Flow and electrical properties of cement composites incorporating mechanical dispersion of carbon nanotube: The effect of carbon nanotube dispersibility. *Cement and Concrete Composites* (Accepted)
- [2]. **Tafesse, M.**, Lee, H. K., Alemu, A. S., Kim, H. K*, and Pyo, S. (2020) On the expansive cracking of a cement matrix containing atomized basic oxygen furnace slag with a metallic iron. *Construction and Building Materials* (Accepted)

- [3]. **Tafesse, M.**, Kim, R. H., Abate, S. Y., Jeon, S. M., Baek, J. J., Yang, B., and Kim, H. K*. Mix proportioning of concrete containing brick chips as coarse aggregate for cost minimization. *Materials* (submitted)
- [4]. Pyo, S., Koh, T., **Tafesse, M.**, & Kim, H. K*. (2019). Chloride-induced corrosion of steel fiber near the surface of ultra-high performance concrete and its effect on flexural behavior with various thickness. *Construction and Building Materials*, 224, 206-213.
- [5]. Kim, H. J., **Tafesse, M.**, Lee, H. K., & Kim, H. K*. (2019). Incorporation of CFBC ash in sodium silicate-activated slag system: Modification of microstructures and its effect on shrinkage. *Cement and Concrete Research*, 123, 105771.
- [6]. Lee, H. K., Nam, I. W., **Tafesse, M.**, & Kim, H. K*. (2019). Fluctuation of electrical properties of carbon-based nanomaterials/cement composites: Case studies and parametric modeling. *Cement and Concrete Composites*, 102, 55-70.
- [7]. **Tafesse, M.**, & Kim, H. K*. (2019). The role of carbon nanotube on hydration kinetics and shrinkage of cement composite. *Composites Part B: Engineering*, 169, 55-64.
- [8]. Pyo, S., **Tafesse, M.**, Kim, B. J., & Kim, H. K*. (2018). Effects of quartz-based mine tailings on characteristics and leaching behavior of ultra-high performance concrete. *Construction and Building Materials*, 166, 110-117.
- [9]. Pyo, S., **Tafesse, M.**, Kim, H., & Kim, H. K*. (2017). Effect of chloride content on mechanical properties of ultra-high performance concrete. *Cement and Concrete Composites*, 84, 175-187.

Domestic journal papers

- [1]. **Tafesse, M.**, & Kim, H. K*. (2017). Effect of Pretreatment of Mine Tailings on the Performance of Controlled Low Strength Materials. *Journal of the Korean Institute of Resources Recycling*, 26(3), 32-38.
- [2]. **Tafesse, M.**, & Kim, H. K*. (2016). Effects of Crushed Coal Bottom Ash on the Properties of Mortar with Various Water-to-binder Ratios. *Journal of the Korean Institute of Resources Recycling*, 25(6), 29-40.

Conference proceedings:

- [1]. **Million Tafesse.**, and Hyeong-Ki Kim., "Utilization of mine tailings as a substitute material in UHPC" *Proceedings of the Korean Society for Composite Materials (KSCM)*, Jeju, South Korea, November 21-23, 2019.
- [2]. **Million Tafesse.**, Beomjoo yang, and Hyeong-Ki Kim., "Brick chips aggregates in cement composite for cost optimization," *Proceedings of the Korean Society for Composite Materials (KSCM)*, Yeosu, South Korea, Spring, 2019.
- [3]. **Million Tafesse.**, and Hyeong-Ki Kim., "Electrical stability of conductive cement composites containing carbon nanomaterials," *Proceedings of the Korean Society for Composite Materials (KSCM)*, Daejeon, South Korea, Autumn, 2018.
- [4]. **Million Tafesse**, Minju Lim, Hyo-Kyoung Lee, & Hyeong-Ki Kim., "Crack detection and modeling of A CNT/Cement composite based on conductivity," *Proceedings of the 4th International Conference on Computational Design in Engineering (CODE 2018)*, Changwon, South Korea, April 1-5, 2018.
- [5]. **Million Tafesse.**, and Hyeong-Ki Kim., "Experimental Evaluation on Flowability and Mechanical Properties of CNT/cement Composites Dispersed by Silica Fume," *Proceedings of the 11th Asian-Australasian Conference on Composite Materials (ACCM-11)*, Cairns, Australia, July 29 to August 1, 2018.
- [6]. **Million Tafesse.**, and Hyeong-Ki Kim., "Flowability, Settlement, and Strength of Controlled low Strength Material containing Sun-Shin Mine Tailings," *Proceedings of International Conference on Frontiers of Composite Materials (ICFCM2016)*, Auckland, New Zealand, November 19-21, 2016.
- [7]. **Million Tafesse.**, and Hyeong-Ki Kim., "Experimental study on shrinkage and hydration kinetics of high-performance concrete by utilizing CNT," *Proceedings of the 10th Asian-Australasian Conference on Composite Materials (ACCM-10)*, Busan, South Korea, October 16 - 19, 2016.
- [8]. Sukhoon Pyo., **Million Tafesse.**, and Hyeong-Ki Kim., "The applications of mine tailings to develop low cost UHPC," *Proceedings of First International Interactive Symposium on UHPC*, Des Moines, IA, USA, no. 92, 6 pages, July 18-20, 2016.